



MID-AMERICA TRANSPORTATION CENTER

Report # MATC-UNL: 004-059

Final Report
WBS: 25-1121-0005-004-059

UNIVERSITY OF
Nebraska
Lincoln

THE UNIVERSITY
OF IOWA

THE UNIVERSITY OF
KU KANSAS

MISSOURI
S&T

LINCOLN
UNIVERSITY
MISSOURI



UNIVERSITY OF
Nebraska
Omaha

University of Nebraska
Medical Center

KU MEDICAL
CENTER
The University of Kansas

Enhancing Erosion Resistance of Rock Shoulder by Considering Hydrodynamics

Chung R. Song, PhD, AE

Associate Professor

Department of Civil and Environmental Engineering
University of Nebraska-Lincoln

Richard L. Wood, PhD

Associate Professor

Basil Abualshar

Graduate Research Assistant

Mark O'Brien

Undergraduate Research Assistant

Bashar Al-Nimri

Graduate Research Assistant

Mitra Nasimi

Graduate Research Assistant

Babur Deliktas

Professor

Civil Engineering

Bursa Uludag University

Aiman Tariq

Graduate Research Assistant

Civil Engineering

Bursa Uludag University

UNIVERSITY OF
Nebraska
Lincoln

2023

A Cooperative Research Project sponsored by
U.S. Department of Transportation- Office of the Assistant
Secretary for Research and Technology

The contents of this report reflect the views of the authors, who are responsible for the facts and the accuracy of the information presented herein. This document is disseminated in the interest of information exchange. The report is funded, partially or entirely, by a grant from the U.S. Department of Transportation's University Transportation Centers Program. However, the U.S. Government assumes no liability for the contents or use thereof.

MATC

Enhancing Erosion Resistance of Rock Shoulder by Considering Hydrodynamics

Chung R. Song, Ph.D., A.E.,
Associate Professor
Civil and Environmental Engineering
University of Nebraska-Lincoln

Richard L. Wood, Ph. D.,
Associate Professor
Civil and Environmental Engineering
University of Nebraska-Lincoln

Basil Abualshar
Graduate Research Assistant
Civil and Environmental Engineering
University of Nebraska-Lincoln

Mark O'Brien
Undergraduate Research Assistant
Civil and Environmental Engineering
University of Nebraska-Lincoln

Bashar Al-Nimri
Graduate Research Assistant
Civil and Environmental Engineering
University of Nebraska-Lincoln

Mitra Nasimi
Graduate Research Assistant
Civil and Environmental Engineering
University of Nebraska-Lincoln

Babur Deliktas
Professor
Civil Engineering
Bursa Uludag University

Aiman Tariq
Graduate Research Assistant
Civil Engineering
Bursa Uludag University

A Report on Research Sponsored by

Mid-America Transportation Center

University of Nebraska–Lincoln

October 2023

Technical Report Documentation Page

1. Report No. 25-1121-0005-059	2. Government Accession No.	3. Recipient's Catalog No.	
4. Title and Subtitle Enhancing Erosion Resistance of Rock Shoulder by Considering Hydrodynamics		5. Report Date October 2023	
		6. Performing Organization Code	
7. Author(s) Chung R. Song, Richard L. Wood, Basil Abualshar, Mark O'Brien, Bashar Al-Nimri, Mitra Nasimi, Babur Deliktas, and Aiman Tariq		8. Performing Organization Report No. 25-1121-0005-059	
9. Performing Organization Name and Address Mid-America Transportation Center Prem S. Paul Research Center at Whittier School 2200 Vine St. Lincoln, NE 68583-0851		10. Work Unit No. (TRAIS)	
		11. Contract or Grant No. 69A3551747107	
12. Sponsoring Agency Name and Address Office of the Assistant Secretary for Research and Technology 1200 New Jersey Ave., SE Washington, D.C. 20590		13. Type of Report and Period Covered Final Report. November 2021 – June 2023	
		14. Sponsoring Agency Code MATC TRB RiP No. 91994-106	
15. Supplementary Notes			
16. Abstract Highway shoulder rocks are exposed to continuous erosion force due to unexpected floodings caused by climate change. The evaluation methods of the erosion resistance of highway shoulder rocks are not currently well-developed. This study developed a new large-scale testing device, the University of Nebraska-Lincoln Erosion Testing Bed (UNLETB), which has the capability of testing the shoulder gravels. Different gradations were tested using UNLETB, and the results distinguished a high-resistant group and a low-resistant group. The low resistant group was treated with different binding agents: Ammonium Lignosulfonate (LIGNO10), Soybean Soap Stock, and DirtGlue. The treated samples showed better erosion resistance based on the binding agent and the sample type. Then, a hydrodynamics-based analysis was conducted using CFD software. UNLETB was modeled using FLOW3D-Hydro, and a comprehensive parametric study was conducted to obtain the hydrodynamics-input parameters for the tested samples. In addition, this study trained ANN (Artificial Neural Network) with test results to conveniently discern the erosion resistance of different gradations. The ANN quickly predicted the acceptable/non-acceptable erosion characteristics of shoulder rocks with close to 99% accuracy based on three simple parameters related to gradation (D_{10} , D_{30} , and D_{60}).			
17. Key Words Erosion Resistant, Rock Shoulder, Sediment Transport, Hydrodynamics-Analysis, Biopolymers, Artificial Intelligence (AI), Artificial Neural Networks (ANN)		18. Distribution Statement	
19. Security Classif. (of this report) Unclassified	20. Security Classif. (of this page) Unclassified	21. No. of Pages 124	22. Price

Table of Contents

Abstract	xi
Chapter 1 Introduction	1
1.1 Background and Significance of Work.....	1
1.2 Problem Statement	3
1.3 Objectives of the Study	5
1.4 Implementation	6
1.5 Work Procedure/Tasks.....	6
Chapter 2 Literature Review	8
2.1 Erosion Mechanism	8
2.2 Testing Methods.....	10
2.2.1 Jet Erosion Test (JET).....	10
2.2.2 Mini Jet Erosion Test (JET).....	12
2.2.3 Erosion Function Apparatus (EFA)	14
2.2.4 Rotating Cylinder Test (RCT)	15
2.2.5 University of Mississippi Erosion Testing Bed (UMETB).....	16
2.3 Shoulder Stabilization.....	18
Chapter 3 Shoulder Rock Properties and Erosion Testing.....	20
3.1 Materials (Rock Shoulder) Properties.....	20
3.2 Testing Apparatus	22
3.2.1 General	22
3.2.2 University of Nebraska Lincoln Erosion Testing Bed (UNLETB) Fabrication/Parts	22
3.2.3 Detailed Test Procedure.....	32
3.3 Erosion Test Results for Untreated Materials	33
3.3.1 Boundary Effect	37
3.3.2 Effect of Fines.....	37
3.3.3 Compaction Effect	38
3.4 Erosion Test Results for Treated Materials	38
3.4.1 Ammonium Lignosulfonate (LIGNO10).....	39
3.4.2 Soybean Soap Stock.....	44
3.4.3 DirtGlue	48
3.4.4 Treatment Methods Comparison.....	51
Chapter 4 : FLOW3D-Hydro Simulation	58
4.1 General	58
4.2 Sediment Transport Model	58
4.2.1 General	58
4.2.2 Packed and Suspended Sediments	59
4.2.3 Bed Morphology	60
4.2.4 Numerical Models and Computational Methods Used in FLOW3D-Hydro	61
4.2.5 Modeling UNLETB	67
4.2.6 Input Parameters	70
Chapter 5 Artificial Intelligence-Approach	88
5.1 General.....	88

5.2 Detailed Explanation for the AI-Approach.....	89
5.3 Test Results.....	96
Chapter 6 Conclusions.....	106
References.....	109
Appendix A Sieve Analysis Test Results	114
Appendix B Individual Erosion Curves.....	118
Appendix C User Manual and Interface for the AI-Approach	124

List of Figures

Figure 1.1 Crushed Rock Surface at Hwy 31 (Rocks in the shoulder were washed out.)	1
Figure 1.2 Graphical Presentation of Gradation of Crushed Rock Surface Course.....	3
Figure 1.3 Drawing for Erosion Susceptible Target Layers 5 and 6, NDOT Plan 1-7(108)-Sheet 2-T1 (NDOT, 2017)	4
Figure 2.1 Schematic of JET by Hanson & Cook (2004)	11
Figure 2.2 Mini JET Device by Al-Madhhachi et al. (2013).....	13
Figure 2.3 Schematic of EFA by Briaud et al. (1999)	14
Figure 2.4 a) View of outside UMETB, b) View of inside UMETB (Song et al. 2011).	16
Figure 3.1 Gradation Curves for the Tested Materials.....	20
Figure 3.2 (a) 1.5 in. Rock Agg Sample, and (b) Class B Sample.....	21
Figure 3.3 External View of UNLETB.....	23
Figure 3.4 Internal View of UNLETB.....	24
Figure 3.5 Air Relief Valve.....	25
Figure 3.6 Empty Sample Box.....	26
Figure 3.7 Sample Box with Soil Sample.....	27
Figure 3.8 Sample Box Base (a) Top view, and (b) Side View.....	28
Figure 3.9 a) 1 HP Sump Pump, and b) $\frac{3}{4}$ HP Sump Pump	29
Figure 3.10 Camera Cover Frame (a) Side view, and (b) Top View	30
Figure 3.11 Waterproof Camera	31
Figure 3.12 Glass Plate Location in UNLETB	32
Figure 3.13 Erosion Curves for All Samples	34
Figure 3.14 Updated Erosion Curves for All Samples.....	36
Figure 3.15 Effect of Fines on the Erosion Behavior of the Combined Package Sample	37
Figure 3.16 Effect of Compaction on the Erosion Behavior of the Class B Sample	38
Figure 3.17 Erosion Test Results for 1 in. Clean Sample Treated with LIGNO10 (Note: The red line refers to the treatment depth)	41
Figure 3.18 Erosion Test Results for 1 in. Coarse Sample Treated with LIGNO10 (Note: The red line refers to the treatment depth)	41
Figure 3.19 Erosion Test Results for Class 2A Sample Treated with LIGNO10 (Note: The red line refers to the treatment depth)	42
Figure 3.20 Erosion Test Results for Gravel Surface Course Sample Treated with LIGNO10 (Note: The red line refers to the treatment depth).....	42
Figure 3.21 Erosion Test Results for Class B Sample Treated with LIGNO10 (Note: The red line refers to the treatment depth)	43
Figure 3.22 Erosion Test Results for 1 in. Clean Sample Treated with Soybean Soap Stock (Note: The red line refers to the treatment depth).....	45
Figure 3.23 Erosion Test Results for 1 in. Coarse Sample Treated with Soybean Soap Stock (Note: The red line refers to the treatment depth).....	46
Figure 3.24 Erosion Test Results for Class 2A Sample Treated with Soybean Soap Stock (Note: The red line refers to the treatment depth).....	46
Figure 3.25 Erosion Test Results for Gravel Surface Course Sample Treated with Soybean Soap Stock (Note: The red line refers to the treatment depth).....	47

Figure 3.26 Erosion Test Results for Class B Sample Treated with Soybean Soap Stock (Note: The red line refers to the treatment depth).....	47
Figure 3.27 Erosion Test Results for 1 in. Clean Sample Treated with DirtGlue	49
Figure 3.28 Erosion Test Results for 1 in. Coarse Sample Treated with DirtGlue.....	49
Figure 3.29 Erosion Test Results for Class 2A Sample Treated DirtGlue	50
Figure 3.30 Erosion Test Results for Gravel Surface Course Sample Treated with DirtGlue	50
Figure 3.31 Erosion Test Results for Class B Sample Treated with DirtGlue.....	51
Figure 3.32 Erosion Test Results for 1 in. Clean Treated Samples (All Biopolymers).....	52
Figure 3.33 Erosion Test Results for 1 in. Coarse Treated Samples (All Biopolymers).....	53
Figure 3.34 Erosion Test Results for Class 2A Treated Samples (All Biopolymers).....	53
Figure 3.35 Erosion Test Results for Gravel Surface Course Treated Samples (All Biopolymers)	54
Figure 3.36 Erosion Test Results for Class B Treated Samples (All Biopolymers).....	54
Figure 4.1 The Physical Processes Causing the Bed Morphology Changes (Fox & Feurich, 2019)	60
Figure 4.2 Side View of UNLETB FLOW3D-Hydro Model	67
Figure 4.3 Top View of UNLETB FLOW3D-Hydro Model.....	68
Figure 4.4 Mesh of UNLETB FLOW3D-Hydro Model	69
Figure 4.5 Boundary Conditions of UNLETB FLOW3D-Hydro Model.....	69
Figure 4.6 Boundary Conditions of UNLETB FLOW3D-Hydro Model.....	70
Figure 4.7 Effect of Turbulence Model on the Erosion Profile of UNLETB FLOW3D-Hydro Model	72
Figure 4.8 Effect of Angle of Repose/Slope on the Erosion Profile of UNLETB FLOW3D-Hydro Model	73
Figure 4.9 Effect of Maximum Packing Fraction on the Erosion Profile of UNLETB FLOW3D-Hydro Model	74
Figure 4.10 Effect of Molecular Diffusion Parameter on the Erosion Profile of UNLETB FLOW3D-Hydro Model	75
Figure 4.11 Effect of Turbulent Diffusion Multiplier on the Erosion Profile of UNLETB FLOW3D-Hydro Model	76
Figure 4.12 Effect of Richardson-Zaki Multiplier on the Erosion Profile of UNLETB FLOW3D-Hydro Model	77
Figure 4.13 Effect of Sediment Density on the Erosion Profile of UNLETB FLOW3D-Hydro Model	78
Figure 4.14 Shields Test Results as Presented in (Buffington, 1999).....	79
Figure 4.15 Effect of the Selected Bedload Equation on the Erosion Profile of UNLETB FLOW3D-Hydro Model	81
Figure 4.16 Effect of Bedload Coefficient on the Erosion Profile of UNLETB FLOW3D-Hydro Model	82
Figure 4.17 Equivalent Roughness Height to Mean Median Grain Size Ratio vs. Critical Shield Parameter (excerpted from (Dey & Ali, 2019)).....	84
Figure 4.18 Effect of Roughness/ D_{50} on the Erosion Profile of UNLETB FLOW3D-Hydro Model	85
Figure 4.19 Effect of Entertainment Parameter on the Erosion Profile of UNLETB FLOW3D-Hydro Model	86

Figure 4.20 Experimental vs. FLOW3D-Hydro Results for Combined Package Class A with Fines Sample	86
Figure 5.1 Workflow of AI for erosion prediction.....	90
Figure 5.2 Synthetic Gradation Curve Generation.....	91
Figure 5.3 One Hot Encoding of Categorical Data.....	93
Figure 5.4 Proposed Neural Network Architecture	94
Figure 5.5 Validation Techniques.....	96
Figure 5.6 Accuracy vs. Epochs of the Trained Model.	98
Figure 5.7 Confusion Matrix.....	102
Figure B.1 Erosion Curve for 1 in. Clean Sample (Initial Results)	118
Figure B.2 Erosion Curve for 1 in. Clean Sample (Updated Results)	118
Figure B.3 Erosion Curve for 1.5 in. Crusher Run Sample	119
Figure B.4 Erosion Curve for 1 in. Coarse Sample (Initial Results)	119
Figure B.5 Erosion Curve for 1 in. Coarse Sample (Updated Results)	120
Figure B.6 Erosion Curve for Combined Package Class A (without fines) Sample	120
Figure B.7 Erosion Curve for Combined Package Class A (with fines) Sample.....	121
Figure B.8 Erosion Curve for 1 in. Crusher Run Sample	121
Figure B.9 Erosion Curve for Gravel Surface Course Sample	122
Figure B.10 Erosion Curve for Class 2A Sample	122
Figure B.11 Erosion Curve for Class B Sample	123
Figure C.1 Step 1 Uploading the prediction_interface.ipynb File to the Google Colab.....	125
Figure C.2 Step 2 Executing the prediction_interface.ipynb Notebook	126

List of Tables

Table 1.1 Current Field Gradation of Erosion Resistant Crushed Rock Surface Course that is Inserted by Special Provision.....	2
Table 1.2 Results of Shoulder or Soil Treatment Methods from Different States.....	4
Table 2.1: Summary of the Advantages and Limitations for Each Testing Method.....	18
Table 3.1 Mean Grain Size (D_{50}) for All Samples	22
Table 3.2 UNLETB Parts	24
Table 3.3 Physical Properties of LIGNO10	39
Table 3.4 Chemical Properties of LIGNO10	39
Table 3.5 Physical and Chemical Properties of Soybean Soap Stock.....	44
Table 3.6 Effect of Biopolymer Treatment on All Treated Sample.....	56
Table 4.1 Richardson-Zaki Coefficient as a Function of Reynold's Number.....	76
Table 4.2 Critical Shields Parameter for Each Sample	80
Table 4.3 Ratio of Nikuradse Equivalent Roughness and Sediment Size for Rivers (Garcia, 2008)	83
Table 4.4 Summary of FLOW3D-Hydro Input Parameters for All Samples.....	87
Table 5.1 Various ANN Models Based on Different Parameters.	97
Table 5.2 Class-Based True Positives, True Negatives, False Positives, and False Negatives .	102
Table 5.3 Class-based Precision, Recall and F-Score Values and Overall Accuracy	104
Table A.1 Sieve Analysis Results for 1.5 in. Rock Agg Sample	114
Table A.2 Sieve Analysis Results for 1.5 in. Crusher Run Sample	114
Table A.3 Sieve Analysis Results for 1 in. Clean Sample	114
Table A.4 Sieve Analysis Results for 1 in. Coarse Sample	115
Table A.5 Sieve Analysis Results for 1 in. Crusher Run Sample	115
Table A.6 Sieve Analysis Results for Gravel Surface Course Sample	115
Table A.7 Sieve Analysis Results for Class B Sample	116
Table A.8 Sieve Analysis Results for Class 2A Sample.....	116
Table A.9 Sieve Analysis Results for Combined Package Class A without Fines Sample	116
Table A.10 Sieve Analysis Results for Combined Package Class A with Fines Sample	117

Acknowledgments

Researchers of this study greatly appreciate the funding from Mid-America Transportation Center (MATC) through the U.S. Department of Transportation and the Nebraska Department of Transportation (NDOT).

Disclaimer

The contents of this report reflect the views of the authors, who are responsible for the facts and the accuracy of the information presented herein. This document is disseminated in the interest of information exchange. The report is funded, partially or entirely, by a grant from the U.S. Department of Transportation's University Transportation Centers Program. However, the U.S. Government assumes no liability for the contents or use thereof.

Abstract

Highway shoulder rocks are exposed to continuous erosion force due to unexpected floodings caused by climate change. The evaluation methods of the erosion resistance of highway shoulder rocks are not currently well-developed. This study developed a new large-scale testing device, the University of Nebraska-Lincoln Erosion Testing Bed (UNLETB), which has the capability of testing the shoulder gravels. Different gradations were tested using UNLETB, and the results distinguished a high-resistant group and a low-resistant group. The low resistant group was treated with different binding agents: Ammonium Lignosulfonate (LIGNO10), Soybean Soap Stock, and DirtGlue. The treated samples showed better erosion resistance based on the binding agent and the sample type. Then, a hydrodynamics-based analysis was conducted using CFD software. UNLETB was modeled using FLOW3D-Hydro, and a comprehensive parametric study was conducted to obtain the hydrodynamics-input parameters for the tested samples. In addition, this study trained ANN (Artificial Neural Network) with test results to conveniently discern the erosion resistance of different gradations. The ANN quickly predicted the acceptable/non-acceptable erosion characteristics of shoulder rocks with close to 99% accuracy based on three simple parameters related to gradation (D_{10} , D_{30} , and D_{60}).

Chapter 1 Introduction

1.1 Background and Significance of Work

Extreme weather conditions are a new norm in modern days with the advent of climate change. Consequently, weather patterns are becoming more unpredictable, and severe drought and flooding are unavoidable. For highway structures, this new weather pattern creates new problems in the pavement system. Particularly during the Winter of 2019, extended heavy rains in Nebraska severely washed out highway shoulder materials in several different places, as shown in Figure 1.1, which is an unexpected challenge for engineers to mitigate. In addition, District Maintenance Operations reported that eroded and dislodged shoulder aggregates are often struck by mower blades to cause longer downtime.



Figure 1.1 Crushed Rock Surface at Hwy 31 (Rocks in the shoulder were washed out.)

Techniques to evaluate erosion resistance of these materials and to mitigate the erosion issue are not sufficiently developed so far. Consequently, a method to evaluate and improve the design of erosion resistant aggregates is needed.

NDOT currently utilizes the gradation of crushed rock surface course, as shown in Table 1.1 and Figure 1.2. A properly compacted crushed rock surface course is believed to provide high bearing stress and erosion resistance (Junliang et al. 2017; USDA, 2017; US Army, 2020). However, materials with these gradations are not always readily available nor tested to perform as intended, as discussed previously in Figure 1.1, the quantitative erosion testing method is not currently well developed. This study combines a dedicated testing method and hydrodynamics analysis technique to test, evaluate, and find the erosion resistant shoulder materials so

- 1) Alternate gradation of crushed rock surface course that can be sourced in Nebraska are attainable when gradation requirements in Table 1.1 are not available.
- 2) Additional reinforcing techniques (such as adding binder materials to gravels) may be recommended to enhance the erosion resistance of the crushed rock surface course shown in Table 1.1 and Figure 1.2.

Table 1.1 Current Field Gradation of Erosion Resistant Crushed Rock Surface Course that is Inserted by Special Provision

Crushed Rock Surface Course		
Sieve Size	Percent Passing	
	Minimum	Maximum
2"	100	
1"	25	45
1/2"	0	15
3/8"	0	10
#4	0	5

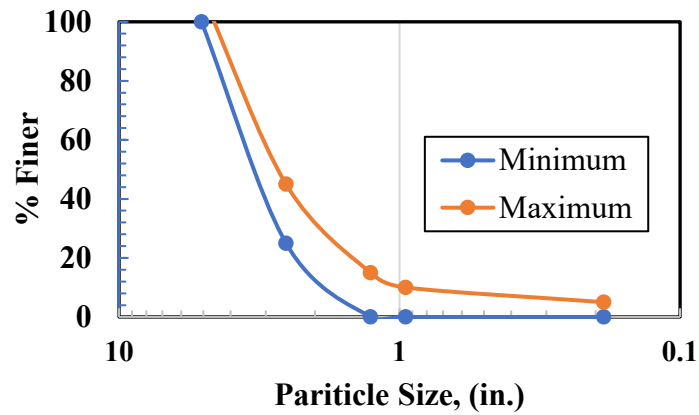


Figure 1.2 Graphical Presentation of Gradation of Crushed Rock Surface Course

1.2 Problem Statement

The current shoulder design of local highways in Nebraska is shown in Figure 1.3. Layer 5 is a 4" thick compacted shoulder with crushed rock surface course mixed with local fine soils, and Layer 6 is a 1" thick crushed rock surface course roller compacted on the top of Layer 5. Potential erosion induced issues such as drop-offs (Jensen and Uerling, 2015), lane-departure crashes (AASHTO, 2008), and mowing issues from dislodged rocks were anticipated or reported for these two layers.

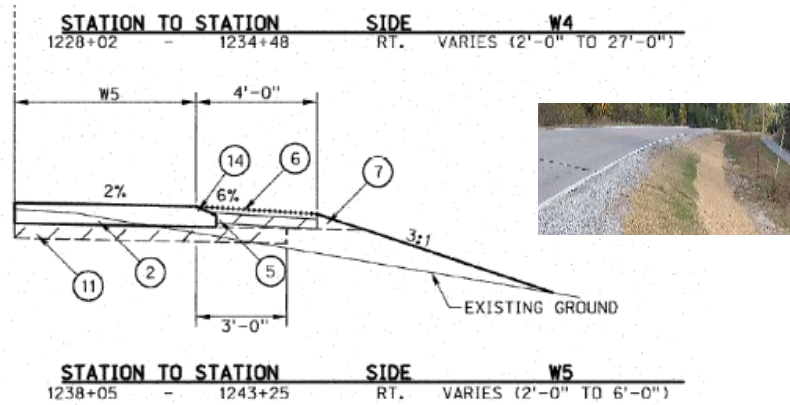


Figure 1.3 Drawing for Erosion Susceptible Target Layers 5 and 6, NDOT Plan 1-7(108)-Sheet 2-T1 (NDOT, 2017)

Several states reported the result of trial tests for shoulder stabilization techniques. However, a generally accepted solution was not yet found. Each state obtained different results with different methods as shown in Table 1.2.

Table 1.2 Results of Shoulder or Soil Treatment Methods from Different States

State	Major Finding	Reference
Maine	Lignosulfonate was effective.	Maine DOT (2007)
Ohio	Vegetation, chemical stabilization, and mechanical stabilization were effective depending on the situation.	Junliang et al. (2017)
Iowa	Soy bin-based soap-stock was effective.	Guo et al. (2013)
Maryland	Combination of Geoweb and grass was effective.	Shirmohammadi (2004)
Louisiana	POSS (Silica Polymer) (Soils in NO, LA) was effective for levee soils.	Kidd et al. (2011)
Virginia	Ammonium Lignosulfonate (known as TDS) was effective. Soiltac and Centrophas AD were not effective.	Bushman et al. (2005) Roosevelt (2005)

One key conclusion identified from a literature review is that previous research was limited to state-specific soils and state-specific environmental conditions, including weather

patterns and unique geology. Moreover, another issue is that the generalization of erosion behavior is difficult due to the complicated nature of interactions with flowing water, rock particles, and the surrounding environment (Song et al., 2012; Briaud et al., 2017).

Nebraska specific shoulder gradation and/or treatment methods need to be researched for Nebraska rocks and Nebraska weather conditions with thoughtful theoretical consideration, laboratory experiment, and validation.

1.3 Objectives of the Study

The objectives of this study are:

- 1) Obtain experimental erosion characteristics of various conditions; three different gradations and four different binding agents. The binding agents include No agent (control), Lignosulfonate, Soybean soap-stock, and DirtGlue. These will be characterized using the University of Nebraska-Lincoln Erosion Testing Bed (UNLETB). The test will be conducted at a lower density than the field crushed rock surface course (no compaction will be applied) to obtain the conservative test results.
- 2) Perform a numerical verification of the experimental results using a hydrodynamics analytical platform.
 - a. For the erosion characteristics (erosion curves) obtained in Objective 1, FLOW3D-Hydro, a computational fluid dynamics (CFD) software, will be calibrated to predict the erosion performance of the above gradations of soils with no binding agent (control).
 - b. Expected products are calibrated erosion parameters with UNLETB testing conditions.
- 3) Obtain simplified field erosion characteristics for different gradations of crushed rock

surface courses with multiple different binding agents.

- 4) Provide an optimized design chart so that NDOT may obtain a conservative gradation of crushed rock surface course (with and without binding agents) based on available choices as follows.
 - a. Combining output from objectives 1 to 3, a recommendations chart that can lead engineers to obtain proper crushed rock surface course will be provided.
 - b. An artificial intelligence-based method known as artificial neural network (ANN) will be utilized for this project that can quickly decide the suitability of a certain gradation to be used as crushed rock shoulder materials based on simple input parameters.
 - c. Calibrated hydrodynamics input parameters for numerical software such as FLOW3D-Hydro will be provided for detailed erosion analyses in the future.

1.4 Implementation

Implementation of the result of this study will be immediate. The tests are designed to be conducted for the same construction materials and lower dry densities than NDOT currently uses (no compaction applied in the test). Therefore, implementation in the field is a direct and conservative match without needing any additional calibration or adjustment. The engineers, therefore, may have flexibility of bringing in rock course materials from the most convenient location while also considering cost.

1.5 Work Procedure/Tasks

The principal investigators include Dr. Chung R. Song and Dr. Richard L. Wood in the Department of Civil and Environmental Engineering at the University of Nebraska-Lincoln (UNL). The research team consisted of the principal investigators along with one fully

committed graduate research student and one partially committed graduate research student. The proposed laboratory tests and numerical simulations were primarily conducted at UNL's Geotechnical Engineering Lab. The project team closely communicated with the TAC members during the research work and had several meetings throughout the duration of the project until completion.

Contact Name	E-mail
Bruce Barret	Bruce.Barrett@nebraska.gov
Matt Park	Matthew.Park@nebraska.gov
Nikolas Glennie	nikolas.glennie@nebraska.gov
Tom Renniger	tom.renniger@nebraska.gov
Lieska Halsey	Lieska.halsey@nebraska.gov
Mark Fischer	Mark.fischer@nebraska.gov

Chapter 2 Literature Review

In this chapter, a literature review was conducted on the erosion testing methods, and the environmentally-friendly techniques used to enhance the erosion resistance.

2.1 Erosion Mechanism

In general, soil erosion is defined as a geological process of washing out and transporting soil particles due to flowing water or wind effects (National Geographic, 2022). In many Civil Engineering applications, meaningful soil erosion occurs due to flowing water.

Classical work for soil erosion was developed by Shields (1936) known as the dimensionless erosion model. Buffington (1999) praised “Shields’ work on incipient motion and bedload transport is a benchmark study that has inspired numerous investigations and is widely applied in fields”. Technically, Shields expressed the bed shear stress at the moment of sediment transport initiation in a dimensionless form as presented in Equation 2.1.

$$\tau_c^* = \frac{\tau_c}{(\rho_s - \rho)gD} \quad (2.1)$$

where

τ_c^* is dimensionless critical shear stress / Critical Shields’ parameter,
 τ_c is critical shear stress (Dimensional),
 ρ_s is sediment density,
 ρ is fluid density, and
 D is characteristic grain size.

The idea of this model is that when the dimensionless bed shear stress exceeds the critical shield parameter, erosion will occur. This model is conceptually sound, still popularly used in soil erosion analysis software such as FLOW3D-Hydro, particularly for coarse-grained soils. This method, however, includes several input parameters that are difficult for engineers to determine.

Another common mathematical model used to describe the erosion process is known as the excess shear stress model, the dimensional model described in Equation 2.2 (Partheniades, 1965; Hanson, 1990a; Hanson, 1990b; Hanson & Cook, 1997; Hanson & Cook, 2004; Hanson & Hunt, 2007; Simon et al., 2010; Al-Madhhachi et al., 2011; Al-Madhhachi et al., 2013; Khanal et al., 2016).

$$\dot{\epsilon}_r = k_d(\tau_e - \tau_c)^a \quad (2.2)$$

where

$\dot{\epsilon}_r$ is erosion rate (m/sec),
 k_d is the erodibility coefficient (m³/ N•sec),
 τ_e is fluid induced shear stress (Pa),
 τ_c is critical shear stress (Pa), and
 a is the empirical exponent which depends on the soil type.

The physical meaning of Equation 2.2 is that erosion in the field occurs when the fluid-induced shear stress at the soil-water contact is higher than the threshold shear stress, called the critical shear stress, and the erodibility coefficient governs the erosion rate. Therefore, two behaviors should be considered when analyzing the erosion process; how deep the erosion would be and how fast the erosion would be. In other words, Equation 2.2 manifests that the critical shear stress represents the possible ultimate erosion depth, and the erodibility coefficient represents the erosion rate. In addition, the exponent (a) depends on the soil type; it is suggested to be 1 for cohesive soils and 1.5 for non-cohesive soils and has an upper limit of 2 (Stein et al., 1993). This exponent leads to dimensional trouble in the model when the exponent (a) is not equal to one. This theory, however, is much easier to use than Shields (1936) hydrodynamics-based approach.

2.2 Testing Methods

Different techniques were developed to evaluate the erosion properties of soils, starting with the traditional flume test (Hanson et al., 2002, 2005; Shaikh et al., 1988a; Shaikh et al., 1988b; Shields, 1936), followed by the Rotating Cylinder Test (RCT) (Moore and Masch, 1962), Erosion Function Apparatus (EFA) (Briaud et al., 1999), submerged jets; Jet Erosion Test, and Mini Jet Erosion Test (Hanson and Cook, 2004), (Simon et al., 2010), University of Mississippi Erosion Testing Bed (UMETB) (Song et al., 2011), Jang et al. 2011), and the University of Nebraska-Lincoln Erosion Testing Bed (UNLETB), which is described in Chapter 3. The procedures of these tests are presented in the following section.

2.2.1 Jet Erosion Test (JET)

Hanson and Cook (2004) developed the JET to estimate the soil erodibility in-situ, considering the submerged jet's hydraulic properties as well as soil erodibility properties. The main idea of submerged jets is to measure the scour depth caused by impinging water with time. Erosion begins when the shear stress induced by the fluid becomes larger than critical shear stress. As time goes on, the fluid-induced shear stress decreases as the erosion depth increases, leading to an equilibrium condition when the fluid-induced shear stress becomes less than soil resistance. Figure 2.1 shows a schematic of the apparatus. One main advantage of submerged jets is they are portable and can be easily conducted in the laboratory or field.

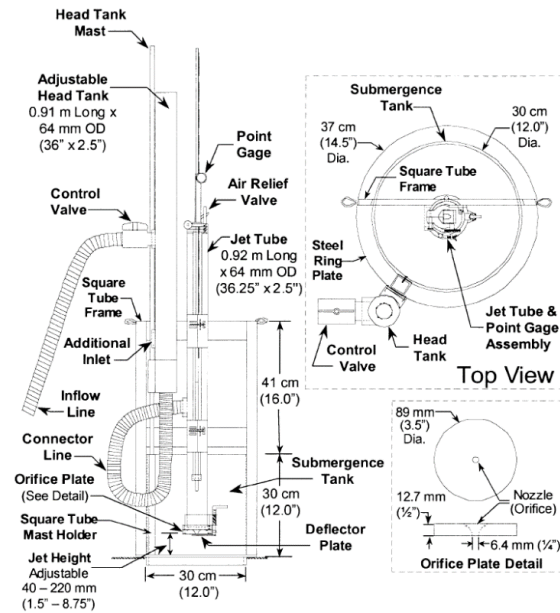


Figure 2.1 Schematic of JET by Hanson & Cook (2004)

The JET testing procedure is as follows based on Hanson & Cook (2004).

- Select the site considering the arrangement of the test apparatus, hoses, and pump.
- Drive the submergence tank into the soil surface.
- Assemble the jet tube and point gauge on the submersible's square tube frame.
- Attach the mast to the submergence tank's head tank mast holder and adjust the head tank height to the submergence tank's top.
- If a pump is utilized for water delivery, install it on the streambank or on a platform in the streambed to keep the engine dry.
- Connect hoses to the pump from the stream channel, the head tank from the pump, and the jet tube from the head tank.
- Determine the height of the jet nozzle using the point gauge.

- Set the point gauge against the deflector plate in front of the jet nozzle. This shuts the nozzle. Open the head tank and jet tube. An air release valve is located at the head of the jet tube.
- After filling the system with water, move the point gauge more than ten nozzle diameters upstream of the jet nozzle to eliminate flow disruption.
- Ahead of filling the submergence tank, measure the distance between the top of the head tank and either the submergence tank or stream channel, whichever is higher. After that, move the deflector plate to begin testing. Take the head reading every 5 to 10 min.
- At specified time intervals, take point gauge measurements on the bed.

Using the time versus depth curve considering diffusion principles, the data can be reduced, and the shear stress parameters are obtained.

2.2.2 Mini Jet Erosion Test (JET)

This device is a miniature version of JET, which can make field tests easier. The Mini-JET was used first by Simon et al. (2010). Figure 2.2 presents the Mini-JET device.

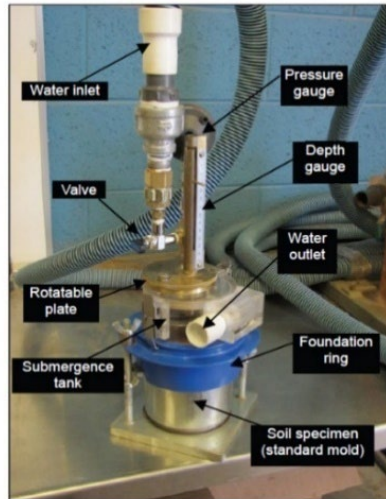


Figure 2.2 Mini JET Device by Al-Madhhachi et al. (2013)

The Mini-JET testing procedure is as follows based on Al-Madhhachi et al. (2013).

- Use the depth gauge to determine the height of the jet nozzle prior to turning on the water by taking depth gauge readings at the nozzle and the soil specimen surface at time zero.
- During the test, rotate the nozzle away from the impinging spot using the rotatable plate when the depth readings are taken.
- Close the jet valve and open the water supply to fill the head tank. Empty the adjustable head tank of all air following depth gauge readings.
- Open the jet valve to fill the submergence tank.
- Take the initial water head reading and keep it constant during the test.
- Rotate the nozzle to start the impingement of the sample and record the time.
- Take the depth readings at time intervals.

Using the time versus depth curve considering diffusion principles, the data can be reduced, and the shear stress parameters are obtained.

2.2.3 Erosion Function Apparatus (EFA)

Briaud et al. (1999) pioneered the idea of EFA to estimate the scour depth versus time beneath a cylindrical bridge pier of a specific diameter in clays. It was later used for different applications. One of the important advantages of this device is to reduce sample disturbance by taking samples using standard Shelby tubes. Figure 2.3 shows a schematic for EFA.

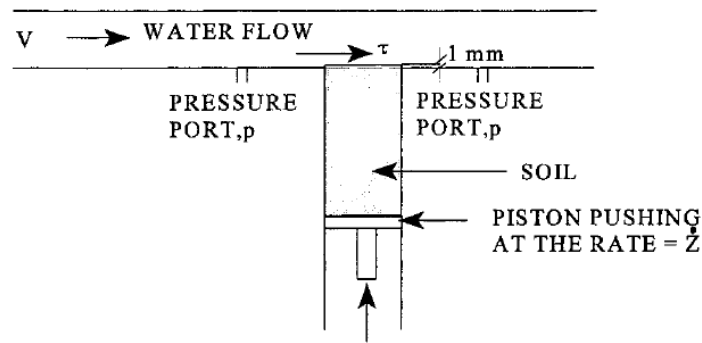


Figure 2.3 Schematic of EFA by Briaud et al. (1999)

The EFA testing procedure is as follows, excerpted from Briaud et al. (2001).

- “After inserting the sample into EFA, the pipe should be filled with water and left for an hour.
- The velocity should be set at 0.3 m/s.
- One millimeter of the soil sample should be extruded towards the flow.
- The required time to erode the one millimeter of the soil sample should be recorded.
- The velocity should be increased to 0.6 m/sec, and the sample should go back to the one-millimeter position either when the initial one millimeter of soil has been eroded or after an hour.

- Again, the required time to erode the one millimeter of the soil sample should be recorded.
- Finally, the previous two steps should be repeated for velocities 1 m/s, 1.5 m/s, 2 m/s, 3 m/s, 4.5 m/s, and 6 m/s.”

2.2.4 Rotating Cylinder Test (RCT)

The Rotating Cylinder Test was developed by Moore & Masch (1962). Then, some improvements were introduced by Chapuis & Gatien (1986). The main idea of RCT is to apply torque on an inner cylindrical soil sample through generated shear stress induced by the fluid motion. The fluid motion is caused by the rotation of an outer cylinder.

The RCT testing procedure is as follows based on Chapuis & Gatien (1986).

- The clay cylinder should be fixed on a pivoting base and contained inside a transparent concentric cylinder that can be turned at a controlled speed of up to 1750 revolutions per minute.
- Water should be supplied into the annular space to determine its erosive properties.
- The rotating outer cylinder imparts rotation to the fluid, transferring shear to the surface of the clay cylinder, which is maintained stationary by a pulley-and-variable-weight system.
- Each test contains many stages performed at a steady rotational speed, and each stage lasts between 10 and 30 minutes.
- The shear stress-induced couple should be continuously recorded.
- The cell should be cleaned with fresh fluid.
- The eroded particles should be weighed after they dry.

The critical shear stress is computed using the torque recorded at the start of the erosion procedure. Then, the erosion rate is determined by measuring the weight at regular time intervals.

2.2.5 University of Mississippi Erosion Testing Bed (UMETB)

The University of Mississippi Erosion Testing Bed was developed and used by Song et al. (2011), Jang et al. (2011) and Kidd et al. (2011) in order to mimic the erosion characteristics of levee soils under a plunging two-dimensional water jet. Figure 2.4 shows essential components of the UMETB.

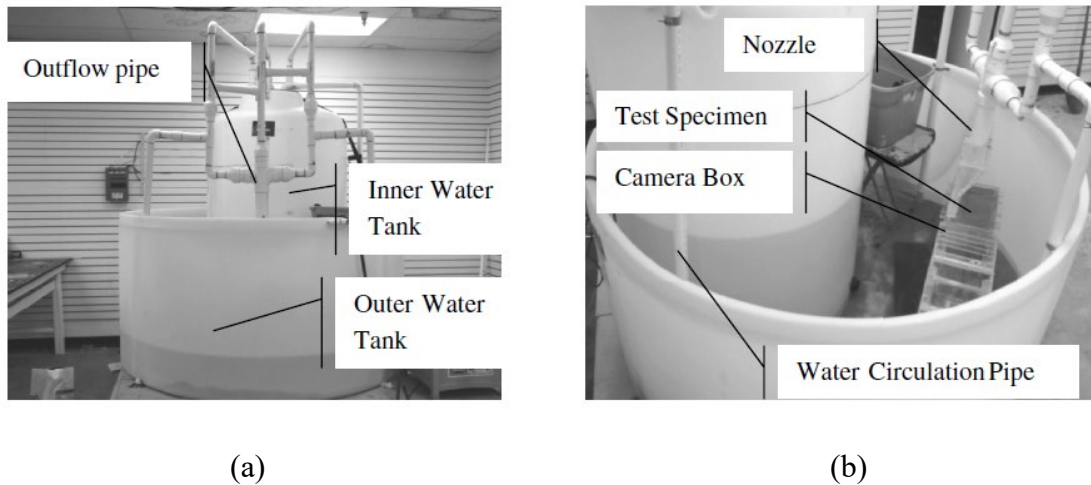


Figure 2.4 a) View of outside UMETB, b) View of inside UMETB (Song et al. 2011).

The UMETB testing procedure is as follows based on Song et al. (2011).

- The dry soil sample should be placed and spread in the specimen box using a small shovel.
- Without disturbing the soil sample, water should be added slowly to saturate it.
- The specimen box should be placed on the test bench, and the nozzle height should be adjusted until the nozzle contacts the top of the flood wall and the water flows smoothly along the wall.
- The camera should be placed and adjusted manually to capture the erosion profile.
- All pumps should be turned on at the same time to supply water to the nozzle.

- The test box should be covered with a plate in order to achieve a constant flow rate before the erosion starts.

After considering advantages and limitations for each testing technique as summarized in Table 2.1, it was decided to use the University of Nebraska-Lincoln Erosion Testing Bed (UNLETB) for this study due to its capability of testing large particles. Detailed discussion of the fabrication and testing procedure of UNLETB are found in Section 3.2.

Table 2.1: Summary of the Advantages and Limitations for Each Testing Method

Testing device	Advantages	Limitations
JET	Can be performed in the lab and in the field.	Cannot measure deep erosion.
Mini-JET	Easy to use and perform in both lab and field.	Any large particle (gravel for example) may cause a disturbance in the test.
EFA	Reduces the disturbance of the soil sample as it is taken using a standard Shelby tube.	Cannot be conducted in the field.
RCT	The shear stress can be derived directly from the torque.	The eroded particles will change the water density which leads to change in the shear stress.
UMETB	The testing procedure is easy. There is no need to stop the flow while taking the readings. Can accommodate large sample size.	It is dependent on image processing. So is not easy to use for cohesive soils because the water that causes the erosion will be mucky.

2.3 Shoulder Stabilization

Soil and rock erosion mitigation is a major challenge for engineers, particularly civil and agriculture engineers. Several states reported the result of trial tests for shoulder rock stabilization techniques. However, a generally accepted solution still needs research.

The Maine Department of Transportation (MaineDOT) utilized lignosulfonate for gravel shoulder stabilization. The results were not consistent. One location showed no erosion and very little vegetation growth, while the other location showed many erosion lines and vegetation growth (Maine DOT, 2007).

The Ohio Department of Transportation (OhioDOT) conducted a comprehensive literature review on the methods and techniques used for shoulder stabilization. The report identified the techniques as belonging to four categories: vegetation, chemical stabilization,

mechanical stabilization, and paving. The OhioDOT selected the proper technique and material based on the categories (Tao et al., 2017).

The Iowa Department of Transportation (IowaDOT) utilized soybean soap stock for shoulder stabilization. The results showed a good performance in some areas and a very good performance in other areas (Guo et al., 2013). In another report, treatment was conducted on six shoulder sections using different techniques. Four test sections were stabilized using either S.S. polymer, foamed asphalt, dust lock soybean oil, and Portland cement, while the subgrade layer was stabilized using Class C fly ash and three geogrids at the other two sections (White et al., 2007), and the result was not very decisive.

In addition, many techniques, materials, and methods were used in different places. For example, a combination of Geo-web and grass was used in Maryland for shoulder stabilization (Shirmohammadi, 2004) and ammonium lignosulfonate was used in Virginia (Bushman et al., 2005).

Motivated by the previous studies, this research selected three different additives to enhance the erosion resistance of the gravel materials: ammonium lignosulfonate, Soybean soap stock, and DirtGlue. Information and details of the three binding agents are provided in sections 3.4.1, 3.4.2, and 3.4.3.

3.1 Materials (Rock Shoulder) Properties

Nine different soil gradations were tested in this study. The soils were chosen as the materials that are already used or may be suitable to use as shoulder materials. First, a series of ASTM Standard D-422 (Sieve Analysis) were conducted on the samples. Then, soil samples were classified based on the Unified Soil Classification System (USCS). Appendix A provides gradation test results. In addition, the gradation curves and USCS symbols for each sample are presented in Figure 3.1.

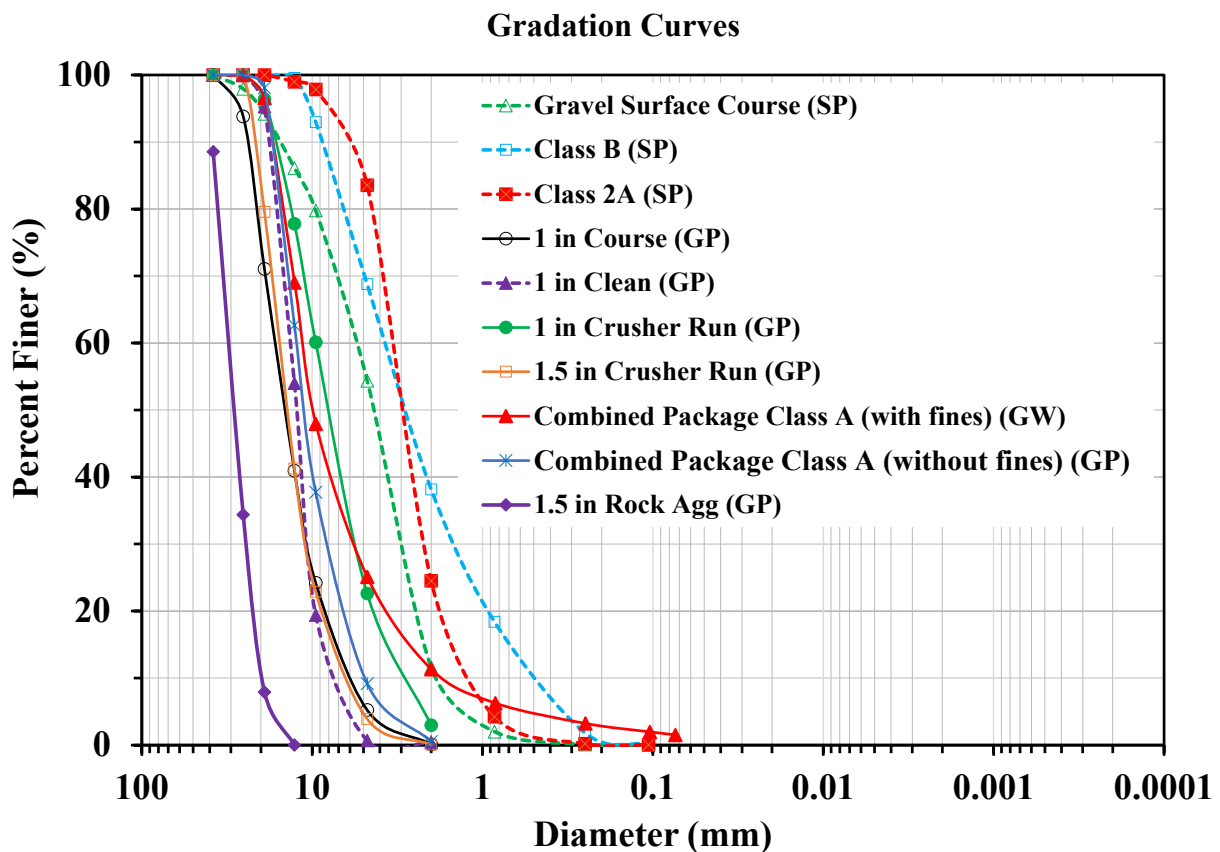


Figure 3.1 Gradation Curves for the Tested Materials

The tested materials were crushed limestones, except for “Class 2A, Class B, and Gravel Surface course samples which were river gravels. Figure 3.2 (a) and (b) present the 1.5 in. Rock Agg sample and Class B sample, respectively.

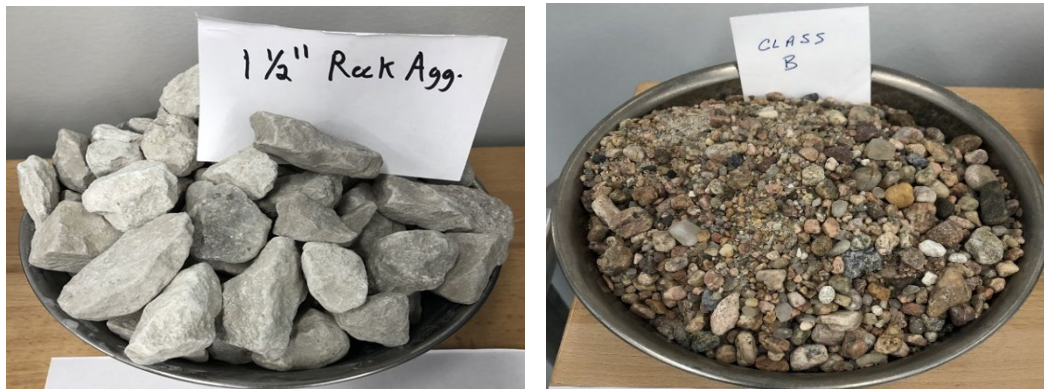


Figure 3.2 (a) 1.5 in. Rock Agg Sample, and (b) Class B Sample

The difference in particle sizes and shapes may affect the hydrodynamics conditions of the erosion process. Therefore, it is expected to see a variable erosion behavior for different samples. One of the main soil index parameters included in most of the hydrodynamics erosion analyses is the mean grain size (D_{50}). The mean grain size for each sample is presented in Table 3.1.

Table 3.1 Mean Grain Size (D_{50}) for All Samples

Sample	Mean Grain Size (in)	Mean Grain Size (mm)
1.5 in. Rock Aggregate	1.103	28
1.5 in. Crusher Run	0.512	13
1 in. Coarse	0.512	13
1 in. clean	0.434	11
Combined Package without fines	0.394	10
Combined Package with fines	0.355	9
1 in. Crusher Run	0.315	8
Gravel Surface Course	0.174	4.4
Class 2A	0.119	3
Class B	0.119	3

3.2 Testing Apparatus

3.2.1 General

The shoulder materials have relatively large diameters, leaving no choice other than constructing a large flume for the erosion test. The flume test is time-consuming, costly, and requires a large amount of material and wide space. Therefore, there is a need to fabricate an apparatus that can test the large materials more efficiently than the traditional flume. This apparatus should satisfy two essential conditions:

- 1) The flow should be sufficient to erode the particles.
- 2) The nozzle diameter should be relatively larger than the maximum particle size.

3.2.2 University of Nebraska Lincoln Erosion Testing Bed (UNLETB) Fabrication/Parts

The University of Nebraska-Lincoln Erosion Testing Bed (UNLETB) was inspired by the University of Mississippi Erosion Testing Bed (UMETB) described in Section 2.1.5 (Jang et al., 2011; Song et al., 2011). The UNLETB is also referred to as a large-scale jet. The primary function of the apparatus is to record the erosion profile in video form while it is subjected to the

impact of a circular water jet with a constant flow rate. Figures 3.3 and 3.4 present UNLETB, and Table 3.2 presents the parts of the apparatus.

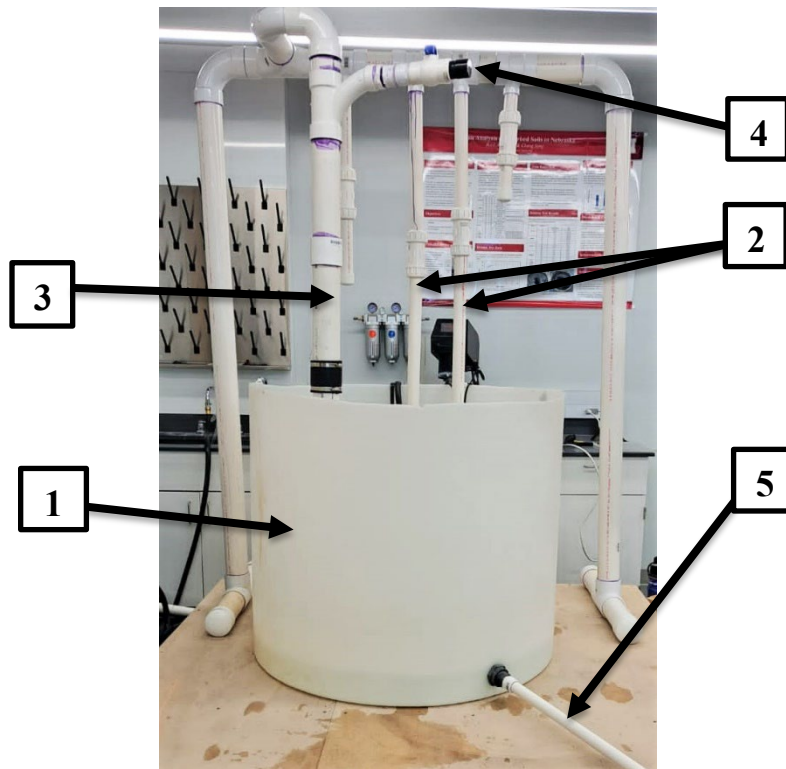


Figure 3.3 External View of UNLETB

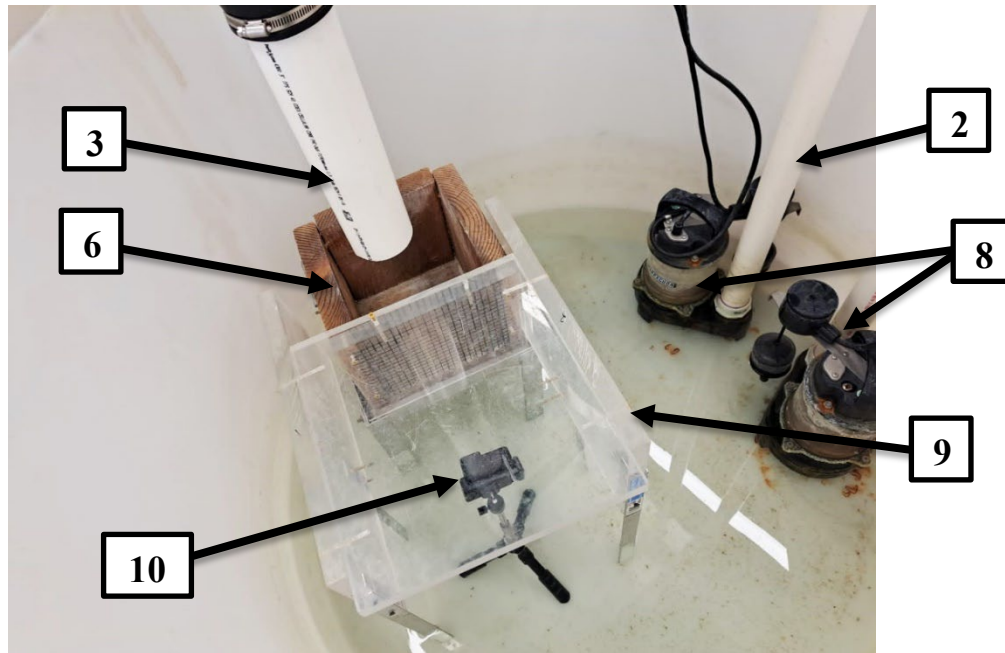


Figure 3.4 Internal View of UNLETB

Table 3.2 UNLETB Parts

Part #	Part Description	Notes
1	Outer tank	
2	PVC connection pipes	
3	PVC nozzle pipe	
4	Air relief valve	
5	Outlet pipe	
6	Sample box	
7	Sample box base	Will be shown in in the following explanation
8	Sump pumps	
9	Camera cover frame	
10	Waterproof camera	
11	Glass plate	Will be shown in in the following explanation

3.2.2.1 Outer Tank

The outer tank is a 3.3 ft diameter tank used as a container for the water during the test. It also contains sump pumps, the sample box base, the sample box, the camera cover frame, and the waterproof camera.

3.2.2.2 PVC Pipes

There are three different uses of PVC pipes in the system: to pump water from the tank (connection pipes), to act as a circular jet (nozzle pipe), and to drain the water out of the system after the end of the test (outlet pipe). The connection and outlet pipes have a diameter of 1.5 in., while the nozzle pipe has a diameter of 3 in.

3.2.2.3 Air Relief Valve

This part was not initially considered in the main design of UNLETB. However, the flow rate of the used pump was not always sufficient to get rid of air in the system, which made the flow not steady. Therefore, the system added an air relief valve to help the flow stabilize quickly. Figure 3.5 shows the air relief valve.



Figure 3.5 Air Relief Valve

3.2.2.4 Sample Box

The sample box function is to contain the soil that needs to be tested. The sample box is a 7.9 in. cubic box made with timber, with an acrylic sheet on the front side. The acrylic sheet's role is to allow the capture of the erosion profile using the camera. The acrylic sheet has a 0.4 in. square grid, helping the analysis of the erosion profile.

Two versions of the sample box were fabricated, with only one difference: the thickness of the front acrylic sheets. The initial version of the sample box contains a 1 in. thick acrylic sheet. However, the box is heavy even without the soil sample. Therefore, the 1 in. acrylic sheet was replaced with 0.5 in. sheet in the next version to be more practical and efficient. A total of five sample boxes were fabricated in this research in order to increase time efficiency. Figures 3.6, and 3.7 present the sample box while empty and with a sample, respectively.

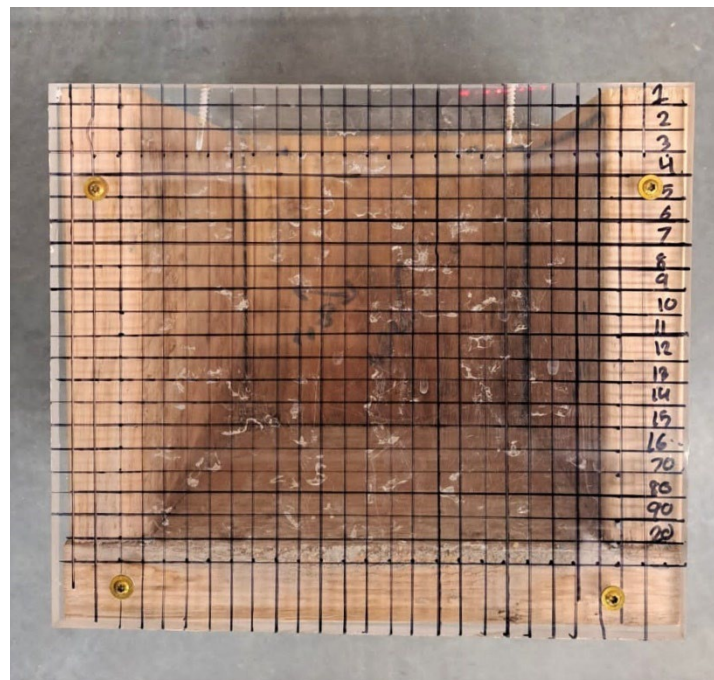


Figure 3.6 Empty Sample Box

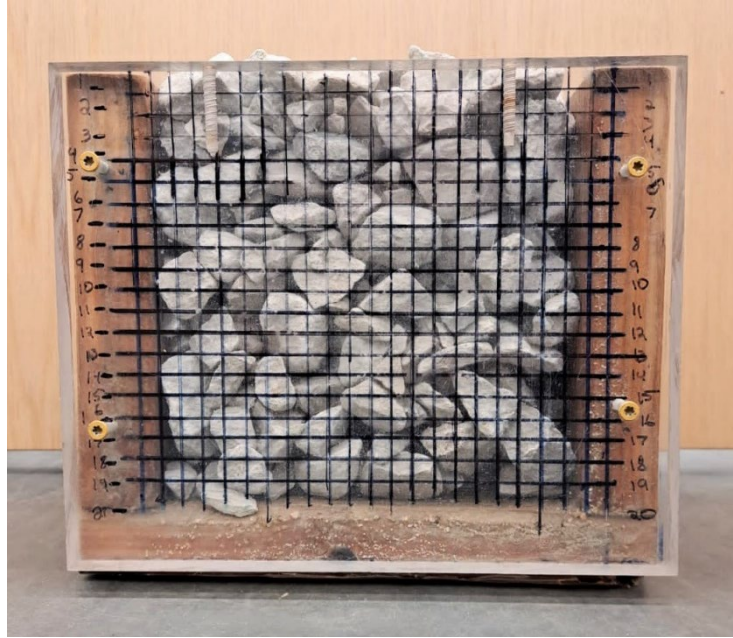


Figure 3.7 Sample Box with Soil Sample

3.2.2.5 Sample Box Base

The sample box base is a metal frame used to carry the sample box, as shown in Figure 3.8 (a) and (b). The dimensions of the frame are 1 ft in length, 1 ft in width, and 1 ft in height.



(a)



(b)

Figure 3.8 Sample Box Base (a) Top view, and (b) Side View

3.2.2.6 Sump Pumps

The sump pumps are used to circulate the water from the tank and apply a certain flow through the nozzle pipe. The initial design used four pumps; two 1 HP pumps and two $\frac{3}{4}$ HP pumps. However, one pump was enough for the test. Therefore, two connection pipes were plugged, and two remained open to make it possible to use two pumps if needed. The applied flow rate was measured to be $0.141 \text{ ft}^3/\text{sec}$ (1.1 Gallons/sec). Figure 3.9 (a) and (b) show the 1 HP and $\frac{3}{4}$ HP pumps, respectively.



(a)



(b)

Figure 3.9 a) 1 HP Sump Pump, and b) $\frac{3}{4}$ HP Sump Pump

3.2.2.7 Camera Cover Frame

The camera cover frame is designed to prevent the water splash and eroded materials from distracting the camera from taking a good quality video for analyzing. Figure 3.10 presents the camera cover frame.

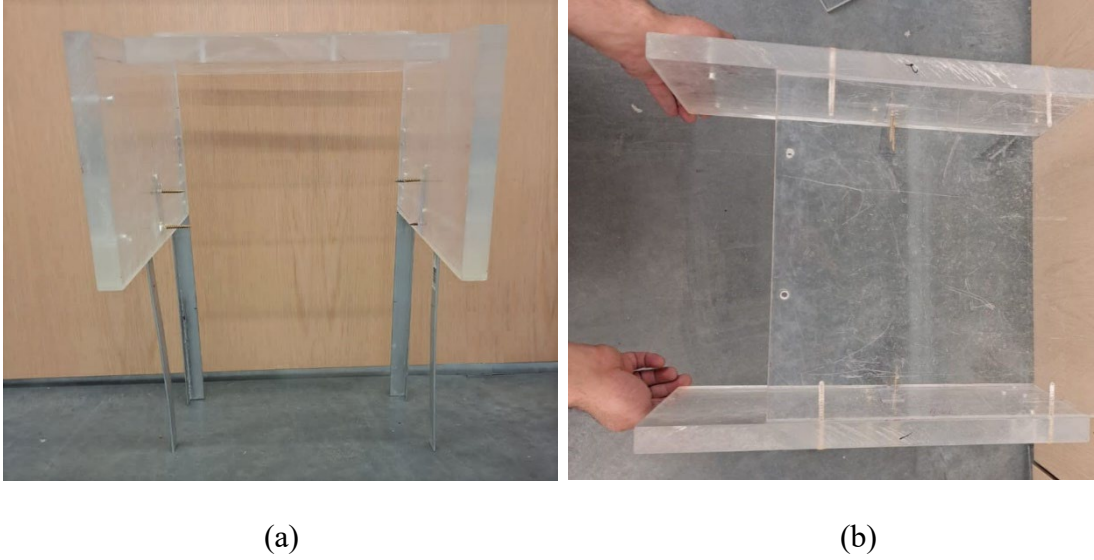


Figure 3.10 Camera Cover Frame (a) Side view, and (b) Top View

3.2.2.8 Waterproof Camera (GoPro10)

The waterproof GoPro 10 camera was used to capture the erosion profile and was set to take 30 frames/sec. The camera can be wirelessly controlled through a mobile app, which makes the process much easier. In addition, it gives good-quality videos. Figure 3.11 presents the camera used in this research.



Figure 3.11 Waterproof Camera

3.2.2.9 Glass Plate

As the sump pumps start working, the flow needs some time until it becomes steady. Therefore, a 1 ft x 1 ft glass plate will be placed at the top of the sample to prevent erosion during the unsteady flow period. Figure 3.12 shows the glass plate location in UNLETB.

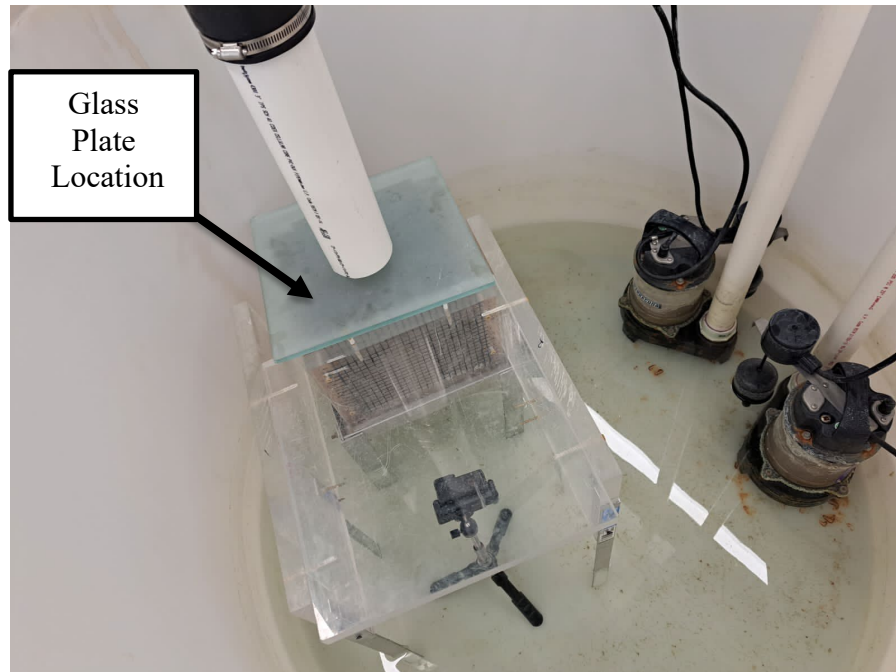


Figure 3.12 Glass Plate Location in UNLETB

3.2.3 Detailed Test Procedure

The Testing Procedure of the University of Nebraska-Lincoln Erosion Testing Bed (UNLETB) is as follows:

- 1) Fill the outer tank with water.
- 2) Place the sample box base in the outer tank.
- 3) Fill the sample box with soil.
- 4) Place the sample box at the top of the sample box base (note: The distance between the nozzle and the sample box is set to be 2.4 in.).
- 5) Connect the camera cover frame to the sample box.
- 6) Slide the glass plate on top of the soil sample.
- 7) Place the camera and adjust the zoom settings to a suitable sample view.
- 8) Turn the pump on by plugging in power.

- 9) Wait until the flow stabilizes (use the air relief valve to make the process faster).
- 10) Start the video recording.
- 11) Remove the glass plate to start the erosion process.
- 12) Wait until the erosion process stops (visual judgment).
- 13) Stop the recording.
- 14) Break the video into individual picture frames.
- 15) Now, use the picture frames with the grid (on the acrylic sheet) to estimate the erosion depth at different times.
- 16) Plot the erosion depth vs. time (erosion profile).

3.3 Erosion Test Results for Untreated Materials

Erosion profiles were plotted for all samples as described in the testing procedure section and presented in Figure 3.13. The erosion curves for individual samples are shown in Appendix B.

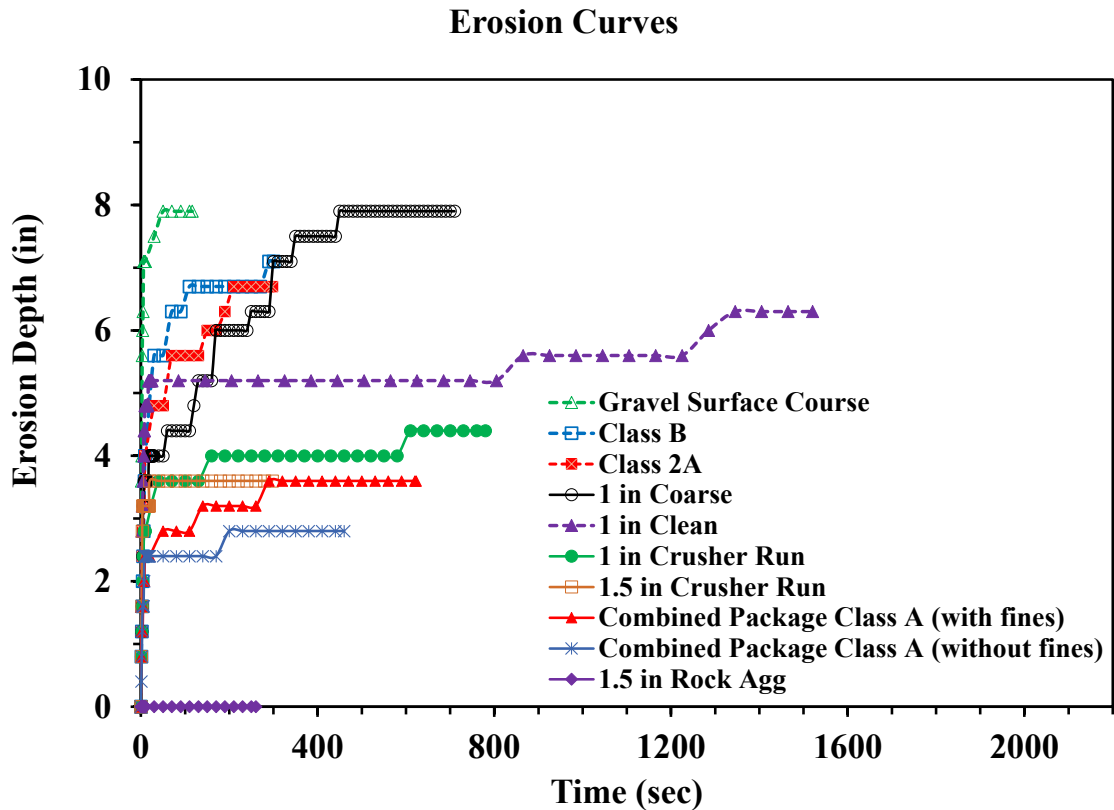


Figure 3.13 Erosion Curves for All Samples

The maximum erosion depth that can be obtained in the erosion curves is 7.9 in. because the sample box height is 7.9 in.

From the obtained erosion curves, it is obvious that obvious the tested materials have variable behavior. The 1.5 in. Rock Agg sample showed the best performance (no erosion); this sample has a poorly graded (uniform) gradation curve with large particles, which makes this behavior expected because the main erosion resistance of the gravels and sands (cohesionless soils) comes from the particles' weights, shapes, and angularity. The Combined Package Class 2A samples (with and without fines) showed a high erosion resistance; they are classified as well, and poorly graded gravels, respectively. The 1.5 and 1 in. crusher run samples showed an

acceptable erosion resistance. On the other hand, the 1 in. Coarse, 1 in. Clean, Class 2A, Class B, and Gravel Surface Course samples showed weak erosion resistance.

Compared with the current NDOT specifications, only the 1.5 in. Rock Agg sample satisfies the required gradation. However, the test results showed there are some materials out of the criteria that provide good erosion resistance.

It was expected that samples with close gradation should show similar erosion behavior. This is because crushed rock samples (all samples except Gravel Surface Course, Class 2A and Class B) have similar shape and angularity. Therefore, the only expected reason that causes a difference in the erosion behavior of those samples is the difference in gradation. However, 1 in. Clean, and 1 in. Coarse samples showed different behavior.

Therefore, it was decided to perform three additional gradation tests and three additional erosion tests on 1 in. Clean, and 1 in. Coarse samples to confirm the initial test results. The gradation tests showed similar to the old tests, but the erosion results were different. Figure 3.14 presents the updated erosion test results.

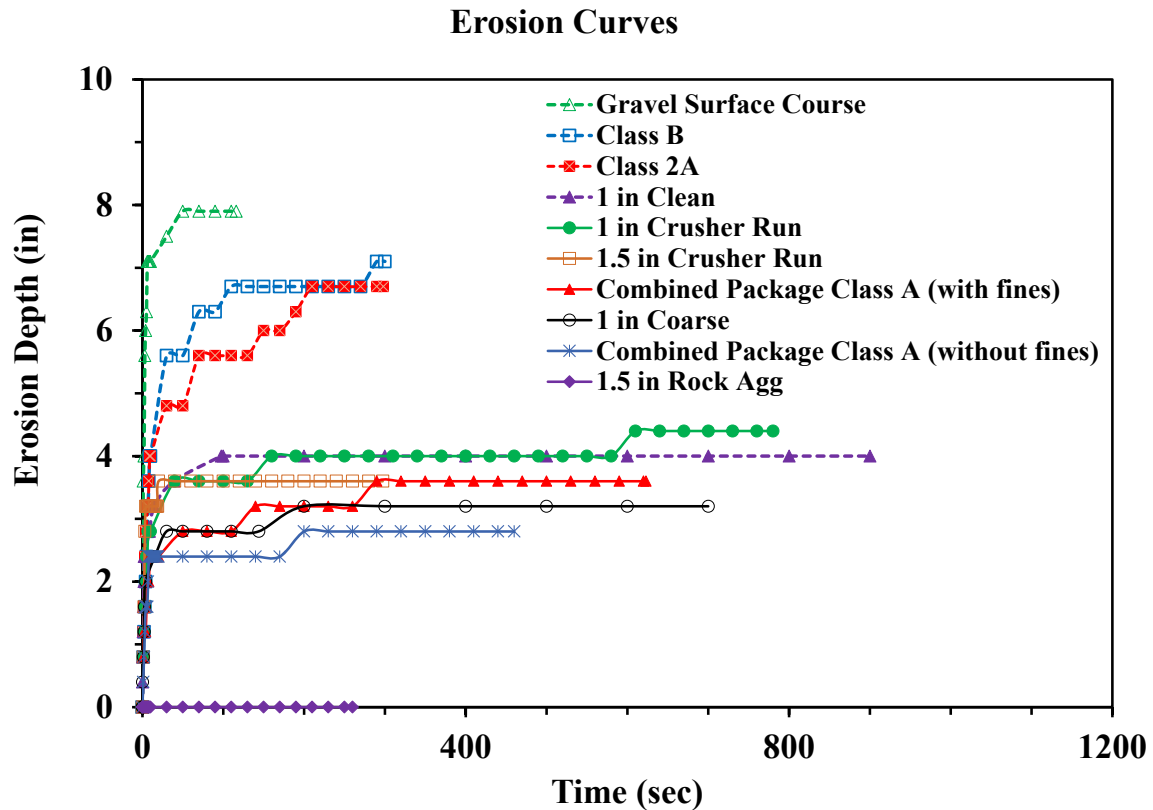


Figure 3.14 Updated Erosion Curves for All Samples

All three new tests showed similar results, different from the old one. Samples 1 in. Clean and 1 in. Coarse showed acceptable results. It is believed that the initial error was due to a problem in the applied flow rate (pumps).

As a summary of the updated results, 1.5 in. Rock Agg showed the best performance with no erosion. Combined package Class A (with and without fines), 1.5 in. Crusher Run, 1 in. Crusher Run, 1 in. Clean and 1 in. Coarse showed an acceptable result. The river gravels (Class 2A, Class B, and Gravel Surface Course) showed a weak erosion resistance (not an acceptable behavior).

3.3.1 Boundary Effect

The box size was chosen to be 7.9 in. x 7.9 in. x 7.9 in. However, this relatively small-sized box may cause a boundary effect, especially on the large particles, such as the 1.5 in. Rock Agg sample. Therefore, a test with a wider box (15.8 in.) was conducted on the 1.5 in. Rock Agg sample, which showed no erosion. The results were similar to the those using the designed box, meaning the box dimensions have no boundary effect on the testing result.

3.3.2 Effect of Fines

The tested samples were brought to the laboratory in large bags or buckets. For some samples there was a substantial percentage of fines in the bottom of the bag. Therefore, a test was conducted to understand the effect of the fines on erosion behavior. The Combined Package sample was chosen to be tested because it contained the highest percentage of fines. The test results are shown in Figure 3.15.

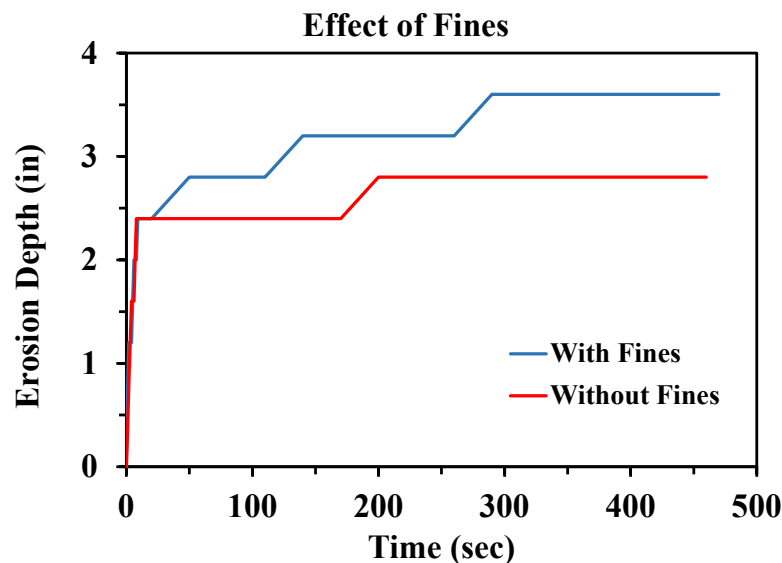


Figure 3.15 Effect of Fines on the Erosion Behavior of the Combined Package Sample

Figure 3.15 shows the sample with fines may erode more than the sample without fines. However, this difference is not large enough to be considered unless the percentage of fines is substantial.

3.3.3 Compaction Effect

It was believed that the density of the small-size particle samples, such as Class 2A, Class B, and Gravel Surface Course, may affect the erosion behavior. Therefore, the erosion test was conducted on Class B six times; three trials were uncompacted samples and three compacted samples. The test results are presented in Figure 3.16, showing that the effect of compaction was not substantial.

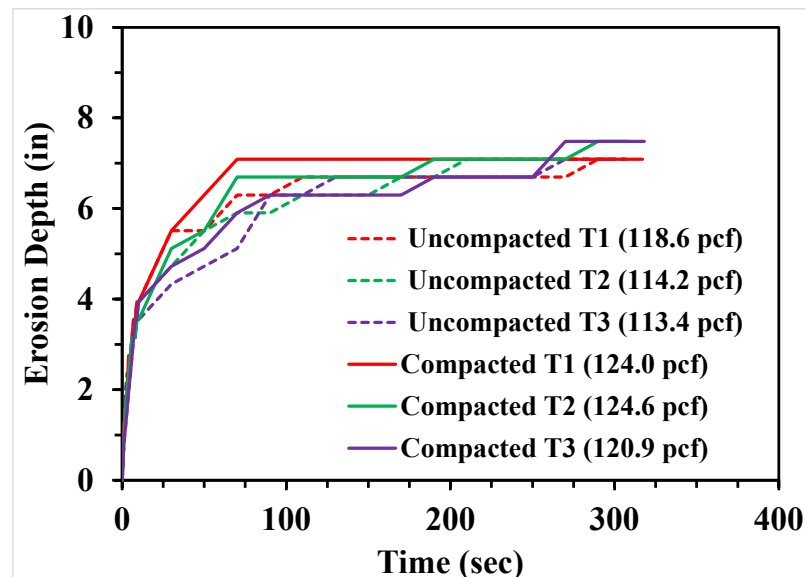


Figure 3.16 Effect of Compaction on the Erosion Behavior of the Class B Sample

3.4 Erosion Test Results for Treated Materials

Three polymers were used to enhance the performance of the samples that showed a weak erosion resistance (Class 2A, Class B, Gravel Surface Course) in addition to the samples

that initially showed weak resistance (1 in. Clean and 1 in. Coarse) even though they showed acceptable results when they were tested again. Those polymers are lignosulfonate, soybean soap stock, and DirtGlue. The used polymers are considered eco-friendly additives that may give a cohesive property to cohesionless soils, leading to higher erosion resistance.

3.4.1 Ammonium Lignosulfonate (LIGNO10)

“Lignosulfonates (Sulfonated Lignin) are environment-friendly, co-products from the production of dissolving pulp. The sulfite pulping process creates Red and Black Liquors which are water-soluble anionic polyelectrolyte polymers with high molecular weight” (The Plaza Group).

Ammonium Lignosulfonate (LIGNO10) provided by The Plaza Group was used in this research. The physical and chemical properties of LIGNO10 are provided in Tables 3.3 and 3.4, respectively.

Table 3.3 Physical Properties of LIGNO10

Physical Properties	Liquid
Solids Concentration	50-51%
pH	5.96%
Specific Gravity (@150C/150C)	1.22
Boiling Point F	213

Table 3.4 Chemical Properties of LIGNO10

Chemical Properties	Liquid Basis
Sodium, ppm	51
Sulfur, as SO ₄ , ppm	11.335
Calcium, ppm	812
Ammonium, ppm	12.5
Total Sugars	8-12%

The 1 in. Coarse, 1 in. Clean, Class 2A, Class B, and Gravel Surface Course samples were treated with LIGNO10. The treatment method is described as follows, and test results are presented in Figures 3.17 to 3.21.

- The LIGNO10 was diluted with water (80% LIGNO10: 20% water) in order to make the solution sprayable.
- The sample box was filled with gravel, but the top two inches were left empty.
- The required amount of the LIGNO10-water solution was chosen to be 2% of the dry weight from the top two inches of the sample.
- One inch of the sample was filled in the sample box.
- A spray bottle sprayed half the required solution evenly on the sample.
- The other inch of the sample was filled and then sprayed with the other half of the solution.
- The sample was left to cure for one week before conducting the erosion test.

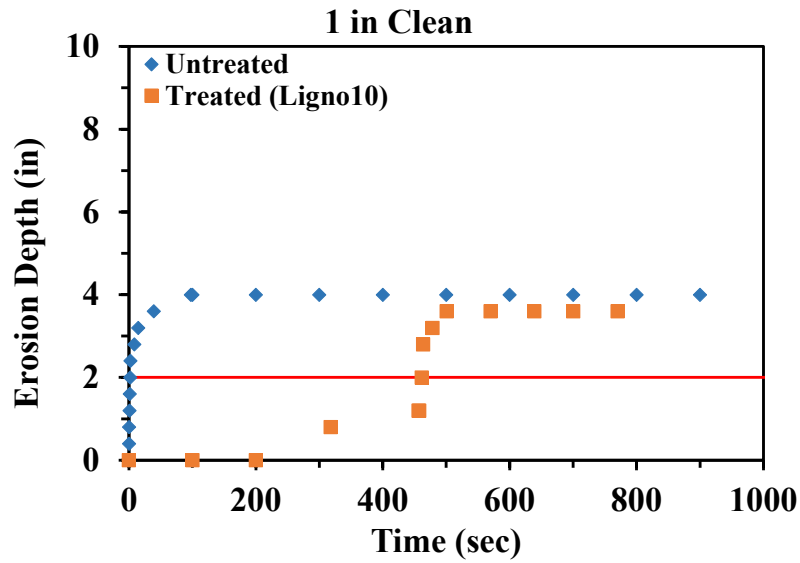


Figure 3.17 Erosion Test Results for 1 in. Clean Sample Treated with LIGNO10 (Note: The red line refers to the treatment depth)

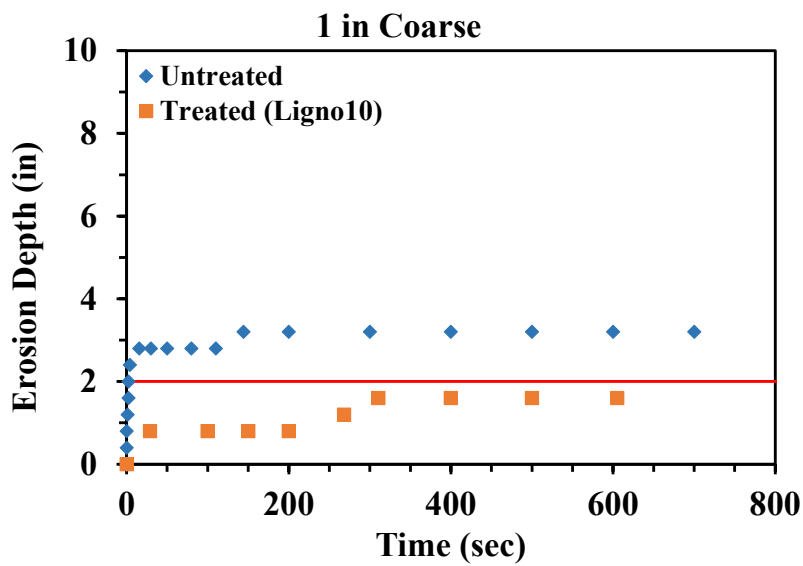


Figure 3.18 Erosion Test Results for 1 in. Coarse Sample Treated with LIGNO10 (Note: The red line refers to the treatment depth)

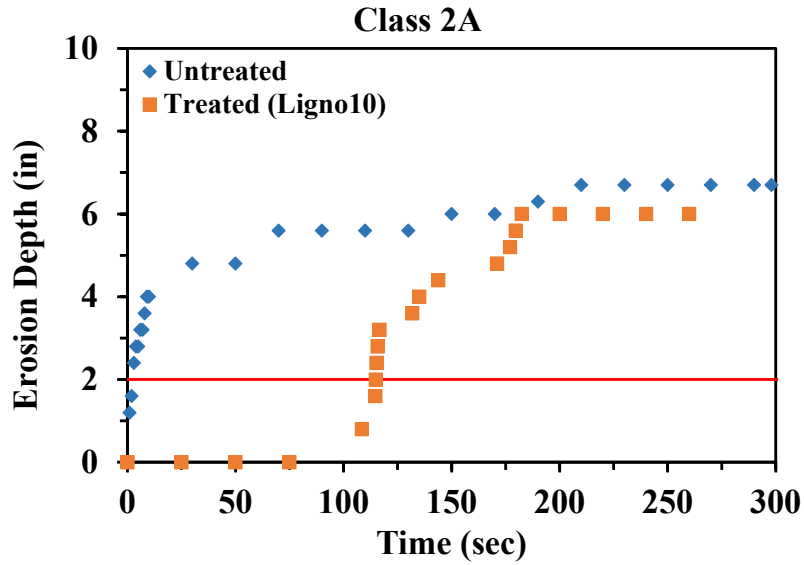


Figure 3.19 Erosion Test Results for Class 2A Sample Treated with LIGNO10 (Note: The red line refers to the treatment depth)

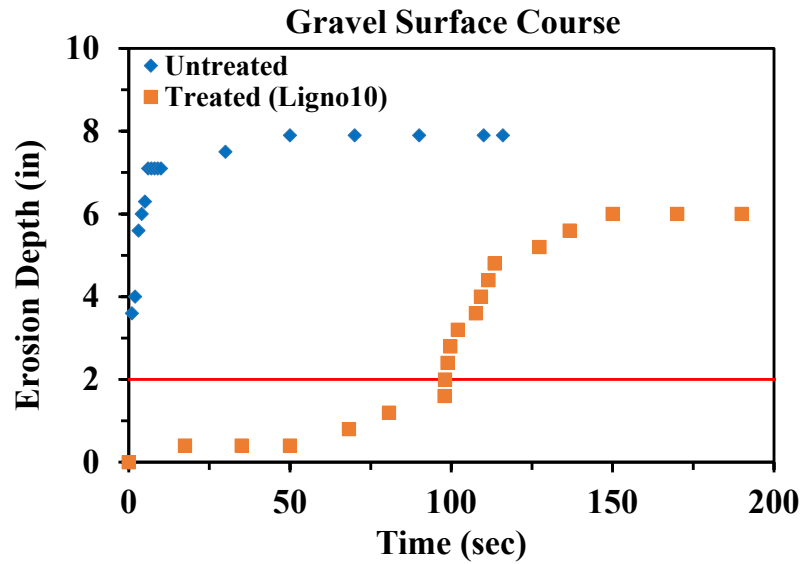


Figure 3.20 Erosion Test Results for Gravel Surface Course Sample Treated with LIGNO10 (Note: The red line refers to the treatment depth)

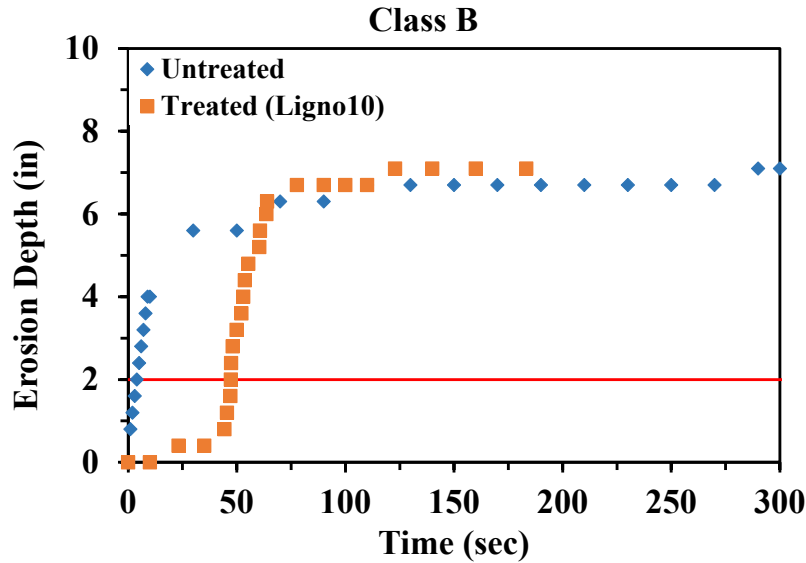


Figure 3.21 Erosion Test Results for Class B Sample Treated with LIGNO10 (Note: The red line refers to the treatment depth)

The test results for the treatment sample showed a substantial enhancement in erosion resistance in all samples for the treated zone. The observed improvement in the erosion resistance may be due to the cohesive property added by the biopolymer to the sample, which changed the erosion mechanism; the erosion occurred chunk by chunk instead of particle-by-particle. Another possible treatment mechanism is the formation of a watertight layer at the surface. Even though LIGNO10 is water-soluble, the applied flow took some time before LIGNO10 dissolved, and the erosion started causing a time lag. This time lag was different depending on the sample. For example, the erosion of the 1 in. Clean sample started after about 5 min, but it started after 0.3 min in the Gravel Surface Course Sample.

Overall, the Lignosulfonate showed a better enhancement in the erosion resistance of the 1 in. Clean, and 1 in. Coarse samples, than the Class 2A, Class B, and Gravel Surface Course

samples. This may be attributed to the particle size, shape, and angularity, which may govern the biopolymer-particle bond strength.

3.4.2 Soybean Soap Stock

Soybean soap stock is one of the soybean oil products. “This soap stock is produced from the degumming process of crude soybean oil. The crude soybean oil is mixed with water and then separated by using a centrifugal method. By performing this separation, the proportion of oil contents, free fatty acids, lecithin, and fatty acids, and could be recognized” (South Dakota Soybean Processors).

South Dakota Soybean Processors provided the product used in this research. The physical and chemical properties of the soybean soap stock are presented in Table 3.5.

Table 3.5 Physical and Chemical Properties of Soybean Soap Stock

Physical state	Solid/Liquid Slurry
Odor and appearance	Red-brown slurry with an earthy, plant-like odor
Specific gravity (g/mL)	1.035
Vapor density	Would be like water
Evaporation rate	Would be like water
Freezing point	Would be like water
Boiling point (°C)	100
pH	7.19 S.U.
Solubility in water	Liquid portion is miscible

The 1 in. Coarse, 1 in. Clean, Class 2A, Class B, and Gravel Surface Course samples were treated with the soybean soap stock. The treatment method is described as follows, and test results are presented in Figures 3.22 to 3.26.

- The sample box was filled with gravel, but the top two inches were left empty.

- The required amount of the soybean soap stock was chosen to be 2% of the dry weight from the top two inches of the sample.
- One inch of the sample was filled in the sample box.
- A spray bottle sprayed half the required solution evenly on the sample.
- The other inch of the sample was filled and then sprayed with the other half of the solution.
- The sample was left to cure for one week before conducting the erosion test.

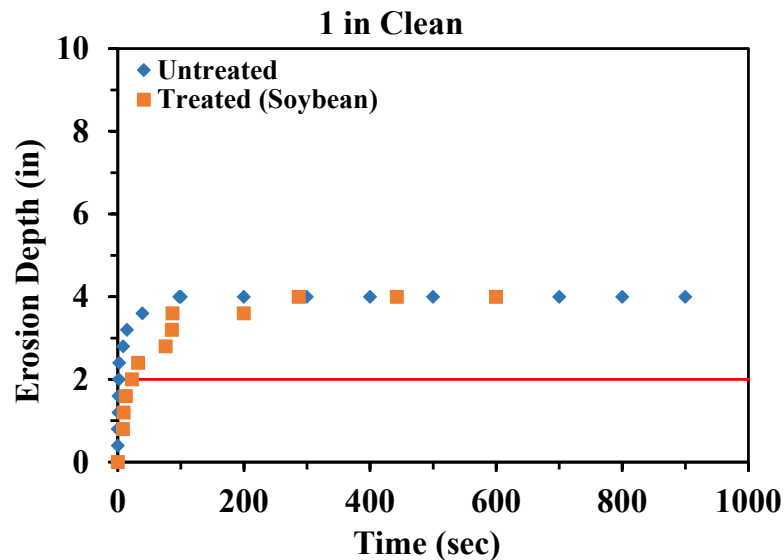


Figure 3.22 Erosion Test Results for 1 in. Clean Sample Treated with Soybean Soap Stock
(Note: The red line refers to the treatment depth)

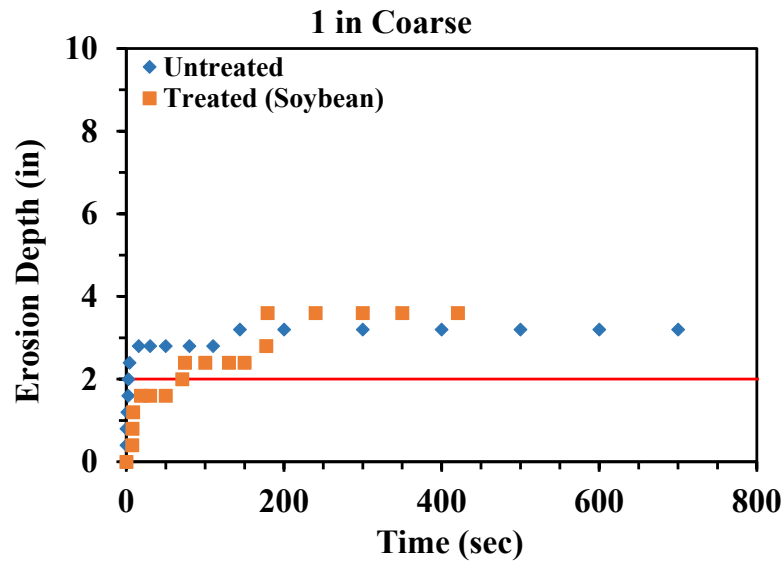


Figure 3.23 Erosion Test Results for 1 in. Coarse Sample Treated with Soybean Soap Stock (Note: The red line refers to the treatment depth)

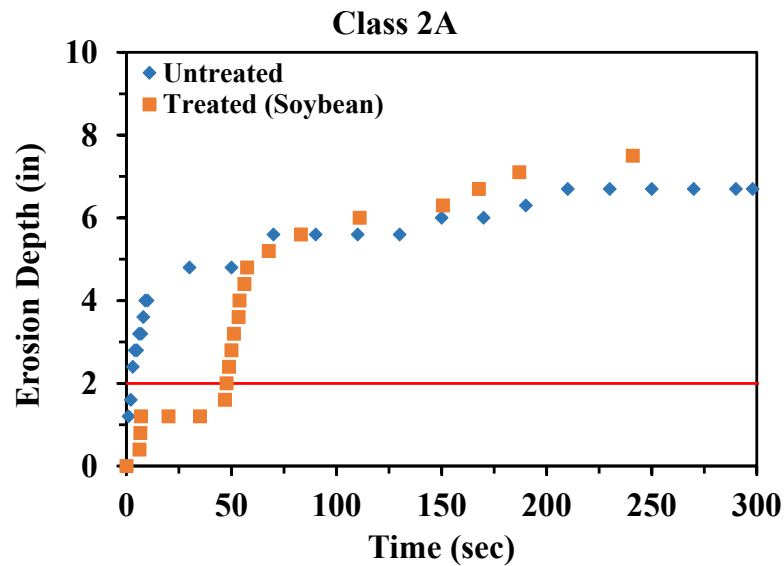


Figure 3.24 Erosion Test Results for Class 2A Sample Treated with Soybean Soap Stock (Note: The red line refers to the treatment depth)

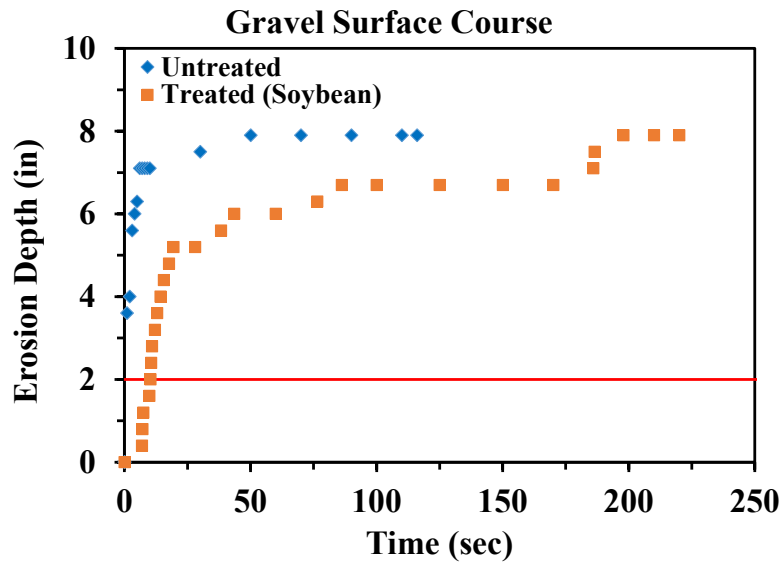


Figure 3.25 Erosion Test Results for Gravel Surface Course Sample Treated with Soybean Soap Stock (Note: The red line refers to the treatment depth)

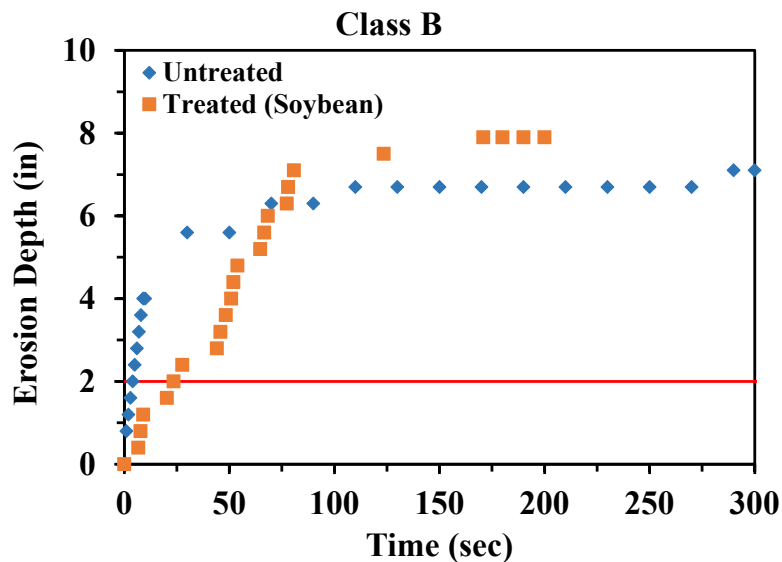


Figure 3.26 Erosion Test Results for Class B Sample Treated with Soybean Soap Stock (Note: The red line refers to the treatment depth)

The test results for the treated sample showed a slight enhancement in erosion resistance in all samples except for 1 in. Clean which showed about no enhancement. However, the

enhancement mechanism seemed to be different from the one obtained by LIGNO10. The enhancement mechanism can be described based on visual observation, as the soybean soap stock coated the soil grains, and made a smooth surface. The smooth surface reduced the roughness of the particles, leading to a reduction in the shear stress induced by the water jet. The variety of the enhancement amount may be attributed to the particle size, shape, and angularity, which may govern the biopolymer-particle bond strength.

3.4.3 DirtGlue

The product used in this research is DirtGlue, provided by Global Environmental Solutions. “DirtGlue is an environmentally safe, powerful styrene/butadiene copolymer that produces highly effective control of dust and erosion thereby stabilizing the soil. DirtGlue polymer emulsions are designed to coat and bond soil particles together. They are formulated to fill the microscopic spaces between soil particles that are essentially in direct contact with each other and will achieve their highest level of performance under those conditions.”

DirtGlue has a wide range of engineering applications, and the mixing ratio with water is decided based on the application. For this research, it was suggested to use a 1:5 ratio for DirtGlue and water, respectively. The application instructions provided by Global Environmental Solutions do not recommend spraying it in a mist form. Therefore, the treatment method was slightly different from the one used for the other polymers; it was poured at the top of the sample. Initially, it was planned to use the same ratio used in the other biopolymers (2% of the dry weight from the top two inches of the sample). However, when that amount was poured on the top of the samples, the solution went through the sample and leaked from the bottom of the sample box, indicating the treatment was applied to the whole sample, not just the top two inches. The samples were tested after one week of the treatment process.

The 1 in. Coarse, 1 in. Clean, Class 2A, Class B, and Gravel Surface Course samples were treated with DirtGlue and test results are presented in Figures 3.27 to 3.31. The treated samples showed no erosion, indicating the treatment was almost perfect.

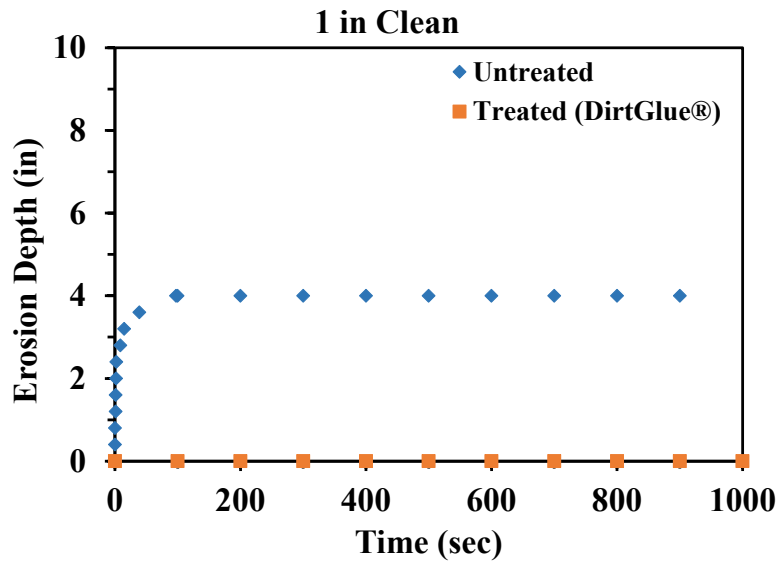


Figure 3.27 Erosion Test Results for 1 in. Clean Sample Treated with DirtGlue

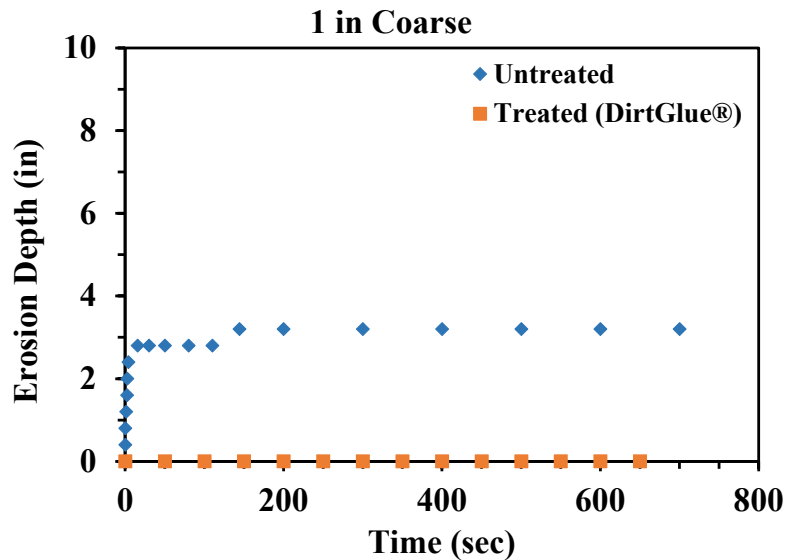


Figure 3.28 Erosion Test Results for 1 in. Coarse Sample Treated with DirtGlue

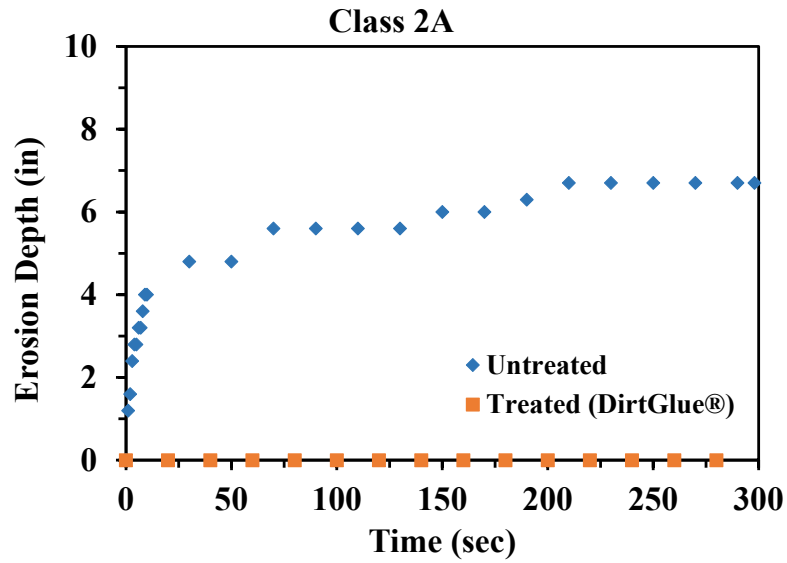


Figure 3.29 Erosion Test Results for Class 2A Sample Treated DirtGlue

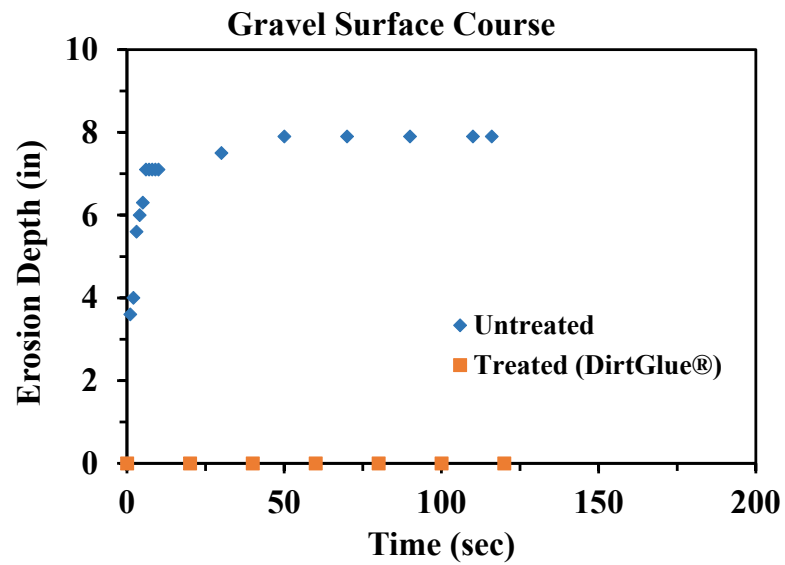


Figure 3.30 Erosion Test Results for Gravel Surface Course Sample Treated with DirtGlue

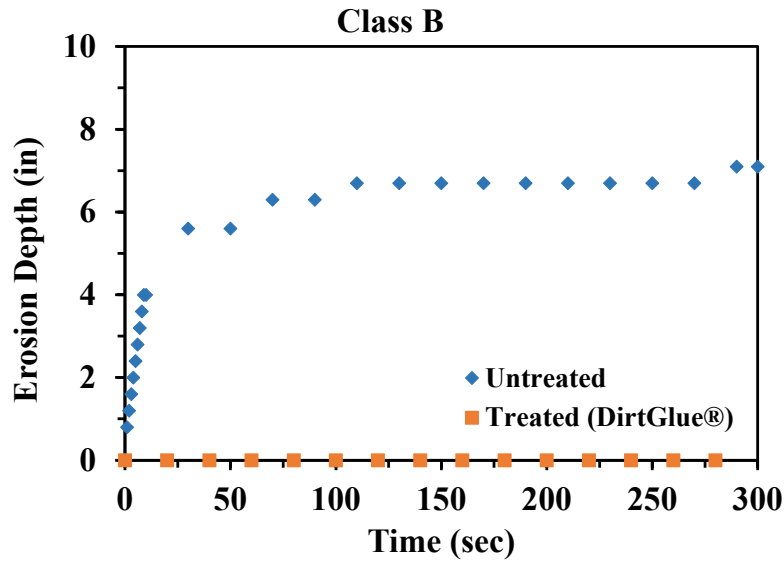


Figure 3.31 Erosion Test Results for Class B Sample Treated with DirtGlue

3.4.4 Treatment Methods Comparison

Different aspects may be taken into consideration to compare the behavior of treated samples with different polymers, such as the observed treatment mechanism, the treatment depth, and the erosion curves.

3.4.4.1 Treatment Mechanism

As discussed before, visually observed treatment mechanisms differed based on the biopolymers used. For example, the observed visual mechanism for the Soybean Soap Stock treated samples reduced the jet-induced shear stress due to the soft oily coat around the soil particles. However, the observed visual mechanism for the LIGNO10 and DirtGlue treated samples was the same, adding a cohesive property to the cohesionless soils. The difference between LIGNO10 and DirtGlue was that LIGNO10 samples were stiff before the test, and they started to become softer with time (the LIGNO10 was dissolved, and the water in the outer tank

became red). On the other hand, the DirtGlue treated samples were stiff and stayed stiff during the test.

3.4.4.2 Treatment Depth

It is important to understand how deep the treatment effect will be if the biopolymer is to be applied in the field. The visual observation showed LIGNO10 and Soybean Soap Stock are viscous solutions, which makes the treatment depth shallow (surface treatment). However, the final erosion depth was reduced for 1 in. Coarse, 1 in. Clean, and Gravel Surface Course samples, indicating a good portion of these samples were treated. On the other hand, DirtGlue has a lower viscosity and easily seeps through the gravel, giving an advantage of sublayer treatment if it is a concern.

3.4.4.3 Erosion Curves

To compare the erosion curves for all used treatment products, the test results were combined and presented in Figures 3.32 to 3.36.

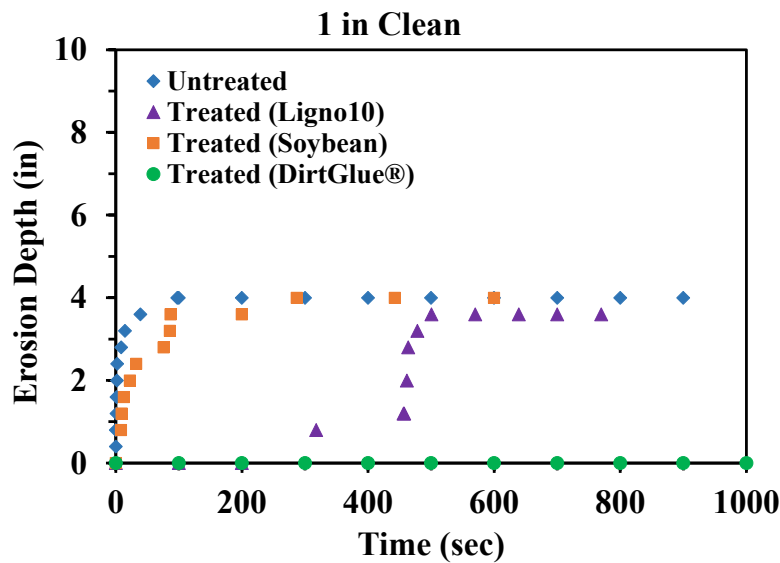


Figure 3.32 Erosion Test Results for 1 in. Clean Treated Samples (All Biopolymers)

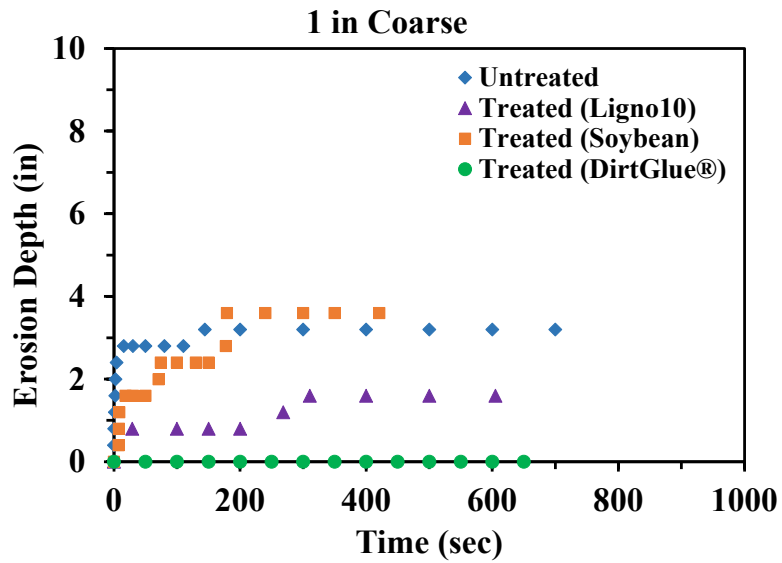


Figure 3.33 Erosion Test Results for 1 in. Coarse Treated Samples (All Biopolymers)

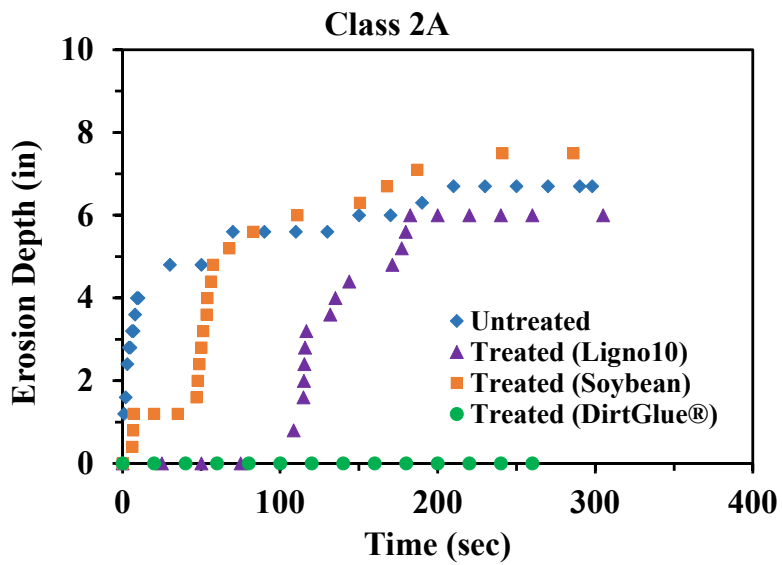


Figure 3.34 Erosion Test Results for Class 2A Treated Samples (All Biopolymers)

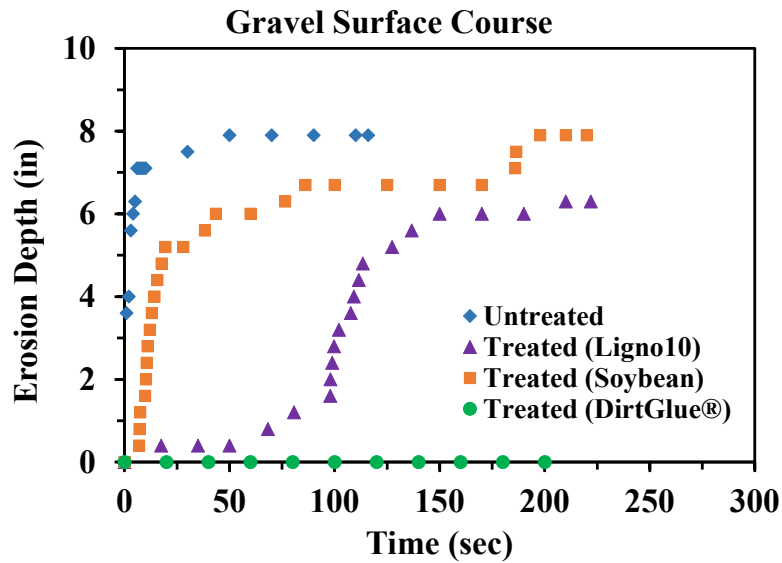


Figure 3.35 Erosion Test Results for Gravel Surface Course Treated Samples (All Biopolymers)

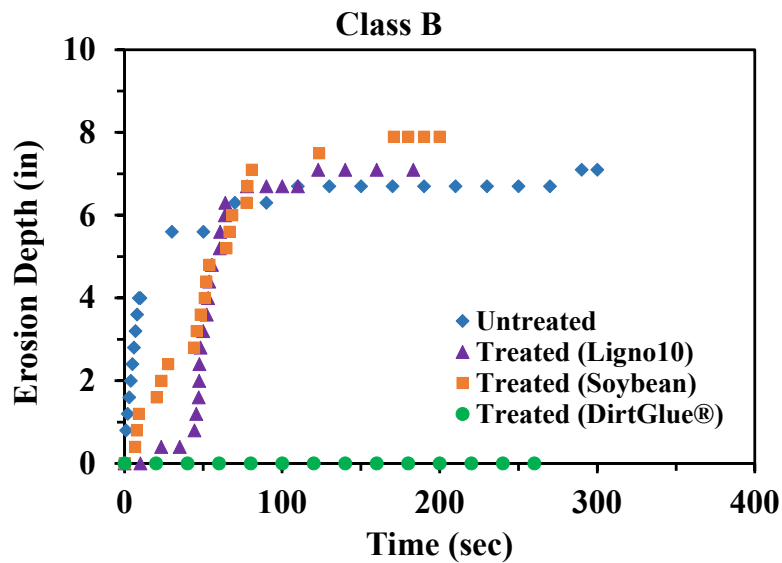


Figure 3.36 Erosion Test Results for Class B Treated Samples (All Biopolymers)

The test results showed variable behaviors depending on the soil sample; LIGNO10 worked better for 1 in. Clean, and 1 in. Coarse samples than the Class 2A, Class B, and Gravel Surface Course samples. However, the comparison could not be conducted on Soybean soap

stock treated sample because the enhancement was minimal. Similar for DirtGlue treated samples, the comparison is hard because there was no erosion.

Comparing the three different products, DirtGlue showed the best performance, as there was no erosion at all. Then, LIGNO10 caused a sufficient improvement by delaying the erosion process and reducing the final depth for some samples. Finally, the Soybean Soap Stock showed a slight improvement in the erosion behavior of the treated zone for most samples except for 1 in. Clean, which showed about no enhancement. Table 3.6 summarizes the effects of the three biopolymers on the treated samples.

Table 3.6 Effect of Biopolymer Treatment on All Treated Sample

Sample/Biopolymer	LIGNO10	Soybean Soap Stock	DirtGlue
1 in. Clean	<p>-Erosion started after around 315 sec.</p> <p>-Took around 461 sec to reach 2 in., while untreated samples took 2 sec to reach that depth.</p> <p>-Overall final depth reduced from 4 in. to 3.6 in.</p>	<p>- Erosion started after 8 sec.</p> <p>-Took around 22 sec to reach 2 in., while untreated samples took 2.5 sec to reach that depth.</p> <p>-Overall final depth was not affected.</p>	No erosion occurred.
1 in. Coarse	<p>-Erosion started after around 28 sec.</p> <p>-Erosion depth did not reach 2 in., while untreated samples took 2 sec to reach that depth.</p> <p>-Overall final depth reduced from 3.2 in. to 1.6 in.</p>	<p>- Erosion started after 7 sec.</p> <p>-Took around 70 sec to reach 2 in., while untreated samples took 2.5 sec to reach that depth.</p> <p>-Overall final depth was not affected.</p>	No erosion occurred.
Class 2A	<p>-Erosion started after around 105 sec.</p> <p>- Took around 115 sec to reach 2 in., while untreated samples took around 3 sec to reach that depth.</p> <p>-Overall final depth reduced from 6.7 in. to 6 in.</p>	<p>-Erosion started after around 6 sec.</p> <p>- Took around 47 sec to reach 2 in, while untreated samples took around 3 sec to reach that depth.</p> <p>-Overall final depth increased from 6.7 in. to 7.5 in.</p>	No erosion occurred.

Gravel Surface Course	<p>-Erosion started after around 17 sec.</p> <p>- Took around 97 sec to reach 2 in., while untreated samples took less than 1 sec to reach that depth.</p> <p>-Overall final depth reduced from 7.9 in. to 6 in.</p>	<p>-Erosion started after around 6 sec.</p> <p>- Took around 10 sec to reach 2 in., while untreated samples took less than 1 sec to reach that depth.</p> <p>-Overall final depth did not change.</p>	No erosion occurred.
Class B	<p>-Erosion started after around 20 sec.</p> <p>- Took around 47 sec to reach 2 in., while untreated samples took 4 sec to reach that depth.</p> <p>- Overall final depth did not change.</p>	<p>-Erosion started after around 6 sec.</p> <p>- Took around 23 sec to reach 2 in., while untreated samples took 4 sec to reach that depth.</p> <p>-Overall final depth increased from 7.1 in. to 7.9 in.</p>	No erosion occurred.

Chapter 4 : FLOW3D-Hydro Simulation

4.1 General

FLOW3D-Hydro is one of the Computation Fluid Dynamics (CFD) tools used for civil and environmental engineering. “FLOW3D-Hydro features a streamlined, water-focused user interface and offers new simulation templates for efficient modeling workflows, as well as expanded training materials geared to the needs of the civil or environmental engineer” (FLOW-3D).

FLOW3D-Hydro can be used to predict soil erosion using its sediment transport model. This model can simulate the erosion phenomena, which can be described in different processes, such as bedload transport, suspension transport, and sedimentation of the sediments. FLOW3D-Hydro can estimate the forces and stresses applied by the flow on a soil bed, leading to different transport modes depending on the stress levels, size, and weight of the sediment. Therefore, the sediment can move by rolling, sliding, in small jumps (bedload transport), or suspended in the flow (suspended load transport). As the flow velocity decreases, the forces acting on the sediment will also decrease, causing the sediments to deposit back into the bed. All processes are included in FLOW3D-Hydro using mass conservation equations. Detailed explanations are provided in the following section.

4.2 Sediment Transport Model

4.2.1 General

FLOW3D-Hydro provides a sediment transport model that considers sediment properties, fluid flow characteristics, and bed morphology. It can predict the sediment's erosion, advection, and deposition, which describes the sediment's motion. The estimation is done by four steps

described in the user manual: suspended sediment transport computation, bedload transport computation, sediment entrainment computation, and sediment settling computation.

4.2.2 Packed and Suspended Sediments

In FLOW3D-Hydro, the sediment may exist as a packed or suspended sediment. The packed sediment can exist in a maximum packing fraction (user-defined), while the suspended sediments exist in low concentration and advect with the flow. Therefore, the morphology of the bed is governed by the mass conservation of the sediment, as shown in Equation 4.1, and the suspended sediment is represented as a concentration, which can be computed using Equation 4.2 (Fox & Feurich, 2019).

$$\emptyset \frac{\partial z}{\partial t} = \frac{\partial q_{bx}}{\partial x} + \frac{\partial q_{by}}{\partial y} + D - E \quad (4.1)$$

where,

(z) is bed elevation,

(\emptyset) is maximum packing fraction,

(q_b) is volumetric bedload transport rate per unit width,

(D) is downward sediment deposition flux, and

(E) upward entrainment flux.

$$\frac{\partial C_i}{\partial t} + \nabla \cdot (u_{s,i} C_i) = \nabla \cdot \nabla (\varepsilon C_i) \quad (4.2)$$

where,

(C) is the suspended sediment mass concentration for species (i),

(u_s) is suspended sediment velocity, and

(ε) is the diffusivity.

4.2.3 Bed Morphology

Bed morphology changes can occur due to the physical processes included in Equation 4.1. More details about these processes are described below, as demonstrated in Figure 4.1.

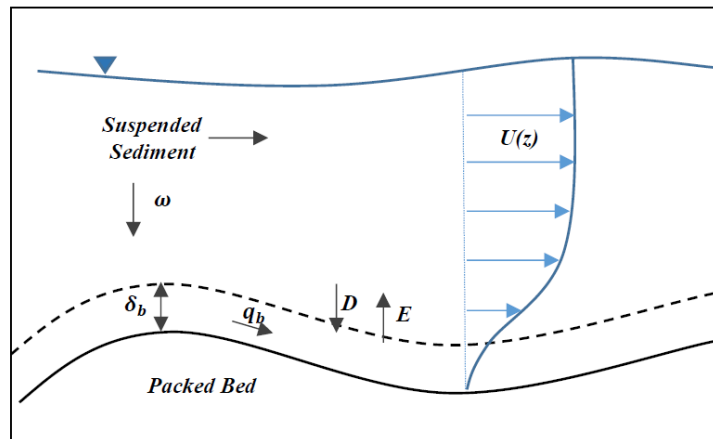


Figure 4.1 The Physical Processes Causing the Bed Morphology Changes (Fox & Feurich, 2019)

4.2.3.1 Bedload Transport

Bedload transport is defined as sediment movement along the bed by sliding, rolling, and saltating (small jumps) without being suspended in the flow. In general conditions, this will be the transport mode for sand and gravel because the turbulent forces caused by the flow will not be sufficient to carry them into suspension.

4.2.3.2 Suspended Load Transport

Suspended transport is defined as the movement of the sediment within the flow when the turbulent forces are enough to carry it. In general conditions, this will be the transport mode for fine-grained soil.

4.2.3.3 Entrainment

Entrainment is defined as the movement of a particle from the packed bed to the suspension.

4.2.3.4 Deposition

The deposition is defined as the movement of a particle from suspension to the packed bed.

4.2.4 Numerical Models and Computational Methods Used in FLOW3D-Hydro

Different numerical models were presented in the literature for the mathematical representations of the physical processes causing the change in bed morphology. The models, equations, and methods used in FLOW3D-Hydro are presented below, as described in the user manual.

4.2.4.1 Dimensionless Diameter

The hydrodynamics erosion theory utilizes a dimensionless diameter of the sediment to make the calculations more practical. The dimensionless diameter is given by Equation 4.3 as described by (Mastbergen and Van Den Berg (2003)).

$$d_{*,i} = d_i \left[\frac{\rho_f(\rho_i - \rho_f) \|g\|}{\mu_f^2} \right]^{\frac{1}{3}} \quad (4.3)$$

where,

ρ_i is the density of the sediment species i ,

ρ_f is fluid density,

d_i is diameter,

μ_f is dynamic viscosity of the fluid, and

$\|g\|$ is the magnitude of the acceleration of gravity \mathbf{g} .

4.2.4.2 Critical Shields Parameter

The dimensionless diameter presented in Equation 4.3 is used to estimate the critical Shields parameter using Equation 4.4; it is the Soulsby-Whitehouse Equation (Soulsby, 1997).

$$\theta_{cr,i} = \frac{0.3}{1+1.2d_{*,i}} + 0.055[1 - \exp(-0.02d_{*,i})] \quad (4.4)$$

where $\theta_{cr,i}$ is the critical Shields parameter, which represents a dimensionless thresholds shear stress. In other words, erosion starts when the dimensionless fluid-induced shear stress (local Shields parameter) exceeds the critical Shields parameter.

4.2.4.3 Modification for the Angle of Repose

In sloped surfaces, the entrainment of the particles by the flow downslope is easier because the bed is not as stable as it is on a flat surface. Therefore, the critical Shields parameter can be modified to include the angle of repose effect, as shown in Equation 4.5 (Soulsby, 1997).

$$\theta'_{cr,i} = \theta_{cr,i} \frac{\cos\psi\sin\beta + \sqrt{\cos^2\beta\tan^2\varphi_i - \sin^2\psi\sin^2\beta}}{\tan\varphi_i} \quad (4.5)$$

where,

β is angle of the bed slope,

φ_i is the user-defined angle of repose for sediment species i , and

ψ is the angle between the flow and the upslope direction.

4.2.4.4 Shear Stress Calculation

The dimensional shear stress is used to calculate the local Shields parameter, which appears in both bedload and entertainment rate equations. As explained before, erosion starts

when the local Shields parameter exceeds the critical Shields parameter. Equation 4.6 is known as the logarithmic law and defines the boundary conditions near the wall (Fox & Feurich, 2019).

$$\frac{u}{u^*} = \frac{1}{k} \ln \left(\frac{y}{c_{rough} d_{50}} \right) + 8.5 \quad (4.6)$$

where,
 u is near bed fluid velocity,
 u^* is shear velocity $= \sqrt{\tau / \rho_f}$,
 k is Von Karmen constant = 0.41,
 y is distance from wall,
 c_{rough} is the roughness multiplier, and
 d_{50} is median particle diameter.

For the roughness height, FLOW3D-Hydro uses Nikuradse sand grain equivalent roughness. The roughness height accounts for additional turbulence at hydraulically rough surfaces and is calculated in the numerical model, as shown in Equation 4.7.

$$k_s = c_{rough} d_{50,packed} \quad (4.7)$$

where,
 k_s is the Nikuradse roughness of the bed surface,
 $d_{50,packed}$ is the local median grain diameter in packed sediment, and
 c_{rough} is a roughness multiplier (user defined).

4.2.4.5 Local Shields Parameter

The local Shields parameter (dimensionless) can be computed using the famous Shields formula based on the local bed shear stress induced by the flow (dimensional), as presented in Equation 4.8 (Shields, 1936).

$$\theta_i = \frac{\tau}{\|g\|d_i(\rho_i - \rho_f)} \quad (4.8)$$

where τ is the local bed shear stress.

4.2.4.6 Bedload Transport

The bedload is initially calculated in dimensionless form, then converted to dimensional form. FLOW3D-Hydro contains three equations for the bedload transport rate: Meyer-Peter Müller equation (Meyer-Peter & Müller, 1948), Nielsen equation (Nielsen, 1992), and Van Rijn equation (van Rijn, 1984), presented in Equations 4.9, 4.10, and 4.11, respectively.

$$\Phi_i = \beta_{\text{MPM},i} (\theta_i - \theta'_{cr,i})^{1.5} c_{b,i} \quad (4.9)$$

$$\Phi_i = \beta_{\text{Nie},i} \theta_i^{0.5} (\theta_i - \theta'_{cr,i}) c_{b,i} \quad (4.10)$$

$$\Phi_i = \beta_{\text{VR},i} d_{*,i}^{-0.3} \left(\frac{\theta_i}{\theta'_{cr,i}} - 1.0 \right)^{2.1} c_{b,i} \quad (4.11)$$

where,

$\beta_{\text{MPM},i}$, $\beta_{\text{Nie},i}$, $\beta_{\text{VR},i}$ are the bedload coefficients,
 $c_{b,i}$ is the volume fraction of species i in the bed material, and
 Φ_i is the dimensionless bed-load transport rate.

The dimensionless bedload transport rate can be converted to a dimensional bedload rate per unit width using Equation 4.12, as described in the user manual.

$$q_{b,i} = \Phi_i \left[\|g\| \left(\frac{\rho_i - \rho_f}{\rho_f} \right) d_i^3 \right]^{\frac{1}{2}} \quad (4.12)$$

where $q_{b,i}$ is the volumetric bedload transport rate per unit width.

It is important to calculate the bedload layer thickness in order to compute the motion of bedload transport in each computational cell. This can be done by using Equation 4.13 (van Rijn, 1984).

$$\frac{\delta_i}{d_i} = 0.3 d_*^{0.7} \left(\frac{\theta_i}{\theta'_{cr,i}} - 1 \right)^{0.5} \quad (4.13)$$

where δ_i is the bedload layer thickness.

In addition, the volumetric bedload transport rate per unit width $q_{b,i}$ is converted to bedload velocity ($u_{bedload}$) to compute sediment velocity in each computational cell using Equation 4.14, as provided by the user manual.

$$u_{bedload,i} = \frac{q_{b,i}}{\delta_i c_{b,i} f_b} \quad (4.14)$$

where f_b is the critical packing fraction of the sediment.

4.2.4.7 Entrainment

The lift velocity at which the particle entrainment occurs is calculated based on (Mastbergen & Van Den Berg 2003) as described in the user manual and presented in Equation 4.15.

$$\mathbf{u}_{lift,i} = \alpha_i \mathbf{n}_s d_*^{0.3} (\theta_i - \theta'_{cr,i})^{1.5} \sqrt{\frac{\|\mathbf{g}\| d_i (\rho_i - \rho_f)}{\rho_f}} \quad (4.15)$$

where,

α_i is the entrainment parameter and

\mathbf{n}_s is the outward pointing normal to the packed bed interface.

4.2.4.8 Deposition

The deposition of the particles can be described by the settling velocity of each particle, which is given by (Soulsby 1997), as described in the user manual and presented in Equation 4.16.

$$u_{settling,i} = \frac{v_f}{d_i} [(10.36^2 + 1.049 d_*^3)^{0.5} - 10.36] \quad (4.16)$$

where v_f is the kinematic viscosity of fluid.

Assuming the direction of the gravity, the settling velocity is written as shown in Equation 4.17.

$$\mathbf{u}_{settling,i} = u_{settling,i} \frac{\mathbf{g}}{\|\mathbf{g}\|} \quad (4.17)$$

The settling velocity can be modified to consider the particle-particle interaction (concentration effect) using the Richardson-Zaki correlation (Richardson & Zaki, 1954). The modification method is presented in Equations 4.18 and 4.19.

$$\mathbf{u}_{settling,i}^* = \mathbf{u}_{settling,i} (1 - \min(0.5, c_s))^\zeta \quad (4.18)$$

where c_s is the total volume fraction of suspended sediment and,

$$\zeta = \zeta_{user} \zeta_0 \quad (4.19)$$

where

ζ_{user} is the Richardson-Zaki coefficient multiplier and ζ_0 is the Richardson-Zaki coefficient.

4.2.5 Modeling UNLETB

4.2.5.1 Geometry

As in any finite element method (FEM) or computational fluid dynamics (CFD) software, FLOW3D-Hydro requires creating a geometry that represents the targeted case study. In this study, the model is designed to mimic the actual UNLETB behavior. Therefore, the model consists of an outer tank, sample box, soil sample, source, and suction. Figures 4.2 and 4.3 present the model's side and top view, respectively.

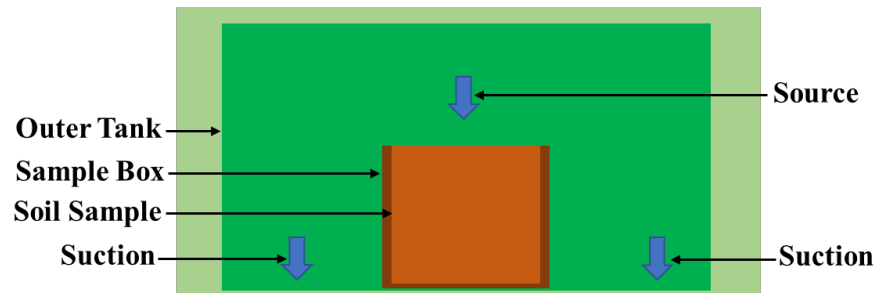


Figure 4.2 Side View of UNLETB FLOW3D-Hydro Model

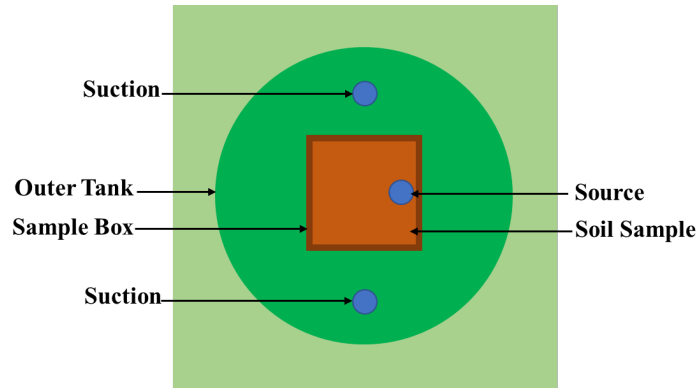


Figure 4.3 Top View of UNLETB FLOW3D-Hydro Model

Initially, the diameter of the actual tank was selected to be 1 m (actual outer tank diameter). However, a trial-and-error process was conducted to reduce the computational time by making the size of the outer tank smaller in a way that maintains the same results as the full-size tank. Therefore, the outer tank diameter became 0.29 m.

The fluid source was defined in FLOW3D-Hydro using the "mass-momentum source" option, with a diameter of 0.0762 m, a flow rate of $0.004 \text{ m}^3/\text{sec}$, and a 0.06 m vertical distance from the soil sample. In addition, two mass-momentum sources were defined with a negative flow rate (suction) to mimic water circulation.

The soil sample was defined as packed sediment with the properties described in the following section of the report.

4.2.5.2 Mesh and Boundary Conditions

As in any FEM or CFD software, it is essential to construct a mesh which determines the computational domain and divides it into elements to make the calculations possible.

The boundary conditions determine the value of a certain quantity or specify a certain condition at the domain boundaries.

In this study, the mesh was defined as a cubic mesh, and the boundaries are defined at the six cube faces, as shown in Figures 4.4 and 4.5.

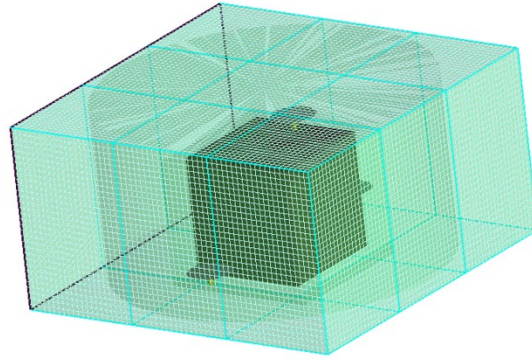


Figure 4.4 Mesh of UNLETB FLOW3D-Hydro Model

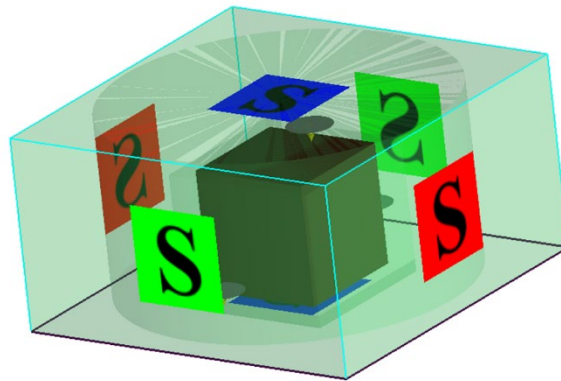


Figure 4.5 Boundary Conditions of UNLETB FLOW3D-Hydro Model

The mesh box size was adjusted with a trial-and-error process to exclude the effect of the boundary conditions on the test results. As a result, the final size of the mesh box was selected to be 0.6 m in length, 0.6 m in width, and 0.72 m in height. The mesh was 0.01 m thick.

A sensitivity analysis was conducted with different reliable boundary conditions, as presented in Figure 4.6, to check the effect of the boundaries on the UNLETB model is negligible. The selected boundaries for the sensitivity analysis were symmetry, wall, specified velocity (0), and stagnation pressure (0).

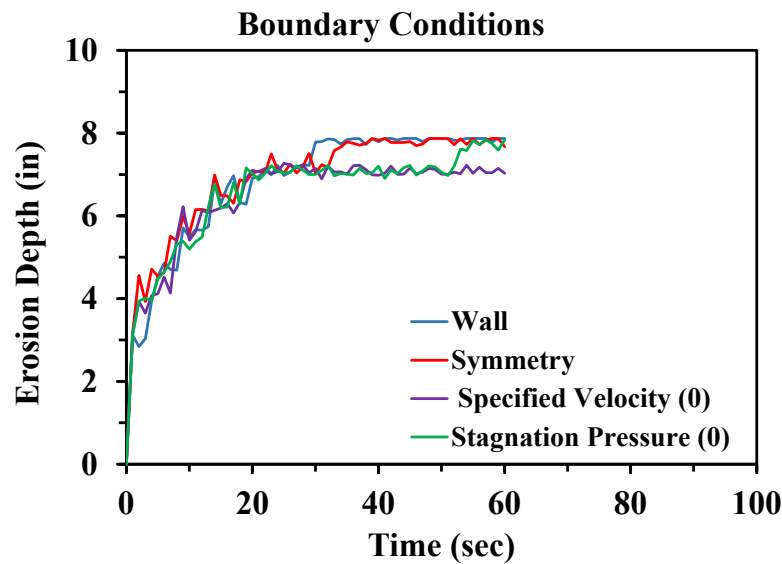


Figure 4.6 Boundary Conditions of UNLETB FLOW3D-Hydro Model

The boundary conditions effect was insignificant with the selected mesh box size. Therefore, the boundary conditions were selected to be the symmetry boundaries for the six mesh cube faces. The symmetry boundary condition applies a zero-gradient condition at the boundary and a zero-velocity condition normal to the boundary.

4.2.6 Input Parameters

In order to get rational results, it is important to understand the physical meaning and the effect of each parameter on the UNLETB model. Therefore, the input parameters used are

provided in this section, in addition to a sensitivity analysis, to observe how the UNLETB model can be affected by changing a certain parameter.

Note the initial parametric sensitivity analysis stage did not target a certain material from the tested ones. Instead, it aimed to understand the effect of each parameter on the model.

4.2.6.1 Fluid Properties

The water properties are predefined in FLOW3D-Hydro. Therefore, this study used the predefined model with the following properties:

- 1) Water density: 998.2 kg/m^3
- 2) Water compressibility: $4.56123\text{e-}10 \text{ 1/Pa}$
- 3) Viscosity: 0.001 kg/m/sec

4.2.6.2 Gravity

FLOW3D-Hydro defines the gravity in the negative Z direction, and the Z- component is equal to -9.81 m/sec^2 .

4.2.6.3 Turbulence Models

FLOW3D-Hydro provides the following five options for the turbulence calculations:

- 1) No Turbulence (laminar)
- 2) Renormalized group (RNG) model
- 3) Two-equation (k - ϵ) model
- 4) Two-equation(k - ω) model
- 5) Large eddy simulation model

In the case of UNLETB, it is obvious that the system should be turbulent. Therefore, the laminar model was excluded. Figure 4.7 provides a sensitivity analysis for a sediment transport model, with everything fixed except the turbulence model.

The sensitivity analysis showed that the difference in the results between the RNG model, k - ϵ model, k - ω model, and the large eddy simulation model does not substantially affect the

erosion profile in the UNLETB model. The two-equation ($k-\epsilon$) model was chosen to be used in the following simulations.

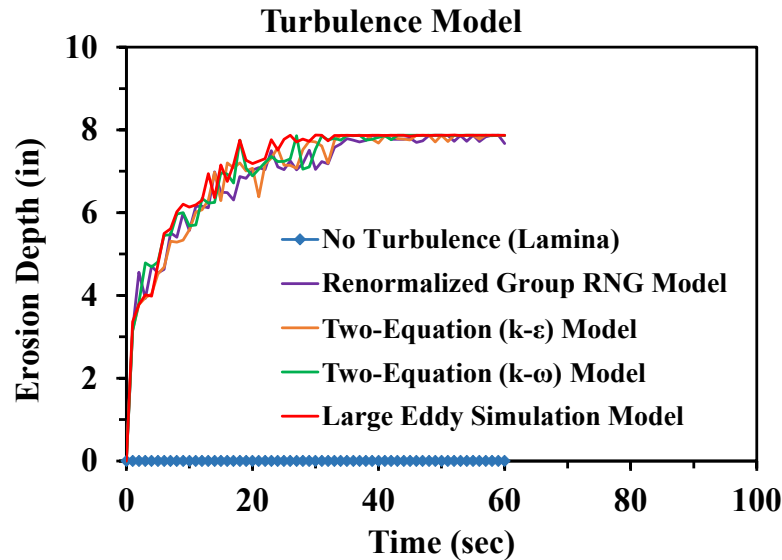


Figure 4.7 Effect of Turbulence Model on the Erosion Profile of UNLETB FLOW3D-Hydro Model

4.2.6.4 Angle of Repose/Slope Effect

The angle of repose can be defined as the maximum angle of a slope or pile of sediment particles that can be maintained without the particles sliding or rolling. It describes the angle at which sediment particles rest on a sloping bed. The FLOW3D model can modify the critical Shields parameter to the angle of repose as described in Equation 4.5 and suggested a range of (30° - 40°). In addition, there was a feature to turn the modification of the slope on and off.

The angle of repose was expected to not make a difference in the results because the targeting data was just the erosion profile. To confirm that idea, a sensitivity analysis was conducted with two angles of repose: 32° and 0° , and the slope effect option was turned on and

off. The simulation results are presented in Figure 4.8, which showed similar behavior to the expected one. Therefore, it was decided to use the typical value (32°) with the slope effect turned on.

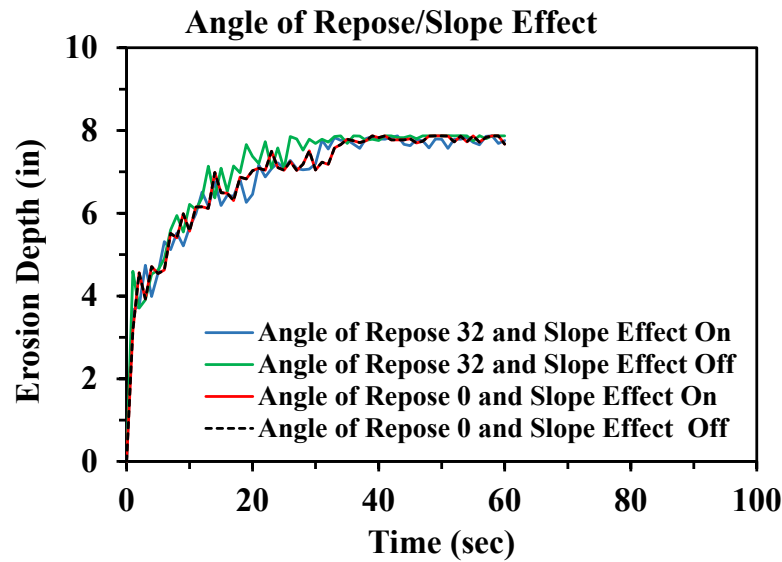


Figure 4.8 Effect of Angle of Repose/Slope on the Erosion Profile of UNLETB FLOW3D-Hydro Model

4.2.6.5 Maximum Packing Fraction

The maximum packing fraction refers to the maximum volume fraction of solid particles present in a given fluid volume. The maximum packing fraction depends on the particles' size, shape, and arrangement, as well as the fluid flow properties. In some references, it is defined as 1-porosity of the soil. In FLOW3D-Hydro, the typical value of the maximum packing fraction is 0.64. It is mentioned in the user manual that 0.64 represents perfect spheres, while the value can be increased for multi-disperse and reduced for monodisperse and irregular sediment particles. Figure 4.9 presents the sensitivity analysis of the maximum packing fraction, showing the effect

was insufficient on the UNLETB model. The maximum packing fraction was chosen to be 0.54 for the tested gravels.

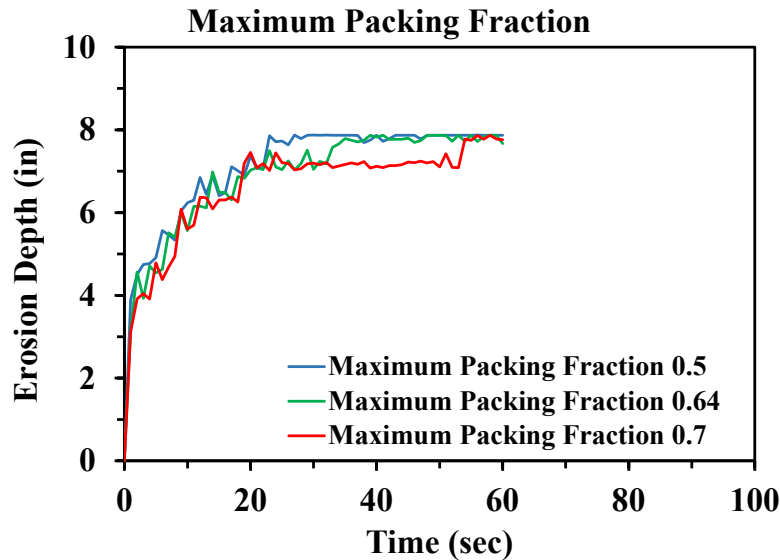


Figure 4.9 Effect of Maximum Packing Fraction on the Erosion Profile of UNLETB FLOW3D-Hydro Model

4.2.6.6 Molecular Diffusion Coefficient, and Turbulent Diffusion Multiplier

In FLOW3D-Hydro, the molecular diffusion coefficient is a physical parameter that describes the diffusion rate of molecules in a fluid. It measures how easily molecules can move through a fluid by random motion or diffusion. The molecular diffusion coefficient is used in the sediment transport model to model the diffusion of sediment particles in the fluid.

The turbulent diffusion multiplier is a dimensionless parameter used to modify the turbulent diffusivity coefficient, which is a parameter that represents the rate of turbulent mixing. The user manual defines it as the inverse of the Schmidt number and gives a typical value about one.

The diffusion of the suspended sediments is activated by sitting nonzero values, the molecular diffusion parameter, and the turbulent diffusion multiplier. Figures 4.10 and 4.11 present the sensitivity analysis of the UNLETB model to the molecular diffusion parameter, and turbulent diffusion multiplier, respectively. The sensitivity analysis showed that the UNLETB model is not sensitive to these two parameters. Therefore, values of zero for the molecular diffusion parameter and 1.43 for the turbulent diffusion multiplier were chosen as the default values in FLOW3D-Hydro.

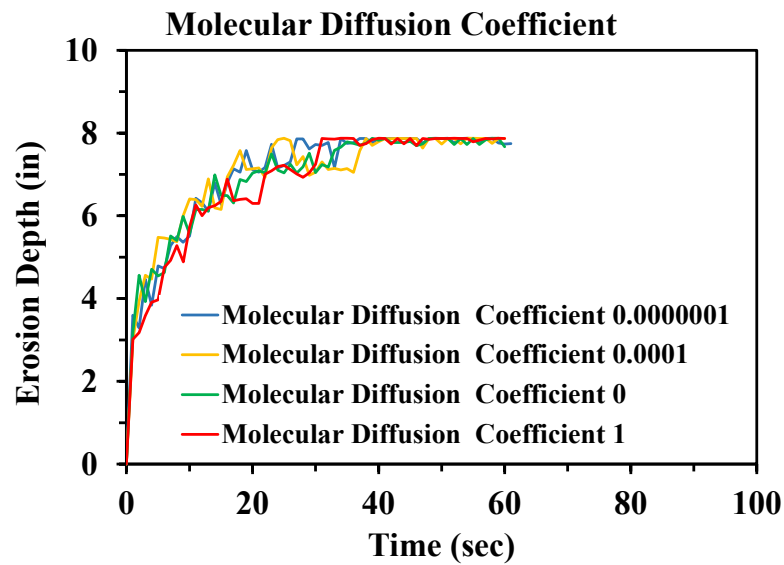


Figure 4.10 Effect of Molecular Diffusion Parameter on the Erosion Profile of UNLETB FLOW3D-Hydro Model

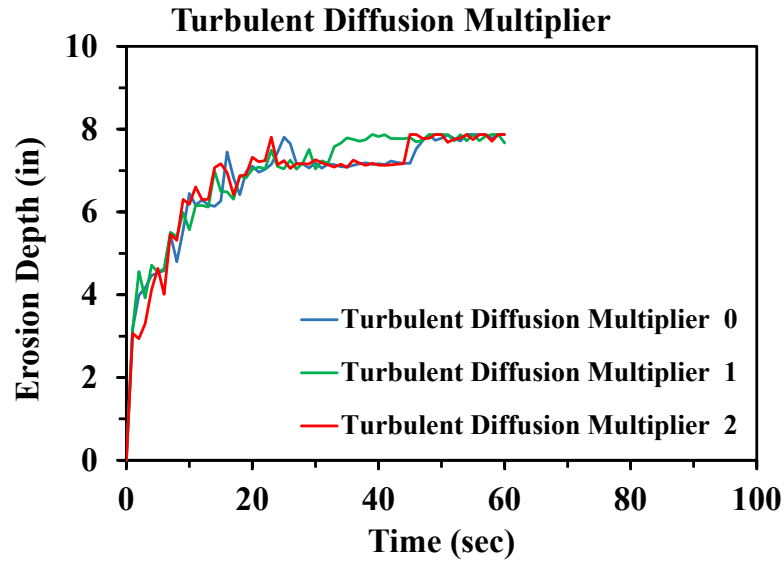


Figure 4.11 Effect of Turbulent Diffusion Multiplier on the Erosion Profile of UNLETB FLOW3D-Hydro Model

4.2.6.7 Richardson-Zaki Multiplier

As described before, the settling velocity can be modified using the Richardson-Zaki correlation to consider the concentration effect. The Richardson-Zaki coefficient is a function of the Reynolds' number of settling particles, as shown in Table 4.1.

Table 4.1 Richardson-Zaki Coefficient as a Function of Reynold's Number

$Re < 0.2$	$\zeta_0 = 4.65$
$0.2 < Re < 1.0$	$\zeta_0 = 4.35 / Re^{0.03}$
$1.0 < Re < 500$	$\zeta_0 = 4.45 / Re^{0.1}$
$500 < Re$	$\zeta_0 = 2.39$

A sensitivity analysis was conducted to understand the effect of the Richardson-Zaki multiplier on the UNLETB model, showing a fair effect of the Richardson-Zaki coefficient on

the erosion profile. The sensitivity analysis is presented in Figure 4.12. It is important to understand the input in FLOW3D-Hydro is the Richardson-Zaki multiplier (not the coefficient). Therefore, to use the definition provided by Richardson-Zaki, the multiplier should be one as this study used.

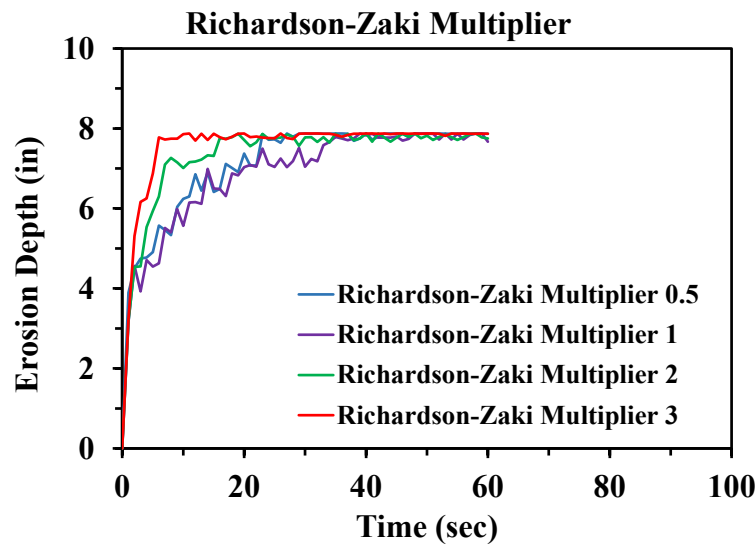


Figure 4.12 Effect of Richardson-Zaki Multiplier on the Erosion Profile of UNLETB FLOW3D-Hydro Model

4.2.6.8 Sediment Density

The input density in the sediment transport model should be the microscopic (grain) density, as described in the user manual. A sensitivity analysis was conducted and presented in Figure 4.13, showing the effect of the sediment density on the UNLETB model is not substantial. Therefore, the default value of the sediment density (2650 kg/m^3) was used in this study.

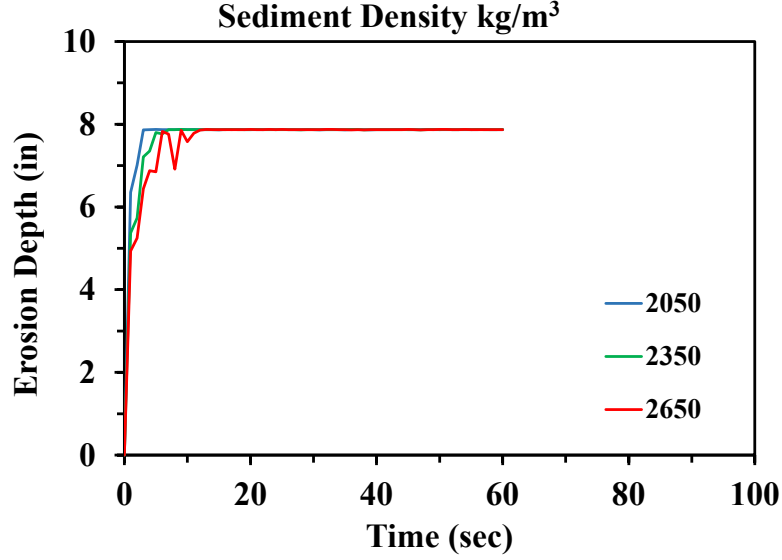


Figure 4.13 Effect of Sediment Density on the Erosion Profile of UNLETB FLOW3D-Hydro Model

4.2.6.9 Critical Shields Parameter

The critical Shields parameter is a dimensionless form of the critical shear stress, representing the threshold stress at which the erosion starts. Shields (1936) conducted flume tests and expressed a low result in similarity, as presented in Equation (4.20).

$$\frac{\tau_c}{(\gamma_f - \gamma)D} = f\left(\frac{u^*D}{\nu}\right) \quad (4.20)$$

where,

τ_c is the dimensional critical shear stress,

γ_f is the unit weight of fluid,

γ is the unit weight of the sediment,

D is the sediment diameter (used as the mean particle diameter in this study),

u^* is the shear velocity, and

ν is the kinematic fluid viscosity.

In Equation 4.20, the left and right terms refer to the critical Shields parameter and the critical Reynolds number for the particle. The test results of Shields (1936) are presented in Figure 4.14 as presented in Buffington (1999).

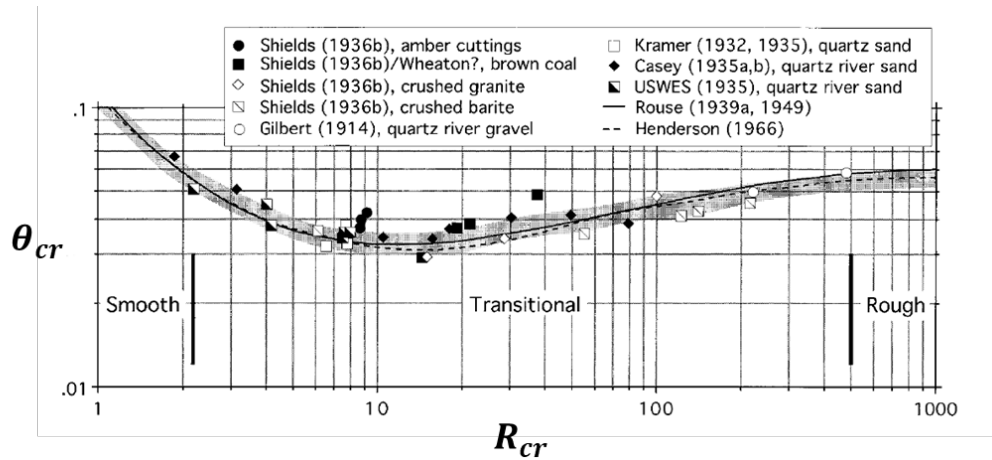


Figure 4.14 Shields Test Results as Presented in (Buffington, 1999)

Soulsby (1997) presented a correlation to predict the critical Shields parameter based on the dimensionless diameter (Equation 4.4). This correlation is used in FLOW3D and was used in this study to predict the input values of the critical Shields parameter. Table 4.2 presents all samples' estimated critical Shields parameters based on the mean grain particle size.

Table 4.2 Critical Shields Parameter for Each Sample

Sample	Critical Shields Parameter
1.5 in. Rock Aggregate	0.0554
1.5 in. Crusher Run	0.0557
1 in. Course	0.0557
1 in. Clean	0.0557
Combined Package without fines	0.0557
Combined Package with fines	0.0556
1 in. Crusher Run	0.0553
Surface Course	0.0513
Class 2A	0.0462
Class B	0.0462

4.2.6.10 Bedload Equation and Bedload Coefficient

As described before, FLOW3D-Hydro provides three equations for the bedload transport rate (Equations 4.9-4.11). Each equation requires the input of a bedload coefficient. Therefore, the sensitivity analysis was initially conducted to compare the three equations with the default bedload coefficients, as presented in Figure 4.15.

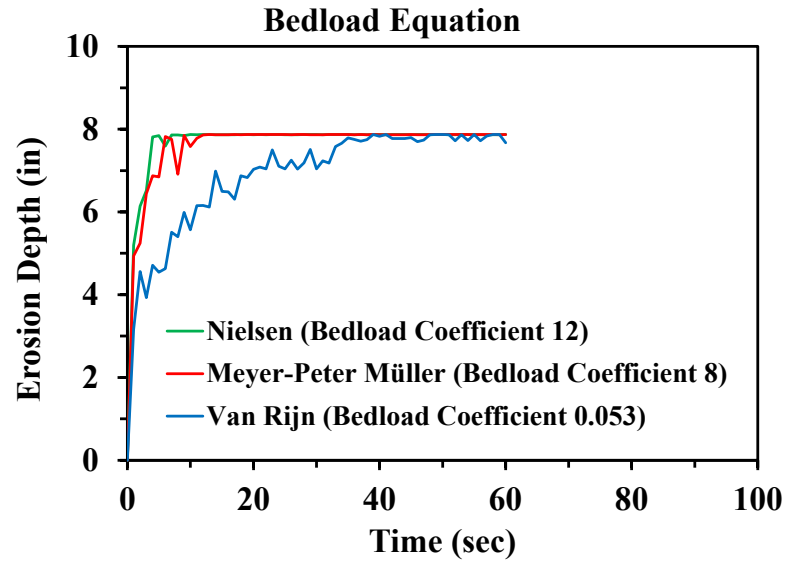


Figure 4.15 Effect of the Selected Bedload Equation on the Erosion Profile of UNLETB FLOW3D-Hydro Model

The Meyer-Peter Müller equation was chosen for this study because the user manual provides a proper range for the bedload coefficient (5.0 for low transport to 13.0 for very high transport). Therefore, an additional sensitivity analysis was conducted on the Meyer-Peter Müller bedload coefficient, as presented in Figure 4.16, showing that the UNLETB model is not sensitive to the bedload coefficient. This behavior may be explained as the sediments were not allowed to move in the bedload form due to the high flow rate and the test setup.

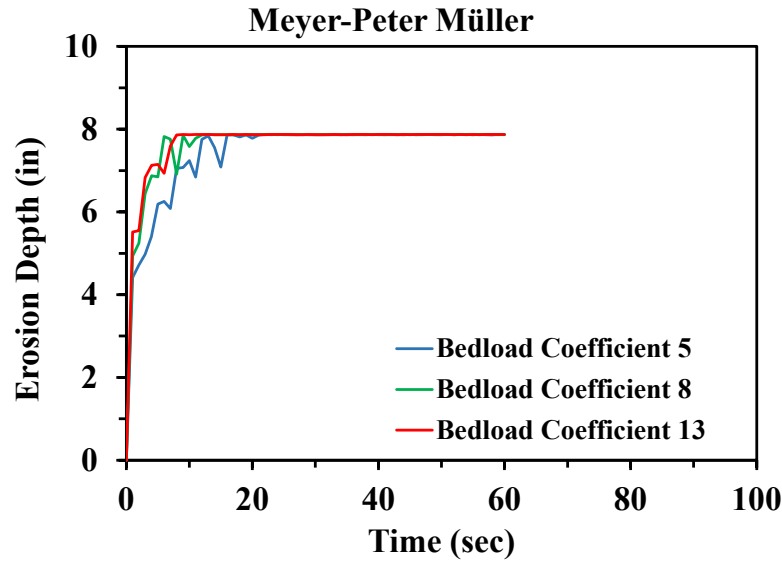


Figure 4.16 Effect of Bedload Coefficient on the Erosion Profile of UNLETB FLOW3D-Hydro Model

An additional sensitivity analysis was conducted through the actual model calibration process showing the effect of the bedload is even lower than the one observed in Figure 4.16.

4.2.6.11 Roughness/ D_{50}

To account for the bed roughness, the input will be in the form of bed roughness/ D_{50} . The roughness used in FLOW3D-Hydro is Nikuradse roughness, which is known as “equivalent sand roughness”. Nikuradse measured the flow resistance of a pipe coated with uniform sands in 1933 and his work was translated in 1950 (Nikuradse, 1950). Garcia (2008) summarized the values used for roughness/diameter in literature, as shown in Table 4.3. In addition, Dey & Ali (2019) provided a chart combining test results from different references correlating the critical shield parameter to the roughness/diameter ratio. This chart is presented in Figure 4.17.

Table 4.3 Ratio of Nikuradse Equivalent Roughness and Sediment Size for Rivers (Garcia, 2008)

Investigator	Measure of sediment size, D	k_s/D
Ackers and White (1973)	D ₃₅	1.23
Aguirre-Pe and Fuentes (1990)	D ₈₄	1.6
Strickler (1923)	D ₅₀	3.3
Katul et al (2002)	D ₈₄	3.5
Keulegan (1938)	D ₅₀	1
Meyer-Peter and Müller (1948)	D ₅₀	1
Thompson and Campbell (1979)	D ₅₀	2
Hammond et al. (1984)	D ₅₀	6.6
Einstein and Barbarossa (1952)	D ₆₅	1
Irmay (1949)	D ₆₅	1.5
Engelund and Hansen (1967)	D ₇₅	2
Lane and Carlson (1953)	D ₈₀	3.2
Gladki (1979)	D ₈₄	2.5
Leopold et al. (1964)	D ₈₄	3.9
Limerinos (1970)	D ₈₄	2.8
Mahmood (1971)	D ₈₄	5.1
Hey (1979), Bray (1979)	D ₈₄	3.5
Ikeda (1983)	D ₈₄	1.5
Colosimo et al. (1986)	D ₈₄	3.6
Whiting and Dietrich (1990)	D ₈₄	2.95
Simons and Richardson (1966)	D ₈₅	1
Kamphuis (1974)	D ₉₀	2
Van Rijn (1982)	D ₉₀	3

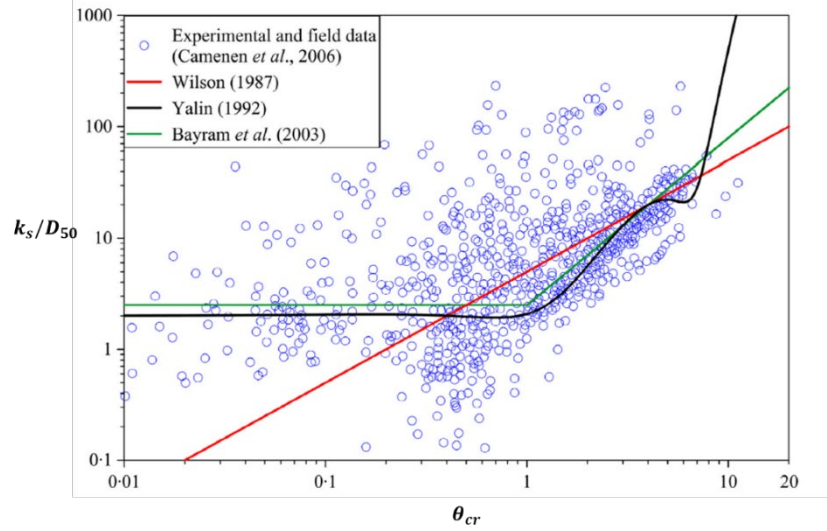


Figure 4.17 Equivalent Roughness Height to Mean Median Grain Size Ratio vs. Critical Shield Parameter (excerpted from (Dey & Ali, 2019))

A sensitivity analysis was conducted to evaluate the effect of the roughness/ D_{50} on the erosion profile of the UNLETB model, as presented in Figure 4.18, showing that the roughness/ D_{50} has a substantial effect.

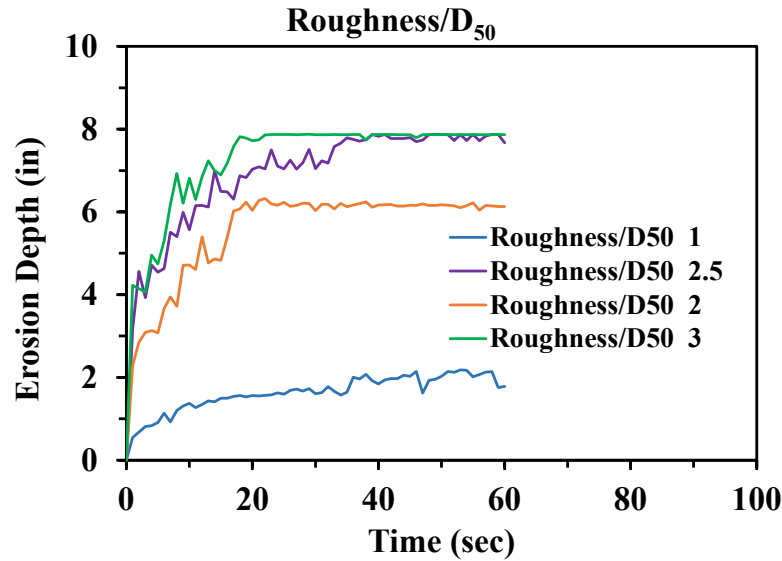


Figure 4.18 Effect of Roughness/D₅₀ on the Erosion Profile of UNLETB FLOW3D-Hydro Model

The recommended value of the roughness/D₅₀ in the FLOW3D-Hydro user manual is 2.5. Based on the literature and tested samples, it was decided to use the range one to three in this study.

4.2.6.12 Entrainment Parameter

The entrainment parameter affects the lift velocity at which the particle's entrainment occurs. The recommended value of the entrainment parameter is 0.018, and the manual mentioned this parameter is used to fit the transport rate to the experimental results. Figure 4.19 demonstrates the sensitivity analysis of the entrainment parameter. The initial analysis showed the effect on UNLETB erosion was not substantial. However, during the calibration of the actual mode the effect would be significant.

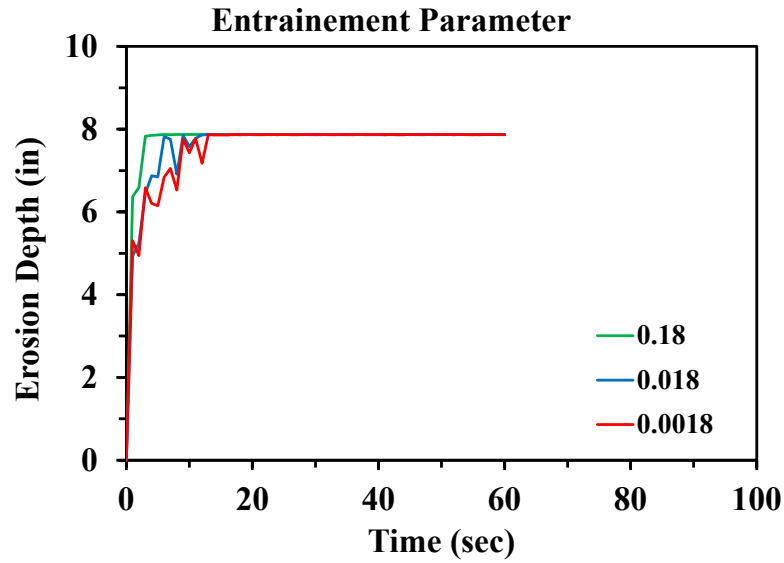


Figure 4.19 Effect of Entertainment Parameter on the Erosion Profile of UNLETB FLOW3D-Hydro Model

An example of a calibrated sample is shown in Figure 4.20, and a summary of the sediment transport input parameters for each sample is presented in Table 4.4.

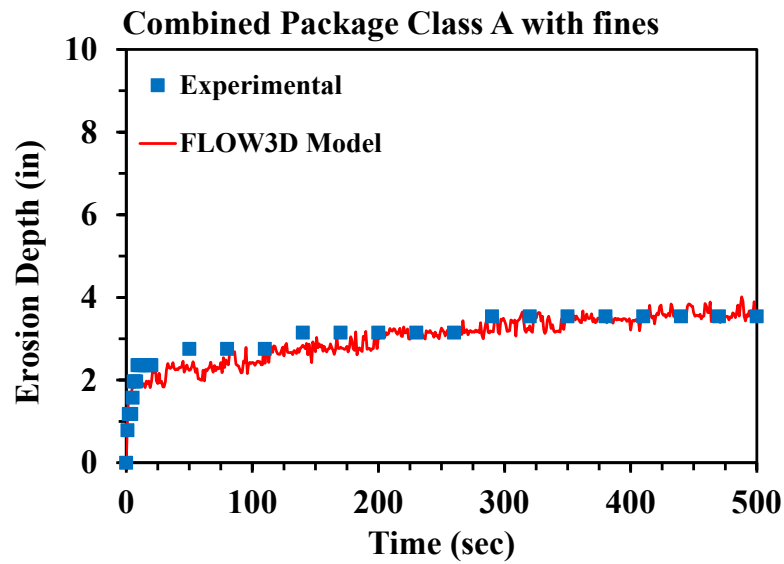


Figure 4.20 Experimental vs. FLOW3D-Hydro Results for Combined Package Class A with Fines Sample

Table 4.4 Summary of FLOW3D-Hydro Input Parameters for All Samples

Soil Type	D ₅₀ ¹	Maximum Packing fraction	Critical Shields Parameter	Bedload Coefficient	Richardson-Zaki Multiplier
1.5 in. Rock Aggregate ²	-	-	-	-	-
1.5 in. Crusher Run	13	0.54	0.0557	8	1
1 in. Coarse	13	0.54	0.0557	8	1
1 in. clean	11	0.54	0.0557	8	1
Combined Package without fines	10	0.54	0.0557	8	1
Combined Package with fines	9	0.54	0.0556	8	1
1 in. Crusher Run	8	0.54	0.0553	8	1
Gravel Surface Course	4.4	0.54	0.0513	8	1
Class 2A	3	0.54	0.0462	8	1
Class B	3	0.54	0.0462	8	1

Table 4.4 cont. Summary of FLOW3D-Hydro Input Parameters for All Samples

Soil Type	Angle of Repose	Turbulent Diffusion Multiplier	Molecular Diffusion Coefficient	Entrainment Parameter	Roughness/ D ₅₀
1.5 in. Rock Aggregate ²	-	-	-	-	-
1.5 in. Crusher Run	32	1.43	0	2.2 ³	0.05 ³
1 in. Coarse	32	1.43	0	1.8	0.005
1 in. clean	32	1.43	0	2.1	0.005
Combined Package without fines	1	1.43	0	1.8	0.005
Combined Package with fines	32	1.43	0	2	0.007
1 in. Crusher Run	32	1.43	0	2.6	0.005
Gravel Surface Course	32	1.43	0	3.5 ³	0.8 ³
Class 2A	32	1.43	0	2.4 ⁴	0.8 ⁴
				2 ⁵	0.05 ⁵
Class B	32	1.43	0	2.4 ⁴	0.8 ⁴
				2 ⁵	0.05 ⁵

¹: Mean grain size is in (mm) unit

²: There was no erosion

³: The entrainment parameter and roughness/D₅₀ does not fit the experimental perfectly (the values in the table are the closest to the experimental)

⁴: The combination of entertainment parameter and Roughness/ D₅₀ fits the initial portion of the erosion curve

⁵: The combination of entertainment parameter and Roughness/ D₅₀ fits the final portion of the erosion curve

Note: The entrainment parameter and roughness/D₅₀ should be taken as a combination to give the proper behavior.

Chapter 5 Artificial Intelligence-Approach

5.1 General

The artificial intelligence-approach (AI-approach) was developed to quickly evaluate whether the material will be suitable for a particular use and based on simple inputs. An artificial neural network (ANN) can be used for this purpose. The main benefit of neural networks is their ability to learn patterns and relationships in data without the need for supplying the governing model structure. ANN is able to adapt and improve its performance through the examination of data without the need for explicit programming. The ANN model should be trained, optimized, and tested thoroughly during its development phase. Training a neural network model involves selecting the best model from the potential models, meaning the optimal set of variables, or hyperparameters, are adjusted without violating constraints during the optimization process. A network performance test involves measuring the network's effectiveness quantitatively or qualitatively.

ANN-based models have been successfully used in many areas closely related to the study of soil erosion. Licznar and Nearing (2003) examined the feasibility of utilizing ANN to reliably calculate and predict the amount of soil erosion resulting from rainfall runoff in highway shoulders through quantitative means. A report by ASCE (ASCE Task committee on application of ANN in hydrology, 2000) details the application of neural networks for rainfall-runoff modeling, stream flow forecasting, and reservoir operations. Harris and Boardmann (1998) proposed expert systems and neural networks as an alternative approach to traditional mathematical models for predicting erosion in the South Downs region of Sussex, England. However, it is true that there are not many studies that have used artificial neural networks to evaluate the erosion behavior of materials based on their physical properties.

This study aims to explore the possibility of using artificial neural networks to decide whether the erosion resistance of gravel is acceptable for use on the highway shoulder based on their D_{10} , D_{30} , and D_{60} values. A multiclass classification ANN model predicting the suitability of material for highway shoulders is trained using the test data from experiments and synthetic data generated using the test data. The performance of the ANN model is evaluated using the handout and k fold cross validation technique. Impact of different input parameters, network architectures and other hyperparameters on the model's accuracy were tested.

5.2 Detailed Explanation for the AI-Approach

The proposed artificial intelligence (AI) based method, popularly known as artificial neural network (ANN), evaluates the erosion behavior for different gradation of highway shoulder gravel. ANN models use interconnected nodes in a layered structure that mimic the thought process of the human brain. These models are able to generalize the relationship between input and output data that are complex and highly nonlinear.

The primary benefit of using ANNs is that they can learn from data sets and create models to predict the behavior of systems without requiring prior knowledge of the relationships between inputs and outputs (Shahin et al., 2008). Among different types of ANN algorithms developed over the years, the feed-forward backpropagation algorithm through supervised learning has been implemented in this work. This method will allow the ANN to improve its ability to make predictions using a corrective feedback system by continuously learning and adjusting the model based on new data.

The overall flow to expand the findings from UNLETB by incorporating the erosion test results into an AI-based system to predict the erosion resistance of various gradation gravels accurately and conveniently is shown in Figure 5.1.

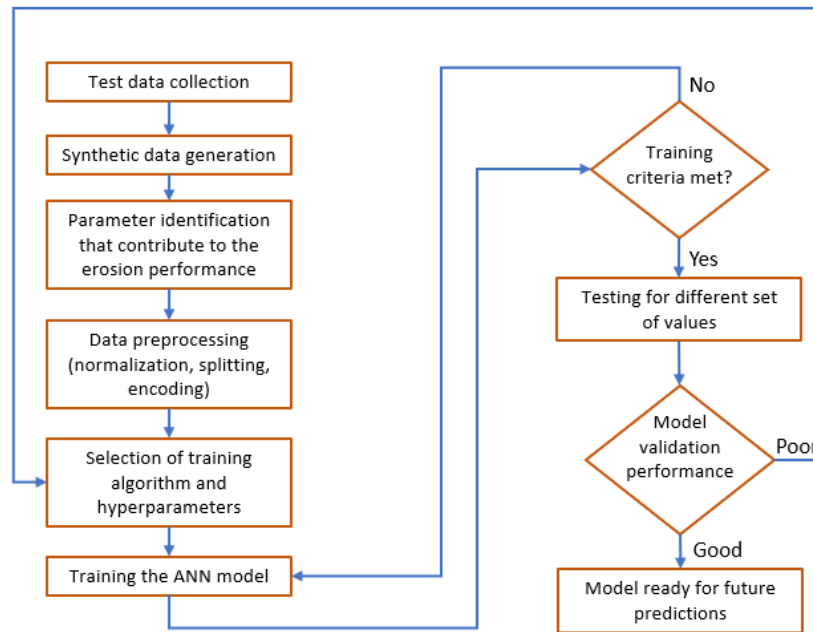


Figure 5.1 Workflow of AI for erosion prediction

The results from sieve analysis, erosion tests and hydrodynamics analysis were collected in a database. Based on the erosion resistance performance, gradation curves of the respective materials were sorted in three groups: Well Performing (WP), Poor Performing (PP), and Not Acceptable (NA). Gradation curves sorted into the WP group demonstrated a high erosion resistance, while the PP group exhibited poor erosion resistance. Moreover, gradation curves in the NA group included large-size gravel with high erosion resistance, but because of their large size they may not be suitable for highway shoulder materials.

In supervised learning, having a rich dataset is of utmost importance to approximately estimate the unknown function that reasonably maps inputs to outputs. The limited data from tests made it challenging to train the ANN model. To overcome this, a scheme was proposed to increase the amount of data in the database. The synthetic data was created by shifting each

gradation curve uniformly in positive and negative directions on the logarithmic scale, thus mimicking the gradation of different materials. Using this strategy, 364 synthetic gradation curves were created using the original nine gradation curves from tests. An example of the synthetic data generated from a gradation curve is illustrated in Figure 5.2. The range of the synthetic gradation curves is between 10-90 only. This is because the inputs required to train the ANN model falls within this range i.e. (D_{10} , D_{30} , D_{60}).

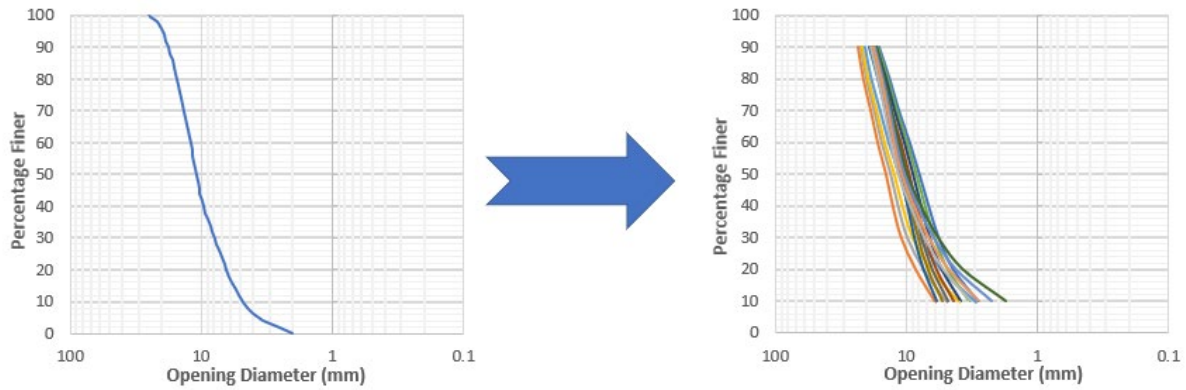


Figure 5.2 Synthetic Gradation Curve Generation

Training ANN should include the input parameters that have direct or indirect impact on the outputs. Therefore, two different combinations of input parameters were tested with the following set of parameters: gravel size pertaining to the D_{10} , D_{30} , or D_{60} , uniformity coefficient (C_u) and coefficient of curvature (C_c). In the first combination, the gravel size for D_{10} , D_{30} , and D_{60} were taken as the input parameters and the output was the performance of that particular gradation i.e. (WP, PP or NA). In the second combination, the uniformity coefficient (C_u) and coefficient of curvature (C_c) were also included as the inputs in addition to D_{10} , D_{30} , and D_{60} , and the outputs were kept the same as the first combination.

It is generally a good practice to normalize the input features in the dataset before using them for training purposes to achieve better performance. Pre-processing typically accelerates the learning process and balances the focus of the training on all variables by ensuring all variables are treated equally. Therefore, all the data in the database was rescaled from the original range to a common range between 0 and 1 using the normalization equation given in Equation 5.1, where X_{norm} is the normalized value, X_{inp} is the actual input value, X_{min} is the smallest value, and X_{max} is the largest value in the input dataset. This way, the original distribution of the data was retained but scale was changed by applying a uniform scaling factor.

$$X_{norm} = \frac{X_{inp} - X_{min}}{X_{max} - X_{min}} \quad (5.1)$$

The outputs of the ANN model are the categorical data (WP, PP, NA), so they must be encoded to numerical values before use in training. A popular technique, one hot encoding, was used in which each label (class) is mapped to a binary vector. To accomplish this, the categorical value was first transformed into the integer values and then each integer value was represented as a binary vector where all elements are set to zero except for the element at the index corresponding to the integer value which is set to one. Figure 5.3 shows the one hot encoding of the output variables.

Categorical Data	WP	PP	NA
Integer Transformation	0	1	2
One Hot Encoding	[1, 0, 0]	[0, 1, 0]	[0, 0, 1]

Figure 5.3 One Hot Encoding of Categorical Data.

The ANN model was created in a three-step process: (1) training using 70% of the data, (2) testing using 15% of the data, and (3) validating using the remaining 15% of the data in the database. If the model meets the training criteria in the first step, it moves on to the testing step where its performance is evaluated using a previously unseen test dataset. If the model does not meet the training criteria, it returns to the first step for additional training. The type and number of hyperparameters used in the ANN model were decided using the trial-and-error method.

According to Burian et al. (2001), the ability of an ANN model to accurately predict outcomes and the overall accuracy of an application tend to improve as the number of hidden neurons decreases. Selecting the appropriate architecture is a crucial and challenging aspect of developing a neural network model. It involves determining the optimal number of layers and the number of nodes within each layer. There is no standard process for determining an optimal ANN architecture. Therefore, the ANN architecture (number of layers and neurons) was incrementally increased, starting with a single hidden layer containing three neurons, until the predictions improved. The best performing ANN model consisted of one input layer with the aforementioned input parameters, one hidden layer with eight neurons, and one output layer with three outputs.

The proposed neural network utilized the Rectified Linear activation function (ReLU) in the hidden layer, which is a commonly used activation function known for its speed and improved performance. The (ReLU) function is a non-linear activation function that has an output range of $[0, \infty]$. It works by checking the net input of a node. If it is less than zero, the function will output zero, but if it is greater than zero, the output will be the same as the input (Agarap, 2018). Since this is a multiclass classification artificial neural network model where the output represents the class that the input vector belongs to, the softmax activation function that converts the vector of numbers into a vector of probabilities will be used in the output layer as addressed by Bridle (1990). The proposed ANN model architecture with ReLU and softmax activation functions is shown in Figure 5.4.

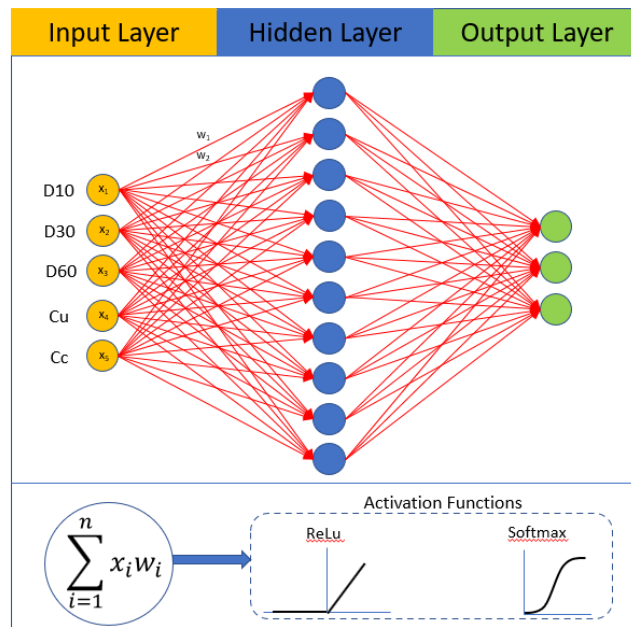


Figure 5.4 Proposed Neural Network Architecture

To train the constructed artificial neural network model, an Adam optimizer proposed by Kingma and Ba (2014) was used. This optimizer is based on the stochastic gradient descent method and is known for its computational efficiency and low memory requirements. The configuration parameters (alpha, beta1, beta2, and epsilon) of this optimizer were kept as default. The categorical cross-entropy loss function was defined during the training process for calculating the difference between the predicted probabilities of a classification model and the actual outputs. This loss function is well-suited for use with the artificial neural network model proposed in this work because the output layer of the model has a softmax activation function. This loss function used in Equation (5.2) to calculate the difference between predicted and actual output, where y is the actual output for a given input and (\hat{y}_i) is the predicted probability for that input.

$$Loss = - \sum_{i=1}^{output\ size} y_i * \log (\hat{y}_i) \quad (5.2)$$

ANN training was initially set to run for 1000 iterations, but it was observed that there was little improvement in the loss value after 300 iterations and the time required to train the network was increasing. As a result, the network was trained for 300 epochs.

Two validation techniques were used to evaluate the performance of the model. The first technique is the hold-out method, in which the data is divided into different sets: one set for training and the other for testing. However, this technique can sometimes lead to a biased model performance. That is why the second validation technique, k-Fold cross validation, is also used.

This technique is considered the golden standard for measuring the performance of an ANN model. In the k-fold cross-validation technique, the data is divided into k subsets and the hold-out method is repeated k times, with each of the k subsets used as the test set and the remaining k-1 subsets used for training. The value of k in this work was selected as five and the average performance from all k tests was calculated. Both validation techniques are shown in Figure 5.5.

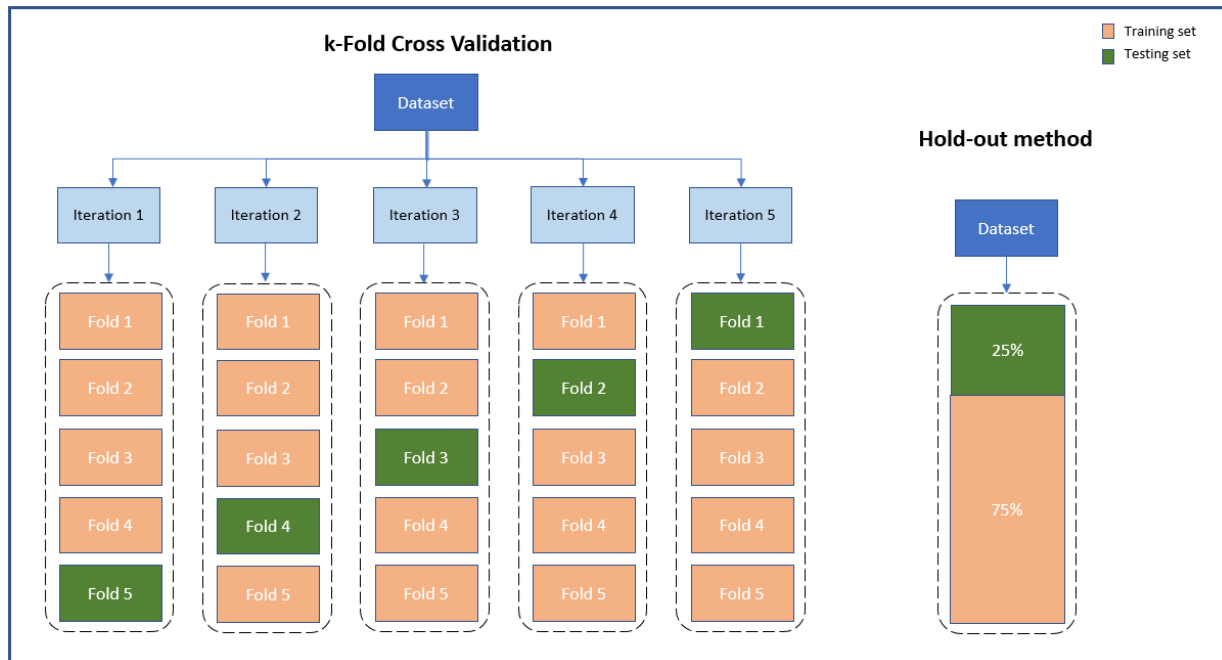


Figure 5.5 Validation Techniques

5.3 Test Results

The best performing ANN model was determined after conducting trials with two combinations of input parameters, different hidden layer neurons, and two different validation methods. Table 5.1 gives information about the various models and the optimal parameter values for each model.

Table 5.1 Various ANN Models Based on Different Parameters.

Input Parameters	Hidden Layers Neurons	Number of Epochs	Hold-out Validation		k-Fold Cross Validation	
			Training Accuracy (%)	Testing Accuracy (%)	Training Accuracy (%)	Testing Accuracy (%)
D ₁₀ , D ₃₀ , D ₆₀	3	32	63.4	66.0	68.0	67.1
	5	64	95.0	92.8	97.5	97.3
	7	128	98.4	98.2	98.7	98.3
	8	300	99.6	1.0	99.0	99.0
D ₁₀ , D ₃₀ , D ₆₀ , C _u , C _c	3	32	78.5	71.4	65.3	65.7
	5	64	96.8	96.4	95.8	95.1
	7	128	98.4	98.2	98.5	97.5
	8	300	99.6	98.2	99.3	99.4

As shown in Table 5.1, there is not much difference in the accuracy values when the C_u and C_c parameters are included in the input layer. Therefore, to reduce the size of the ANN model and the associated computational time, the input parameters in the first combination with only three variables (D₁₀, D₃₀, D₆₀) were chosen.

The accuracy values achieved using the hold-out validation and k-Fold cross validation showed a slight difference mostly because hold-out validation is susceptible to variance, especially if the data is small. Therefore, the accuracy achieved using k-Fold cross validation were accepted as an accurate estimate of the model's generalization performance because this method can better detect overfitting. Various trials were conducted using a combination of different hidden layer sizes and epochs. Initially the training started on a model with three neurons in the hidden layer and trained 32 times. Using this model, an accuracy of approximately

67% was achieved. The model's performance improved as the number of neurons and epochs increased.

The model with eight neurons in the hidden layer and trained on 300 epochs showed the best performance among all the models. The accuracy of the trained model using this combination reached up to 99% both on training and testing data. This indicates the model does not suffer from overfitting. As a result, the overall improvement in the accuracy of the model was 48% from the initial model. Using the ANN model, the erosion resistance behavior of gravel can be predicted with 99% accuracy based on its D_{10} , D_{30} , and D_{60} values obtained from a sieve analysis test. Figure 5.6 illustrates the improvement in the accuracy of the best trained model as the number of iterations increases.

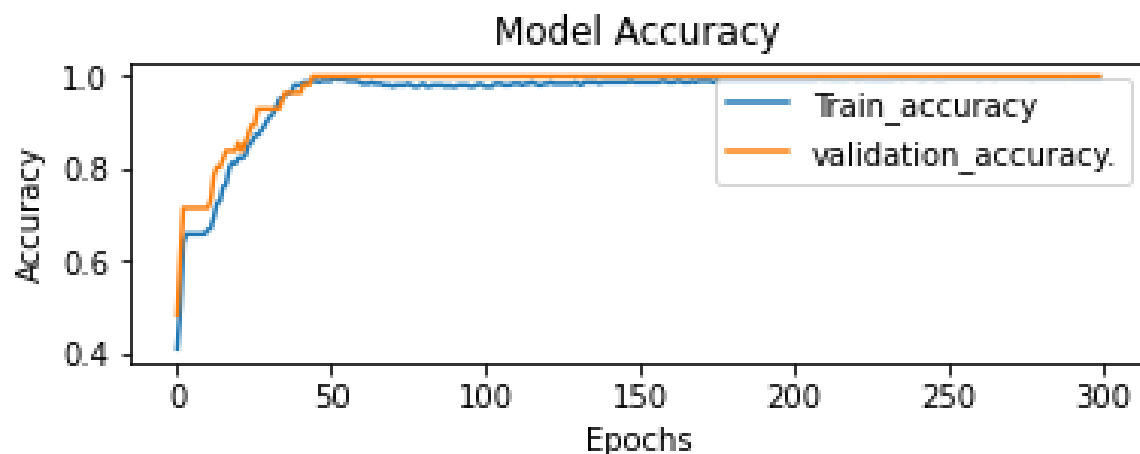


Figure 5.6 Accuracy vs. Epochs of the Trained Model.

The robustness of an ANN model for classification problems is measured by the number of accurate predictions made. This determines how well the model is performing in terms of classification accuracy, and whether the model is effective. For this reason, the confusion matrix is mostly used to evaluate the performance of the ANN classification model. A confusion matrix

provides a summary of how well the model can predict the correct class label for a set of data. Each row of the matrix represents the actual class of a sample, while each column represents the predicted class of the same sample. The elements of the matrix are the number of samples that were predicted as belonging to a certain class. A confusion matrix typically contains four elements: true positive (TP), true negative (TN), false positive (FP), and false negative (FN). It is necessary to obtain these elements to evaluate the model's accuracy, precision, recall, and F1 score and to identify areas for improvement.

True positives denote the number of samples correctly predicted as positive by the model. In other words, it refers to the number of instances where a predicted class matched the actual class for a particular category. These instances were located in the diagonal section (top left to bottom right) of the confusion matrix.

True negatives refer to the number of samples correctly predicted as negative by the model. Basically, it is the count of instances where the model predicted the negative class and the actual class was also negative. True negatives for a specific class were determined by adding up the values in all rows and columns except for the row and column of the class in question.

False positives represent the number of samples that were incorrectly predicted as positive by the model but were actually negative. To put it briefly, it is the count of instances where the model predicted the positive class, but the actual class was negative. False Positives for a particular class were calculated by summing up all the values in the column of that class, excluding the True Positive value.

False negatives refer to the number of samples that were incorrectly predicted as negative by the model but were actually positive. In other words, it is the count of instances where the model predicted the negative class, but the actual class was positive. False Negatives for a

specific class can be determined by adding all the values in the row pertaining to that class, excluding the True Positive value.

The values TP, TN, FP and FN in the confusion matrix can be used to evaluate the ANN model performance using various metrics such as Accuracy, Precision, Recall, and F1 Score.

The accuracy metric represents the overall accuracy of the multiclass classification ANN model. It is defined as the number of correct predictions (True Positives) divided by the sum of all values in the confusion matrix, (i.e., true positives + false positives). The accuracy metric can be calculated using Equation 5.3.

$$Accuracy = \frac{\sum True Positives}{\sum True Positives + \sum False Positives} \quad (5.3)$$

The precision metric represents the ability of the model to correctly identify positive cases as well as measuring the prediction accuracy of a particular class. It is determined by dividing the true positive predictions of a class by the sum of true positives and false positives predictions. The precision metric can be calculated using Equation 5.4.

$$Precision = \frac{True Positive}{True Positive + False Positive} \quad (5.4)$$

Recall metric represents the ability of the model to detect all positive cases. It is calculated as the number of true positive predictions divided by the sum of true positive and false negative predictions, as shown in Equation 5.5.

$$Recall = \frac{True\ Positive}{True\ Positive + False\ Negative} \quad (5.5)$$

The F1 score metric combines the precision and recall measurements into a single value. It is calculated by taking the harmonic mean of the precision and recall values, which gives equal weight to both measurements. A high F1 score means the model is performing well in both identifying positive cases accurately and detecting all positive cases. A low F1 score, on the other hand, indicates the model needs improvement in either precision or recall. The F1 score metric is calculated using Equation 5.6.

$$F1\ Score = 2 * \frac{Precision * Recall}{Precision + Recall} \quad (5.6)$$

The average confusion matrix of the validation dataset using k-Fold cross validation is shown in Figure 5.7. This matrix compares the actual target values (true labels) with those predicted by the ANN model and gives a holistic view of how well the classification model works and what types of mistakes are present. The main diagonal cells (top left to bottom right) represent the average number of correctly predicted outputs, while the off-diagonal cells represent the average number of wrongly predicted outputs across all five folds. The majority of the values in the off-diagonal are zero, indicating the ANN model exhibits excellent classification capabilities. Out of 75 instances in the validation dataset, 74 (27 + 25 + 22) correct predictions were made as presented in the main diagonal. The cell located in the first row and second column indicates a 0.6 sample (or 1 sample) was incorrectly predicted as belonging to the PP class, when it belonged to the WP class. The model accurately predicted the rest of the instances related to the class PP and NA.

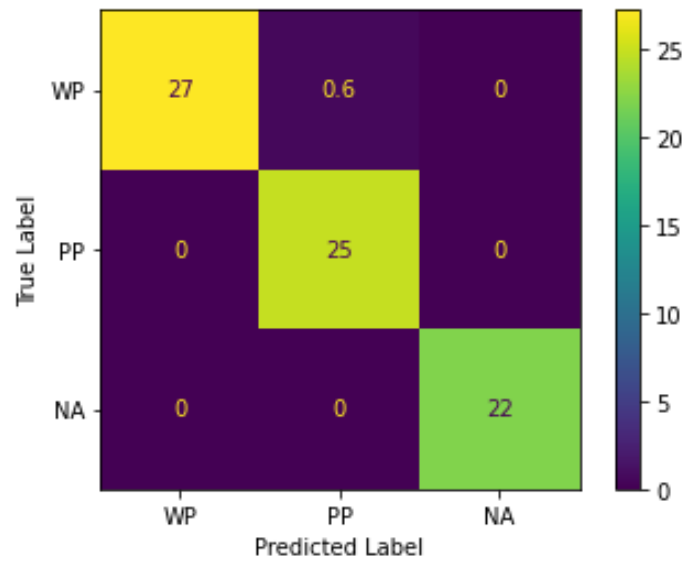


Figure 5.7 Confusion Matrix

The data in the confusion matrix can be used to evaluate the model performance by first calculating the matrix elements i.e., TP, TN, FP, FN and then calculating various metrics based on Equation 5.3-5.6. The values of these confusion matrix elements are calculated in Table 5.2.

Table 5.2 Class-Based True Positives, True Negatives, False Positives, and False Negatives

Metric Class	True Positives	True Negatives	False Positives	False Negatives
WP	27	$25 + 0 + 0 + 22 = 45$	$0 + 0 = 0$	$1 + 0 = 1$
PP	25	$27 + 0 + 0 + 22 = 49$	$1 + 0 = 1$	$0 + 0 = 0$
NA	22	$27 + 1 + 0 + 25 = 53$	$0 + 0 = 0$	$0 + 0 = 0$

The true positive values for the WP, PP, and NA classes from Table 5.2 indicate the model correctly identified 27, 25, and 22 instances as belonging to their respective positive class. In other words, the model made accurate predictions of 27 instances being positive for the WP class, 25 instances being positive for the PP class, and 22 instances being positive for the NA class.

The true negative values for the WP, PP, and NA classes represent the number of instances that the model correctly predicted the instance as belonging to the negative class. The true negative value for the WP class was 45, meaning the model correctly identified 45 instances as not belonging to the WP class. Similarly, the true negative values were 49 and 53 for the PP and NA classes, respectfully.

The false positive values for the WP, PP, and NA classes were calculated as 0, 1, and 0 respectively, meaning the model made one incorrect prediction for the PP class, labeling an instance as positive (i.e., belonging to the PP class) when it was a negative (i.e., not belonging to the PP class). The WP and NA classes did not have any instances of false positive predictions.

A false negative value of 1 for the WP class, 0 for the PP class, and 0 for the NA class means the model incorrectly predicted an instance in the WP class as negative (i.e., not belonging to the WP class) when in fact it was positive (i.e., belonging to the WP class). There were no false negative instances observed for the PP and NA classes.

The performance of the ANN model was calculated using evaluation metrics such as the overall accuracy, class-based precision, recall, and F-score given in Equations 5.3-5.6. The values of these newly calculated matrices are presented in Table 5.3.

Table 5.3 Class-based Precision, Recall and F-Score Values and Overall Accuracy

Metric Class	Precision	Recall	F1 Score	Overall Accuracy
WP	$\frac{27}{27 + 0} = 1$	$\frac{27}{27 + 1} = 0.96$	0.98	99%
PP	$\frac{25}{25 + 1} = 0.96$	$\frac{25}{25 + 0} = 1$	0.98	
NA	$\frac{22}{22 + 0} = 1$	$\frac{22}{22 + 0} = 1$	1	

The precision metrics of the WP, PP, and NA classes were calculated as 1, 0.96, and 1, respectively. A precision of 1 for class WP and NA implies that 100% of the predictions made by the ANN model for the WP and NA classes were accurate, whereas a precision of 0.96 for class PP means that 96% of the predictions made by the model were accurate, i.e., out of all positive cases predicted by the model for class PP, 96% were actually positive.

The recall metrics for the WP, PP, and NA classes were 0.96, 1, and 1, respectively. A recall of 0.96 for class WP suggests that 96% of all positive cases for class WP were correctly predicted by the model, i.e., out of all the actual positive cases for class WP, 96% were predicted as positive by the model. A recall of 1 for class PP and NA means that 100% of all positive cases for class PP and NA were correctly predicted by the model, i.e., all the actual positive cases for class PP and NA were predicted as positive by the model.

The F1 scores for the WP, PP, and NA classes were calculated as 0.98, 0.98, and 1, respectively. An F1 score of 0.98 for class WP and PP indicates that the model had a good balance between precision and recall for class WP and PP respectively. The F1 score for both classes was close to 1, which portrays the model performed exceptionally well. The F1 score of 1

for class NA indicates the model had a perfect balance between precision and recall for class NA. This means the model had perfect accuracy in identifying positive cases (precision) and a perfect ability to detect all positive cases (recall).

The overall accuracy of the ANN model was calculated as 99%. This confirms 99% of all predictions made by the model were correct.

Appendix C includes a user manual for the presented AI approach.

Chapter 6 Conclusions

The main objective of this study was to evaluate the erosion resistance of the materials used for highway shoulders. To efficiently test those relatively large materials, a new testing device called the University of Nebraska-Lincoln Erosion Testing Bed (UNLETB) was fabricated. The materials were tested to compare erosion behavior, then the low erosion resistance materials were treated using three different biopolymers and polymers: Lignosulfonate, soybean soap stock, and DirtGlue. In addition, a hydrodynamic-based erosion analysis was conducted using FLOW3D-Hydro to calibrate the UNLETB testing device to a numerical model. An extensive parametric study was conducted to get the proper values of the input parameters for the sediment transport model. Finally, an AI approach was proposed to quickly determine whether a certain material was suitable for use in the shoulders based on their D_{10} , D_{30} , and D_{60} results. The findings of this research can be concluded in the following points:

1) Erosion Testing Device

- The University of Nebraska-Lincoln Erosion Testing Bed (UNLETB) was fabricated to test the large size materials.
- UNLETB turned out to be a reliable and efficient method to evaluate the erosion resistance of the highway shoulder materials.

2) Erosion Test Results for Untreated Samples

- The 1.5 in. Rock Agg sample showed the highest erosion resistance.
- The Combined Package Class A (with fines without fines), 1 in. Coarse, 1 in. Clean, 1.5 in. Crusher Run, and 1 in. Crusher Run showed good erosion resistance.

- The Class 2A, Class B, and Gravel Surface Course samples showed weak erosion resistance. Therefore, binding agents were applied to enhance their erosion resistance.

3) Erosion Test Results for Treated Samples

- Three environmentally friendly binding agents were used to improve the erosion resistance for the materials that showed a weak erosion resistance; the binding agents were Ammonium Lignosulfonate (LIGNO10), Soybean Soap Stock, and DirtGlue.
- The treatment efficiency varies depending on the sample and the used biopolymers/polymers.
- The 1 in. Coarse, 1 in. Clean, Class 2A, Class B, and Gravel Surface Course samples showed no erosion when treated with DirtGlue.
- The 1 in. Coarse, 1 in. Clean, Class 2A, Class B, and Gravel Surface Course samples showed a significant enhancement in erosion resistance when treated with LIGNO10. The observed erosion mechanism was an initial watertight layer, which caused a delay in the erosion.
- The 1 in. Coarse, 1 in. Clean, Class 2A, Class B, and Gravel Surface Course samples showed a slight enhancement in the erosion resistance when treated with soybean soap stock. The erosion mechanism observed a reduction of the fluid induced shear stress due to the oily coat around the particles.

4) Hydrodynamics-based simulation

- FLOW3D-Hydro was used to model UNLETB, and the numerical model was calibrated to match the computed results with the experimental.

- A comprehensive parametric study was conducted to demonstrate the effect of each input parameter on UNLETB erosion profile, and the sensitivity of the model to each parameter.

5) Artificial Intelligence Approach

- The ANN model achieved high accuracy levels in its predictions and was able to distinguish between the different erosion behavior of shoulder rocks within these three groups based on information from gradation curves. Extensive examination of the model's performance using diverse methodologies yielded exceptionally favorable outcomes.
- This model provides valuable insights into the behavior of shoulder rocks under erosion and can support engineers and researchers in making informed decisions regarding shoulder rock selection for erosion applications.
- The successful implementation of the ANN classification model, combined with its ability to accurately categorize erosion into three groups, highlights the potential for the application of machine learning techniques in solving complex problems in the field of geotechnical engineering.

References

- AASHTO (2008). "Driving Down Lane-Departure Crashes: A National Priority". American Association of State Highway and Transportation Officials, Washington, D.C. 20001.
- Ackers, P., & White, W. R. (1973). Sediment transport: new approach and analysis. *Journal of the Hydraulics Division*, 99(11), 2041-2060.
- AASHTO (2008). "Driving Down Lane-Departure Crashes: A National Priority". American Association of State Highway and Transportation Officials, Washington, D.C. 20001.
- Ackers, P., & White, W. R. (1973). Sediment transport: new approach and analysis. *Journal of the Hydraulics Division*, 99(11), 2041-2060.
- Agarap, A. F. (2018). Deep learning using rectified linear units (relu). *arXiv preprint arXiv:1803.08375*.
- Aguirre-Pe, J., & Fuentes, R. (1990). Resistance to flow in steep rough streams. *Journal of Hydraulic Engineering*, 116(11), 1374-1387.
- Al-Madhhachi, A. T., Hanson, G. J., Fox, G. A., Tyagi, A. K., & Bulut, R. (2013). MEASURING SOIL ERODIBILITY USING A LABORATORY "MINI" JET. *Transactions of the ASABE*, 56(3), 901–910.
- ASCE Task Committee on Application of Artificial Neural Networks in Hydrology. (2000). Artificial neural networks in hydrology. I: Preliminary concepts. *Journal of Hydrologic Engineering*, 5(2), 115-123.
- Bayram, A., Camenen, B., & Larson, M. (2003). Equivalent roughness under sheet flow conditions. In *Proc. Coastal Sediment (Vol. 3)*.
- Bray, D. I. (1979). Estimating average velocity in gravel-bed rivers. *Journal of the Hydraulics Division*, 105(9), 1103-1122.
- Briaud, J. L., Govindasamy, A. V. and Shafii, I. (2017), "Erosion Charts for Selected Geomaterials," *J. Geotech. Geoenviron. Eng.*, 2017, 143(10): 04017072.
- Briaud, J. L., Ting, F. K. C., Chen, H. C., Cao, Y., Han, S. W., Kwak, K. W., & Member, S. (2001). EROSION FUNCTION APPARATUS FOR SCOUR RATE PREDICTIONS. 5(February), 105–113.
- Briaud, J., Ting, F. C. K., Chen, H. C., Gudavalli, R., Perugu, S., & Member, S. (1999). SRICOS: PREDICTION OF SCOUR RATE IN COHESIVE SOILS AT BRIDGE PIERS. 125(April), 237–246.

- Bridle, J. S. (1990). Probabilistic interpretation of feedforward classification network outputs, with relationships to statistical pattern recognition. In *Neurocomputing* (pp. 227-236). Springer, Berlin, Heidelberg.
- Buffington, J. M. (1999). THE LEGEND OF A. F. SHIELDS. *Journal of Hydraulic Engineering*, 125(4).
- Burian, S. J., Durrans, S. R., Nix, S. J., & Pitt, R. E. (2001). Training artificial neural networks to perform rainfall disaggregation. *Journal of Hydrologic Engineering*, 6(1), 43-51.
- Bushman, W. H., Freeman, T. E., & Hoppe, E. J. (2005). Stabilization techniques for unpaved roads. *Transportation Research Record*, 1936, 28–33. <https://doi.org/10.3141/1936-04>
- Camenen, B., Bayram, A., & Larson, M. (2006). Equivalent roughness height for plane bed under steady flow. *Journal of Hydraulic Engineering*, 132(11), 1146-1158.
- Chapuis, R. P., & Gatien, T. (1986). An improved rotating cylinder technique for quantitative measurements of the scour resistance of clays. *Canadian Geotechnical Journal*, 23(1), 83–87. <https://doi.org/10.1139/t86-010>
- Colosimo, C., Copertino V, A., and Veltri, M (1986). Average velocity estimation in gravel-bed rivers. In *Fifth Congress Asian and Pacific Regional Division of the IAHR* (Vol. 2, pp. 1-16).
- Dey, S., & Ali, S. Z. (2019). Bed sediment entrainment by streamflow: State of the science. *Sedimentology*, 66(5), 1449–1485. <https://doi.org/10.1111/sed.12566>
- Einstein, H. A., & Barbarossa, N. L. (1952). River channel roughness. *Transactions of the American Society of civil Engineers*, 117(1), 1121-1132.
- Fox, B., & Feurich, R. (2019). CFD analysis of local scour at bridge piers.
- Garcia, M. H. (2008). *Sedimentation Engineering: Processes, Measurements, Modeling, and Practice*. ASCE. <https://doi.org/10.1061/9780784408148>
- Gladki, H. (1979). Resistance to flow in alluvial channels with coarse bed materials. *Journal of hydraulic research*, 17(2), 121-128.
- Guo, F., Guerra, M., Jahren, C., & White, D. (2013). Pilot construction project for granular shoulder stabilization. https://lib.dr.iastate.edu/intrans_reports/96
- Hammond, F. D. C., Heathershaw, A. D., & Langhorne, D. N. (1984). A comparison between Shields' threshold criterion and the movement of loosely packed gravel in a tidal channel. *Sedimentology*, 31(1), 51-62.
- Hanson, G. J., & Cook, K. R. (2004). Apparatus, test procedures, and analytical methods to measure soil erodibility in situ. *Applied Engineering in Agriculture*, 20(4), 455–462.

- Hanson, G. J., Cook, K. R., & Hunt, S. L. (2005). PHYSICAL MODELING OF OVERTOPPING EROSION AND BREACH FORMATION OF COHESIVE EMBANKMENTS. 48(5), 1783–1794.
- Hanson, G. J., Robinson, K. M., & Cook, K. R. (2002). SCOUR BELOW AN OVERFALL: PART II. PREDICTION. 45(1), 957–964.
- Harris, T. M., & Boardman, J. (1998). Alternative approaches to soil erosion prediction and conservation using expert systems and neural networks. In *Modelling soil erosion by water* (pp. 461–477). Springer, Berlin, Heidelberg.
- Hey, R. D. (1979). Flow resistance in gravel-bed rivers. *Journal of the Hydraulics Division*, 105(4), 365–379.
- Irmay, S. (1949). On steady flow formulae in pipes and channels. In *Proc., IAHR 3rd Congress*.
- Ikeda, H. (1983). Experiments on bedload transport, bed forms, and sedimentary structures using fine gravel in the 4-meter-wide flume. *Environmental Research Center Papers*, 2, 1–78.
- Jang, W., Song, C. R., Kim, J., Cheng, A. H.-D., & Al-Ostaz, A. (2011). Erosion Study of New Orleans Levee Materials Subjected to Plunging Water. *Journal of Geotechnical and Geoenvironmental Engineering*, 137(4), 398–404. [https://doi.org/10.1061/\(asce\)gt.1943-5606.0000439](https://doi.org/10.1061/(asce)gt.1943-5606.0000439)
- Junliang, T., Zhe L. and Pandey, G. (2017), "Evaluation of Post Flooding Shoulder Reconditioning." Ohio DOT, FHWA/OH-2017-1
- Kamphuis, J. W. (1974). Determination of sand roughness for fixed beds. *Journal of Hydraulic Research*, 12(2), 193–203.
- Katul, G., Wiberg, P., Albertson, J., & Hornberger, G. (2002). A mixing layer theory for flow resistance in shallow streams. *Water Resources Research*, 38(11), 32–1.
- Keulegan, G. H. (1938). *Laws of turbulent flow in open channels* (Vol. 21, pp. 707–741). Gaithersburg, MD, USA: National Bureau of Standards.
- Kidd, J. T., Song, C. R., Al-Ostaz, A., Cheng, A. H.-D., & Jang, W. (2011). Erosion Control Using Modified Soils. *International Journal of Erosion Control Engineering*, 4(1), 1–9. <https://doi.org/10.13101/ijece.4.1>
- Kingma, D. P., & Ba, J. (2014). Adam: A method for stochastic optimization. *arXiv preprint arXiv:1412.6980*.
- Lane, E. W., & Carlson, E. J. (1953). Some factors affecting the stability of canals constructed in coarse granular materials. In *Proceedings: Minnesota International Hydraulic Convention* (pp. 37–48). ASCE.
- Leopold, L. B., Wolman, M. G., & Miller, J. P. (1964). *Fluvial processes in geomorphology*.

- Licznar, P., & Nearing, M. A. (2003). Artificial neural networks of soil erosion and runoff prediction at the plot scale. *Catena*, 51(2), 89-114.
- Limerinos, J. T. (1970). Determination of the Manning coefficient from measured bed roughness in natural channels (Vol. 1898). Washington, DC: US Government Printing Office.
- Mahmood, K. (1972). Flow in sand-bed channels.
- Maine DOT, T. R. D. (2007). "Utilizing lignosulfonates for gravel shoulder stabilization." Maine DOT Transportation Research Division.
- Mastbergen, D. R., & Van Den Berg, J. H. (2003). Breaching in fine sands and the generation of sustained turbidity currents in submarine canyons. *Sedimentology*, 50(4), 625–637. <https://doi.org/10.1046/j.1365-3091.2003.00554.x>
- Meyer-Peter, E., & Müller, R. (1948). Formulas for bed-load transport. *Proceedings of the 2nd Meeting of the International Association for Hydraulic Structures Research*, 39–64.
- Moore, L., & Masch, F. D. (1962). Experiments on the Scour Resistance of Cohesive Sediment. 67(4).
- Nielsen, P. (1992). *Coastal Bottom Boundary Layers and Sediment Transport*. World Scientific.
- Nikuradse, J. (1950). Laws of Flow in Rough Pipes. *Journal of Applied Physics*, 3(November), 399. <http://scholar.google.com/scholar?hl=en&btnG=Search&q=intitle:LAWS+OF+FLOW+IN+ROUGH+PIPES#0>
- Richardson, J., & Zaki, W. N. (1954). Sedimentation and fluidisation: Part I. *Transactions of the Institution of Chemical Engineers*.
- Roosevelt, D. S. (2005). "Use of Soil Stabilizers on Highway Shoulders." Virginia Department of Transportation 36 p.
- Shahin, M. A., Jaksa, M. B., & Maier, H. R. (2008). State of the art of artificial neural networks in geotechnical engineering. *Electronic Journal of Geotechnical Engineering*, 8(1), 1-26.
- Shaikh, A., Ruff, J. F., & Abt, S. R. (1988). EROSION RATE OF COMPACTED NAMONTMORILLONITE SOILS. 114(3), 296–305.
- Shaikh, B. A., Ruff, J. F., Charlie, W. A., & Abt, S. R. (1988). EROSION RATE OF DISPERSIVE AND NONDISPERSIVE CLAYS. 114(5), 589–600.
- Shields, A. (1936). Application of similarity principles and turbulence research to bed-load movement.
- Shirmohammadi, A. (2004). Soil/Aggregate Mix for Highway Shoulders.

- Simons, D. B., & Richardson, E. V. (1966). Resistance to flow in alluvial channels. US Government Printing Office.
- Simon, A., Thomas, R. E., & Klimetz, L. (2010). Comparison and Experiences With Field Techniques To Measure Critical. 2nd Joint Federal Interagency Conference, Las Vegas, 826, 13.
- Song, C.R., Al-Ostaz, A., Cheng, A. H.-D. and Mantena, R. P. (2012), Structural, Material, and Geotechnical Solutions to Levee and Floodwall Construction and Retrofitting, Vol. II, Final Report Submitted to DHS/SERRI, 400p.
- Song, C. R., Kim, J., Wang, G., & Cheng, A. H.-D. (2011). Reducing Erosion of Earthen Levees Using Engineered Flood Wall Surface. *Journal of Geotechnical and Geoenvironmental Engineering*, 137(10), 874–881. [https://doi.org/10.1061/\(asce\)gt.1943-5606.0000500](https://doi.org/10.1061/(asce)gt.1943-5606.0000500)
- Soulsby, R. (1997). Dynamics of marine sands.
- Strickler, A. (1981). Contributions to the question of a velocity formula and roughness data for streams, channels and closed pipelines.
- Tao, J., Luo, Z., & Pandey, G. (2017). Evaluation of post flooding shoulder reconditioning. <http://cdm16007.contentdm.oclc.org/cdm/ref/collection/p267401ccp2/id/14690>
- Thompson, S. M., & Campbell, P. L. (1979). Hydraulics of a large channel paved with boulders. *Journal of Hydraulic Research*, 17(4), 341-354.
- US ARMY (2020), US Army field Manual 5-430-00-1, accessed Dec. 3, 2020, <https://www.globalsecurity.org/military/library/policy/army/fm/5-430-00-1/CH5.htm>
- USDA (2017), Agricultural Engineering Technical Note No. AEN-4, 63p. accessed Dec. 3, 2020
- van Rijn, L. (1984). Sediment Transport, Part I: Bed load transport. *Journal of Hydraulic Engineering*, 110(10), 1431–1456.
- White, D. J., Jahren, C. T., Suleiman, M., & Mekkawy, M. (2007). Effective Shoulder Design and Maintenance.
- Whiting, P. J., & Dietrich, W. E. (1990). Boundary shear stress and roughness over mobile alluvial beds. *Journal of hydraulic engineering*, 116(12), 1495-1511.
- Wilson, K. C. (1987). Analysis of bed-load motion at high shear stress. *Journal of Hydraulic Engineering*, 113(1), 97-103.
- Yalin, M.S. (1992) *River Mechanics*. Pergamon, Oxford. Excerpted from (Dey and Ali 2019)

Appendix A Sieve Analysis Test Results

Table A.1 Sieve Analysis Results for 1.5 in. Rock Agg Sample

Standard Sieves	Sieve size (in.)	Sieve size (mm)	% Retained	% Passing
1 1/2"	1.5	38.1	11.46	88.54
1"	1	25.4	65.6	34.4
3/4"	0.75	19.05	92.09	7.91
1/2"	0.5	12.7	100	0

Table A.2 Sieve Analysis Results for 1.5 in. Crusher Run Sample

Standard Sieves	Sieve size (in.)	Sieve size (mm)	% Retained	% Passing
1 1/2"	1.5	38.1	0	100
1"	1	25.4	0	100
3/4"	0.75	19.05	20.42	79.58
1/2"	0.5	12.7	58.72	41.28
3/8"	0.375	9.525	77.13	22.87
#4	0.187	4.75	96.09	3.91
#10	0.0787	2	99.94	0.06

Table A.3 Sieve Analysis Results for 1 in. Clean Sample

Standard Sieves	Sieve size (in.)	Sieve size (mm)	% Retained	% Passing
1 1/2"	1.5	38.1	0	100
1"	1	25.4	0	100
3/4"	0.75	19.05	4.72	95.28
1/2"	0.5	12.7	46	54
3/8"	0.375	9.525	80.59	19.41
#4	0.187	4.75	99.3	0.7
#10	0.0787	2	99.62	0.38

Table A.4 Sieve Analysis Results for 1 in. Coarse Sample

Standard Sieves	Sieve size (in.)	Sieve size (mm)	% Retained	% Passing
1 1/2"	1.5	38.1	0	100
1"	1	25.4	6.17	93.83
3/4"	0.75	19.05	28.93	71.07
1/2"	0.5	12.7	59.06	40.94
3/8"	0.375	9.525	75.79	24.21
#4	0.187	4.75	94.77	5.23
#10	0.0787	2	99.88	0.12

Table A.5 Sieve Analysis Results for 1 in. Crusher Run Sample

Standard Sieves	Sieve size (in.)	Sieve size (mm)	% Retained	% Passing
1 1/2"	1.5	38.1	0	100
1"	1	25.4	0	100
3/4"	0.75	19.05	3.61	96.39
1/2"	0.5	12.7	22.21	77.79
3/8"	0.375	9.525	39.86	60.14
#4	0.187	4.75	77.38	22.62
#10	0.0787	2	97.04	2.96

Table A.6 Sieve Analysis Results for Gravel Surface Course Sample

Standard Sieves	Sieve size (in.)	Sieve size (mm)	% Retained	% Passing
1 1/2"	1.5	38.1	0	100
1"	1	25.4	2.06	97.94
3/4"	0.75	19.05	5.79	94.21
1/2"	0.5	12.7	13.87	86.13
3/8"	0.375	9.525	20.2	79.8
#4	0.187	4.75	45.62	54.38
#10	0.0787	2	88.39	11.61
#20	0.0335	0.85	97.99	2.01
#60	0.0098	0.25	99.91	0.09
#140	0.0042	0.106	99.97	0.03

Table A.7 Sieve Analysis Results for Class B Sample

Standard Sieves	Sieve size (in.)	Sieve size (mm)	% Retained	% Passing
1 1/2"	1.5	38.1	0	100
1"	1	25.4	0	100
3/4"	0.75	19.05	0	100
1/2"	0.5	12.7	0.41	99.59
3/8"	0.375	9.525	7.01	92.99
#4	0.187	4.75	31.21	68.79
#10	0.0787	2	61.83	38.17
#20	0.0335	0.85	81.58	18.42
#60	0.0098	0.25	98.17	1.83
#140	0.0042	0.106	99.92	0.08

Table A.8 Sieve Analysis Results for Class 2A Sample

Standard Sieves	Sieve size (in.)	Sieve size (mm)	% Retained	% Passing
1 1/2"	1.5	38.1	0	100
1"	1	25.4	0	100
3/4"	0.75	19.05	0	100
1/2"	0.5	12.7	1	99
3/8"	0.375	9.525	2.16	97.84
#4	0.187	4.75	16.46	83.54
#10	0.0787	2	75.48	24.52
#20	0.0335	0.85	95.76	4.24
#60	0.0098	0.25	99.79	0.21
#140	0.0042	0.106	99.94	0.06

Table A.9 Sieve Analysis Results for Combined Package Class A without Fines Sample

Standard Sieves	Sieve size (in.)	Sieve size (mm)	% Retained	% Passing
1 1/2"	1.5	38.1	0	100
1"	1	25.4	0	100
3/4"	0.75	19.05	1.88	98.12
1/2"	0.5	12.7	37.34	62.66
3/8"	0.375	9.525	62.26	37.74
#4	0.187	4.75	90.81	9.19
#10	0.0787	2	99.46	0.54

Table A.10 Sieve Analysis Results for Combined Package Class A with Fines Sample

Standard Sieves	Sieve size (in.)	Sieve size (mm)	% Retained	% Passing
1"	1	25.4	0	100
3/4"	0.75	19.05	3.46	96.54
1/2"	0.5	12.7	30.98	69.02
3/8"	0.375	9.525	52.05	47.95
#4	0.187	4.75	74.91	25.09
#10	0.0787	2	88.69	11.31
#20	0.0335	0.85	93.74	6.26
#60	0.0098	0.25	96.78	3.22
#140	0.0042	0.106	98.03	1.97
#200	0.003	0.075	98.49	1.51

Appendix B Individual Erosion Curves

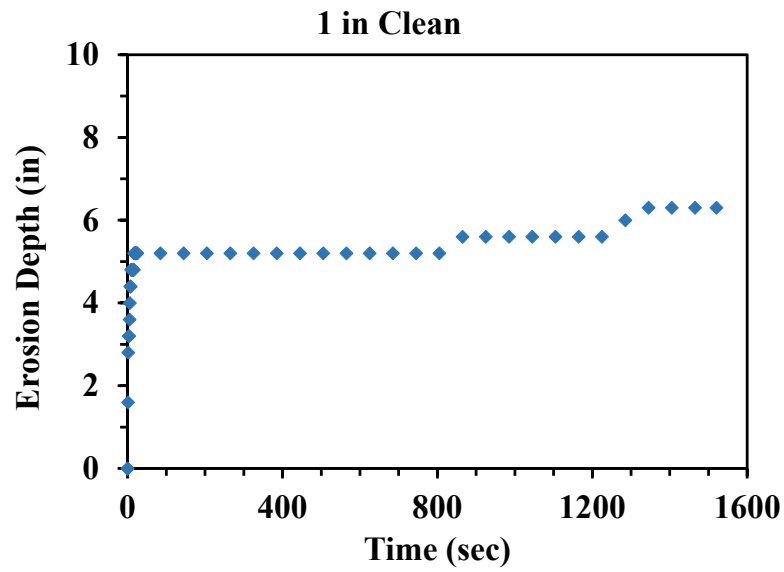


Figure B.1 Erosion Curve for 1 in. Clean Sample (Initial Results)

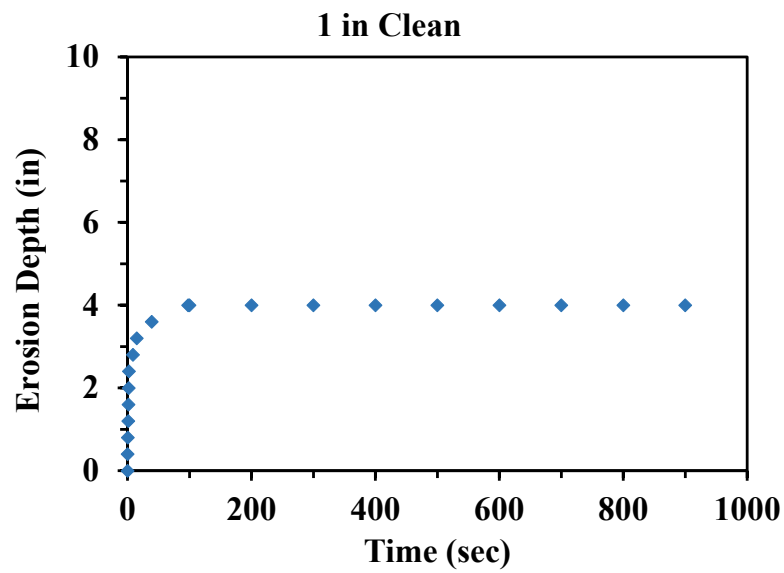


Figure B.2 Erosion Curve for 1 in. Clean Sample (Updated Results)

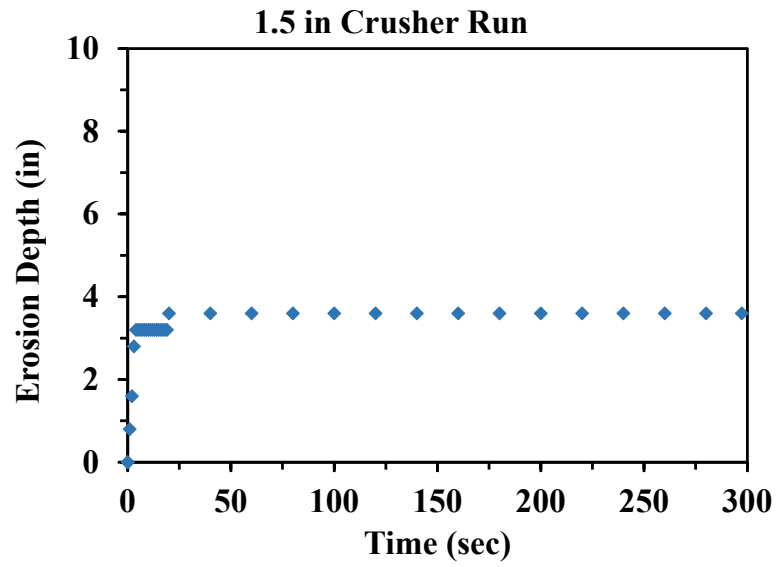


Figure B.3 Erosion Curve for 1.5 in. Crusher Run Sample

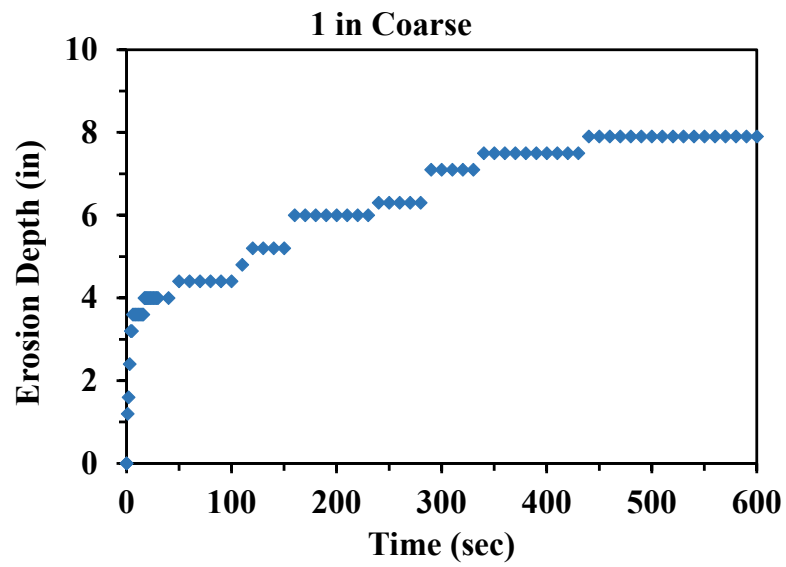


Figure B.4 Erosion Curve for 1 in. Coarse Sample (Initial Results)

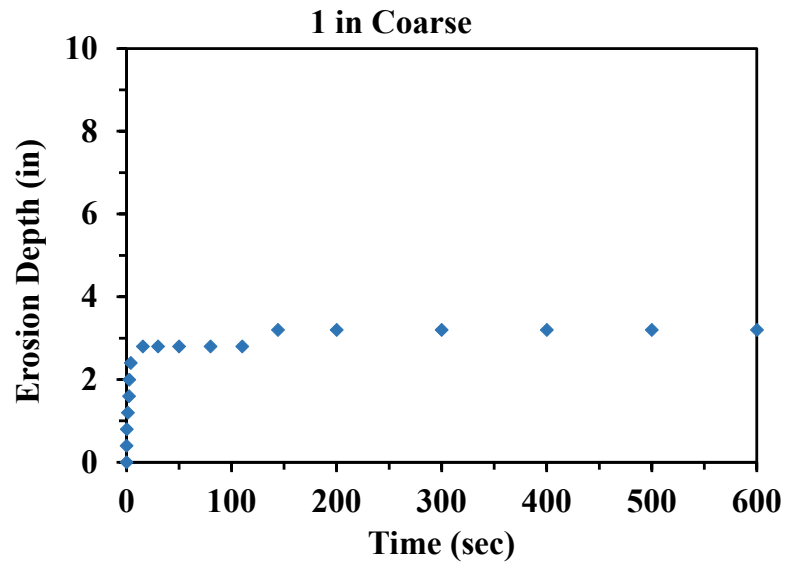


Figure B.5 Erosion Curve for 1 in. Coarse Sample (Updated Results)

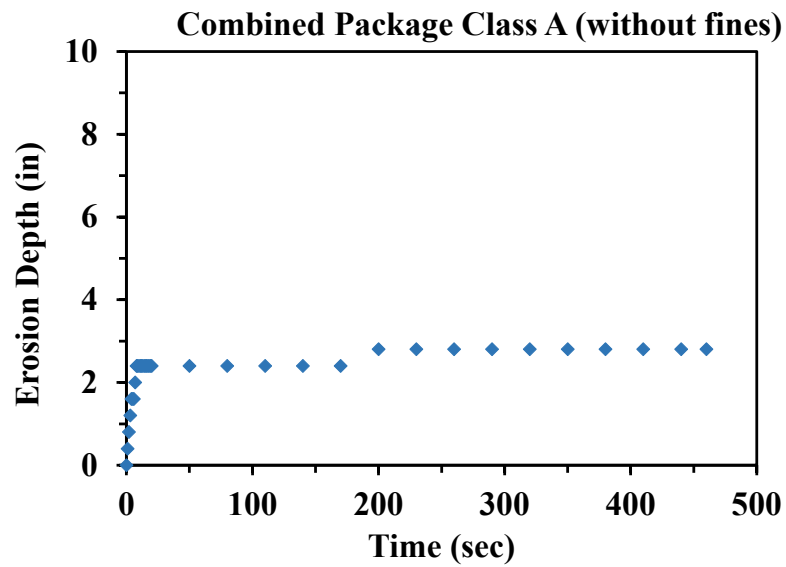


Figure B.6 Erosion Curve for Combined Package Class A (without fines) Sample

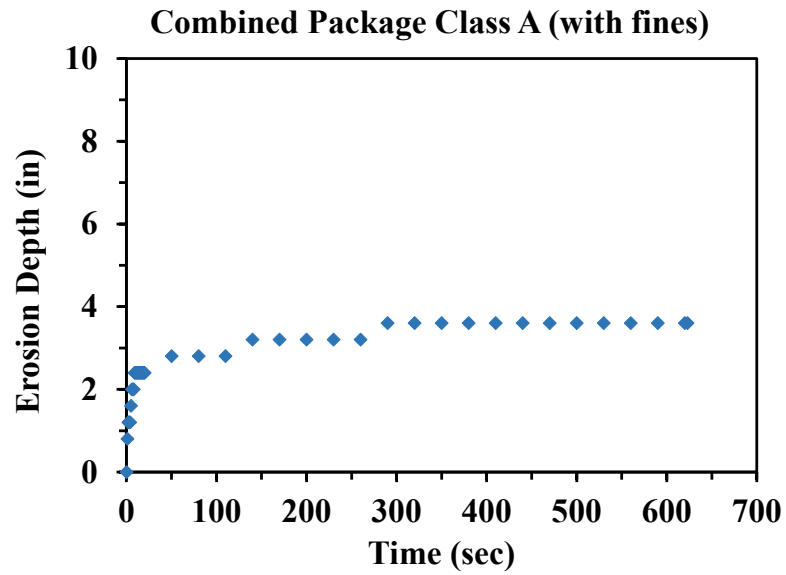


Figure B.7 Erosion Curve for Combined Package Class A (with fines) Sample

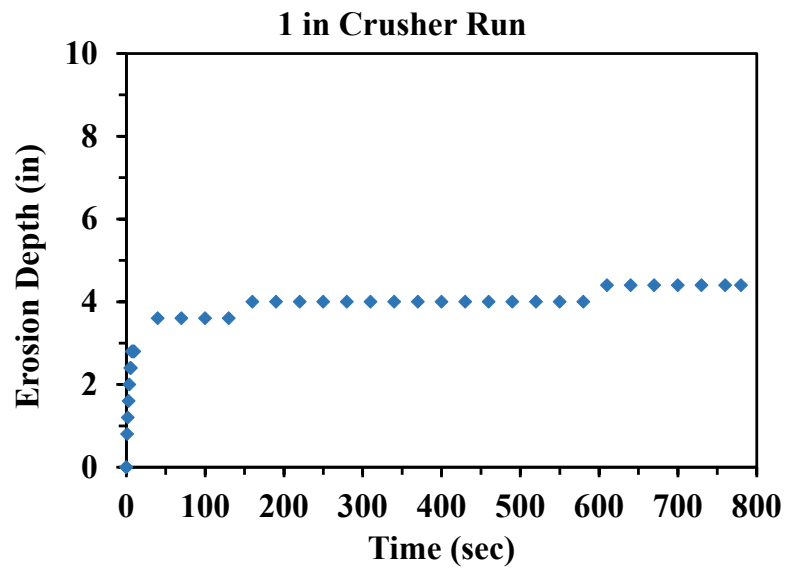


Figure B.8 Erosion Curve for 1 in. Crusher Run Sample

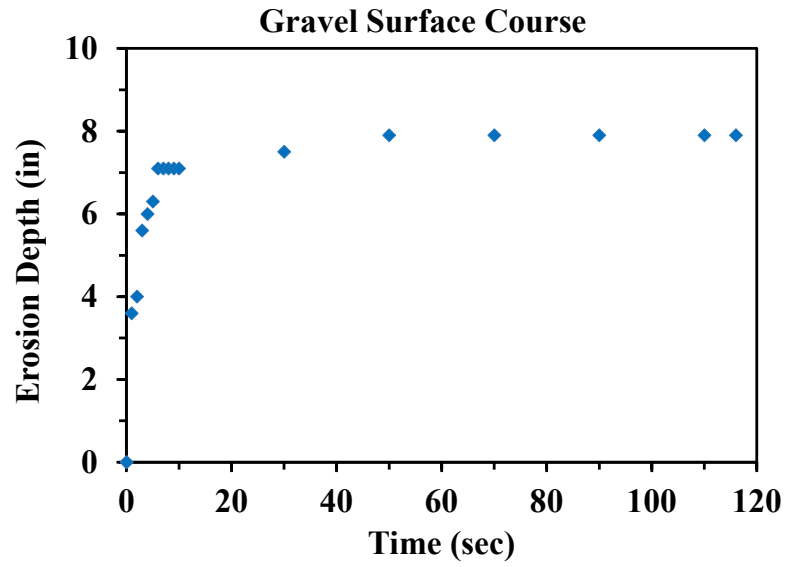


Figure B.9 Erosion Curve for Gravel Surface Course Sample

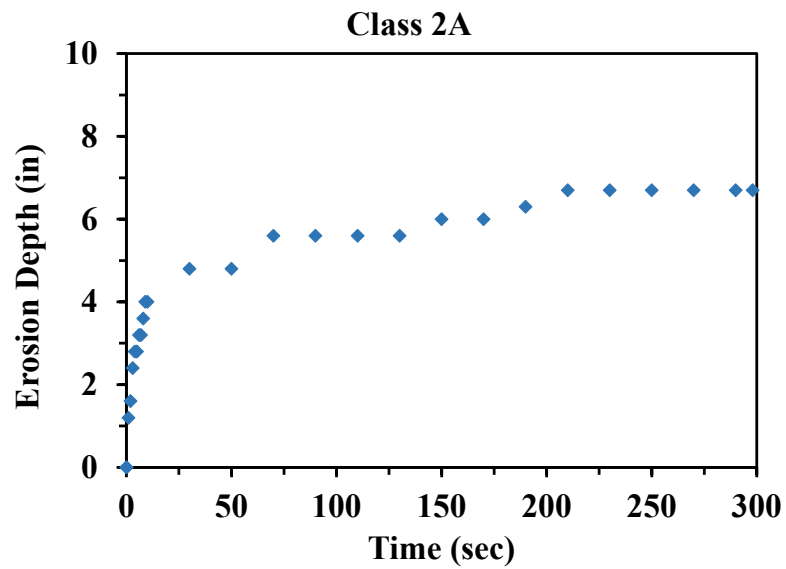


Figure B.10 Erosion Curve for Class 2A Sample

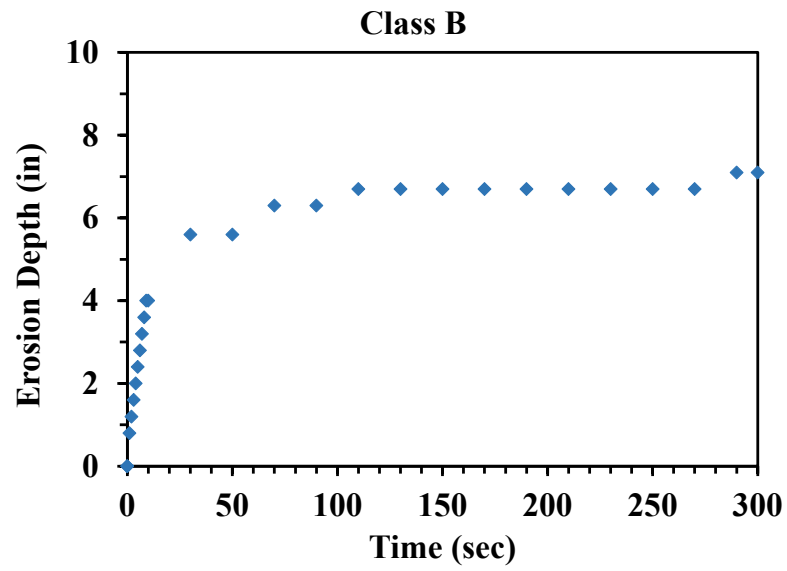


Figure B.11 Erosion Curve for Class B Sample

Appendix C User Manual and Interface for the AI-Approach

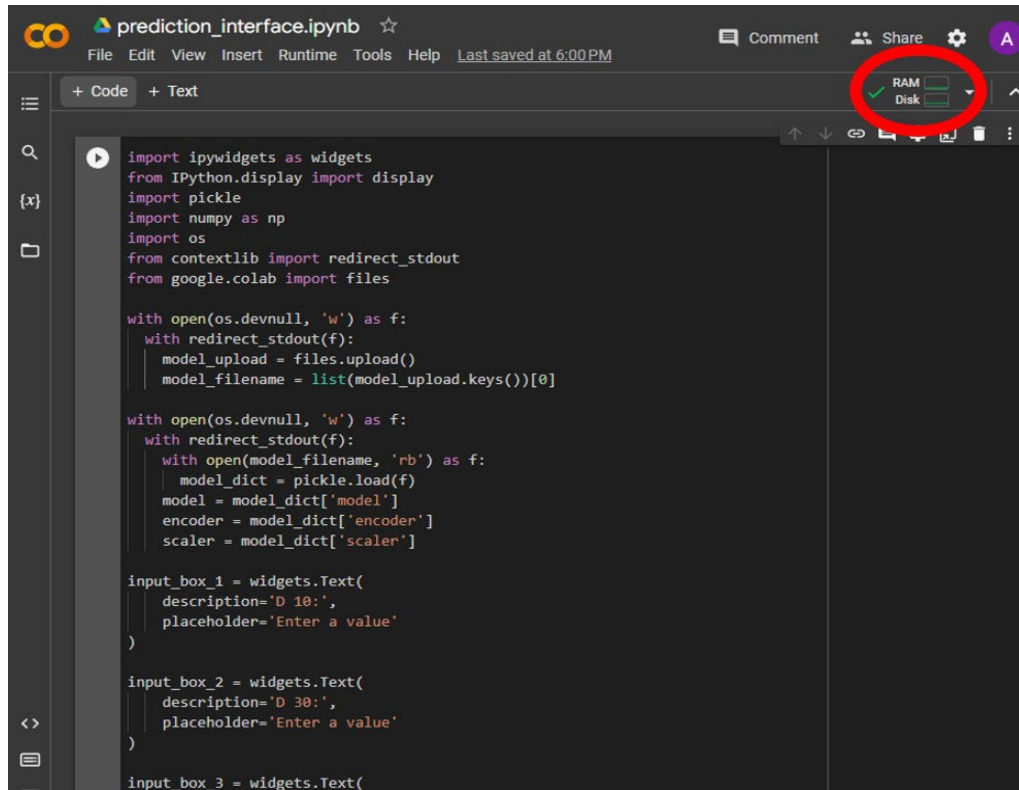
Step 1 – Uploading the prediction_interface.ipynb file to the Google Colab

1. Open your web browser and navigate to the Google Colab website (colab.research.google.com).
2. Click on “Sign in” in the top right corner and sign in with your Google account credentials.
3. Once you are signed in, click on “New notebook” to create a new Colab notebook.
4. A new notebook will open. Click on “File” in the top left-hand corner of the notebook.
5. Click on “Upload notebook” from the dropdown menu.
6. A file explorer window will open. Locate the prediction_interface.ipynb file on your computer and select it.
7. The prediction_interface.ipynb file will start uploading to Colab. Wait for the upload to complete.
8. Click on “Connect” in the upper right-hand corner of the notebook. Wait for a few seconds until the green tick mark appears.

Step 2 – Executing the prediction_interface.ipynb notebook

1. Execute the code by clicking on the play button or using the shortcut Shift+Enter.
2. Upload the saved ANN model file (i.e ann_model.pkl) using the ‘Choose File’ widget at the bottom of the code and wait for the upload to complete.
3. Enter the D_{10} , D_{30} , and D_{60} values in the three input boxes displayed. Make sure to enter a value in all three input boxes.
4. Click on the "Predict" button to predict the output of values entered in the input boxes.

5. To make more predictions, there is no need to execute the whole code again from the start. Just clear the previous input values and hit the predict button.



```
import ipywidgets as widgets
from IPython.display import display
import pickle
import numpy as np
import os
from contextlib import redirect_stdout
from google.colab import files

with open(os.devnull, 'w') as f:
    with redirect_stdout(f):
        model_upload = files.upload()
        model_filename = list(model_upload.keys())[0]

with open(os.devnull, 'w') as f:
    with redirect_stdout(f):
        with open(model_filename, 'rb') as f:
            model_dict = pickle.load(f)
            model = model_dict['model']
            encoder = model_dict['encoder']
            scaler = model_dict['scaler']

input_box_1 = widgets.Text(
    description='D 10:',
    placeholder='Enter a value'
)

input_box_2 = widgets.Text(
    description='D 30:',
    placeholder='Enter a value'
)

input_box_3 = widgets.Text(
```

Figure C.1 Step 1 Uploading the prediction_interface.ipynb File to the Google Colab

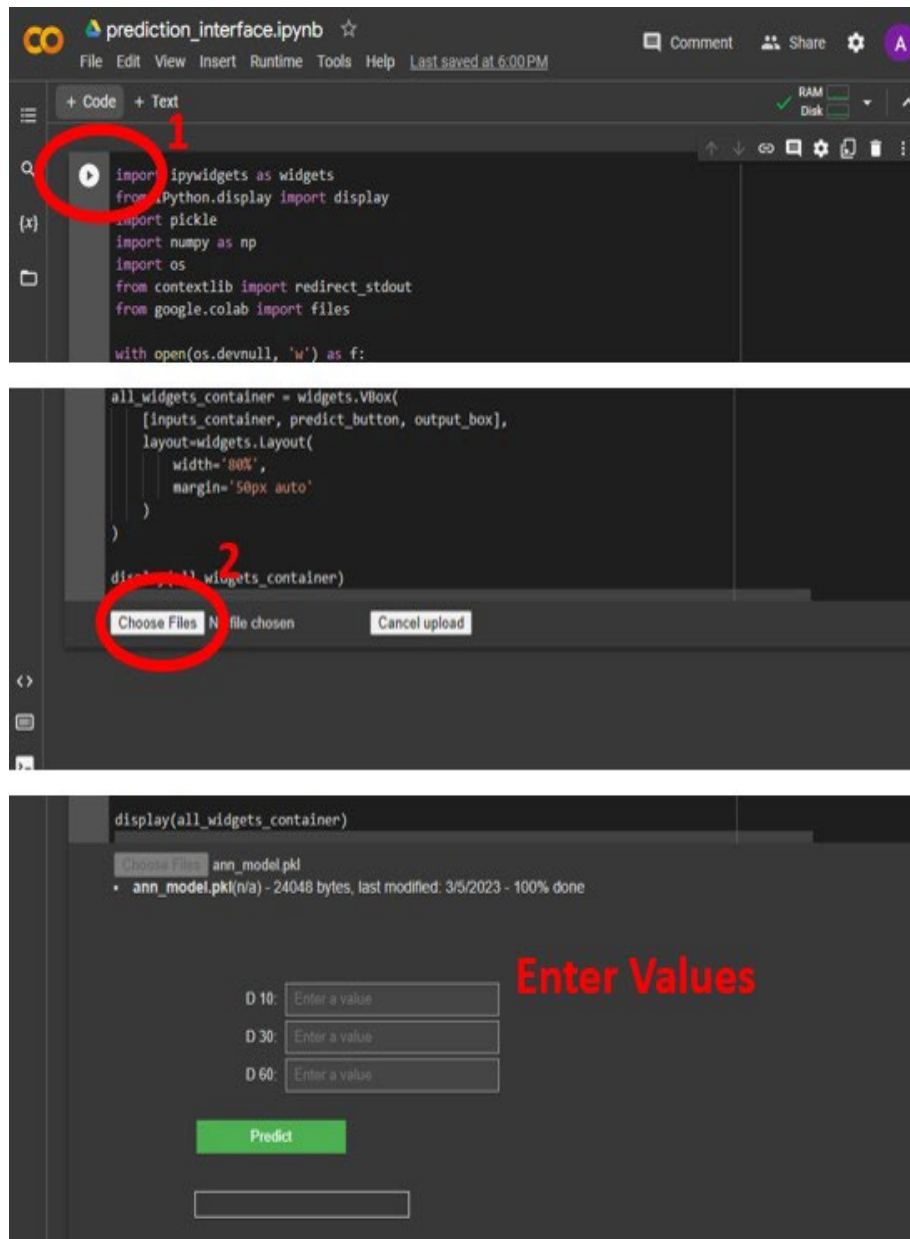


Figure C.2 Step 2 Executing the prediction_interface.ipynb Notebook